Chondrogenesis and BMP2-Induced Regeneration of the Adult Mouse Middle Phalanx (P2) post Amputation

AN ABSTRACT

SUBMITTED ON THE 8th DAY OF APRIL 2014

TO THE DEPARTMENT OF CELL AND MOLECULAR BIOLOGY

IN PARTIAL FULFILLMENT OF THE REQUIREMENTS
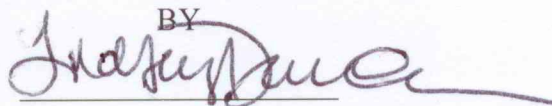
OF THE SCHOOL OF SCIENCE AND ENGINEERING

OF TULANE UNIVERSITY

FOR THE DEGREE
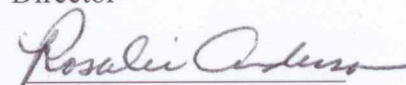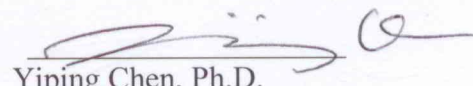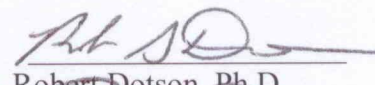
OF

DOCTOR OF PHILOSOPHY

BY

_____
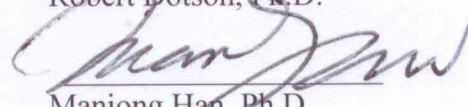
Lindsay Dawson

APPROVED BY: _____

Ken Muneoka, Ph.D.
Director

_____
Rosalie Anderson, Ph.D.

_____
Yiping Chen, Ph.D.

_____
Robert Dotson, Ph.D.

_____
Manjong Han, Ph.D.

Abstract

Humans and mice lack the broad regenerative capacity of Urodele amphibians, capable only of partial regeneration of the terminal phalanx (P3), i.e., amputation mid-way through P3 results in essentially complete regeneration of the digit tip mediated via blastema formation and subsequent direct bone formation, culminating in distal bone growth, patterning, and function. Conversely, amputation injuries occurring proximal to the mid-point of P3 result in scar formation. Here, in part, we studied the endochondral bone healing response following amputation of the middle phalanx (P2). We showed the endochondral ossification healing response post amputation of P2 is analogous to the fracture healing response of P2 and other long bones of the body, ultimately proving useful in yielding insight into effectively inducing regeneration of the amputated digit. We showed the periosteal-derived chondrocytes of P2 play an integral role in the bone healing process in that they provide a template for subsequent bone formation following amputation injury. We also showed the periosteal-derived cells can be targeted through the temporal application of BMP2 to accumulate and proliferate at the distal digit tip and thus induce regeneration of the amputated bone. Our studies indicated that P2 amputation injuries of various time points, i.e. previously healed injuries, can be induced to regenerate via re-wounding of the periosteal tissue and subsequent BMP2 application, and thus is immeasurably promising from a translational therapeutic perspective.

Lastly, we studied the fracture healing response in conjunction with the intramembranous regeneration response of P3. Following fracture of the digit, we showed the relative lack of periosteal callus formation, the lack of periosteal chondrogenesis, and a novel endosteal/marrow chondrogenic response. Unlike P2, the periosteal tissue of the fractured P3 bone does not respond to BMP2-treatment via endochondral bone growth, instead the bone heals via intramembranous ossification, possibly via intrinsic differentiation limitations and extrinsic factors. Notably, we showed that in the absence of the periosteal tissue of the amputated P3 bone, the regeneration response was greatly attenuated.

Taken together, our work blending regeneration and fracture repair may prove useful in enhancing regeneration studies with methods and ideas not previously considered.

Chondrogenesis and BMP2-Induced Regeneration of the Adult Mouse Middle Phalanx (P2) post Amputation

A DISSERTATION

SUBMITTED ON THE 8th DAY OF APRIL 2014

TO THE DEPARTMENT OF CELL AND MOLECULAR BIOLOGY

IN PARTIAL FULFILLMENT OF THE REQUIREMENTS

OF THE SCHOOL OF SCIENCE AND ENGINEERING

OF TULANE UNIVERSITY

FOR THE DEGREE

OF

DOCTOR OF PHILOSOPHY

BY

(signature)

Lindsay Dawson

APPROVED BY: _(signature)_

Ken Muneoka, Ph.D.
Director

(signature)

Rosalie Anderson, Ph.D.

(signature)

Yiping Chen, Ph.D.

(signature)

Robert Dotson, Ph.D.

(signature)

Manjong Han, Ph.D.

Acknowledgements

Table of Contents

List of Figures

General Introduction:

Mammalian Digit Regeneration: Terminal Phalanx & Sub-terminal (Middle) Phalanx:

Mammals lack the extensive regenerative capacity of Urodele amphibians, capable only of regenerating the distal digit tip, the terminal phalanx (P3), post amputation injury (Han et al., 2008; Fernando et al., 2011). The mammalian digit regeneration response is limited however; amputation mid-way through P3 results in essentially complete regeneration of the digit tip, while amputation injuries including and proximal to the P3 nail matrix result in scar formation (Neufeld and Zhao 1993; Borgens, 1982; Han et al., 2008; Turner et al, 2010; Fernando et al., 2011; Agrawal et al., 2011; Agrawal et al., 2012; Mu et al., 2013). Earlier studies have suggested a link between preservation of the proximal nail organ and successful bone regeneration post amputation, showing that proximal amputation injuries regenerate if the proximal portion of the nail is not amputated (Zhao et al., 1995; Mohammad et al., 1999.) Accordingly, grafting studies in which the nail organ was transplanted into the regeneration-incompetent middle phalanx (P2) amputation injury milieu indicated new bone formation associated with the transplanted nail, thus suggesting the nail organ itself could induce bone growth (Mohammad et al., 1999). A recent study has shown the necessity of Wnt activation in epidermal cells localized to the distal nail matrix post P3 amputation injury, with Wnt signaling essential in both nail regeneration and the downstream bone regeneration response (Takeo et al., 2013). Regeneration-incompetent proximal amputation injuries transect the proximal portion of the nail matrix, thus amputating the distal nail matrix comprised of Wnt-expressing cells, and ultimately inhibiting regeneration of the digit (Takeo et al., 2013). Regeneration-competent amputation mid-

way through P3 transects multiple tissue types, including the nail plate, nail bed, dorsal epidermis and associated dermis, and the distal portion of the P3 bone (Muller et al., 1999). Following adult mouse distal amputation, instead of scar formation, P3 undergoes an initial inflammatory response, characterized by the influx of macrophages and neutrophils (Simkin, Unpublished), followed by osteoclast-mediated degradation through the distal portion of the P3 bone, thus exposing the marrow cavity (Fernando et al., 2011). The degraded bone stump is eventually expelled as epidermal tissue migrates below it, essentially enabling a secondary bone 'self-amputation' at a plane proximal to the original amputation level (Fernando et al., 2011). Successive formation of the blastema, a population of undifferentiated mesenchymal cells and lineage-committed progenitor cells, occurs in the region between the open marrow cavity and the wound epidermis (Fernando et al., 2011; Rinkevich et al., 2011; Lehoczky et al., 2011). The cells of the blastema do not undergo chondrogenesis; instead they differentiate directly into bone forming cells, osteoblasts, which produce woven bone in a proximal-to-distal fashion, ultimately regenerating the digit tip (Han et al., 2008, Fernando et al., 2011). Importantly, the intramembranous bone regeneration response of P3 differs from its developmental mechanisms, in that P3 initially forms via a proximal epiphyseal growth plate, with subsequent appositional bone growth distally (Han et al., 2008). Regeneration-incompetent amputation levels of the neonate P3 digit have the potential to undergo induced regeneration after exogenous application of BMP2 or 7 at the time of wound closure (Yu et al., 2010). Importantly, BMP-induced regeneration of the neonate P3 digit occurs via endochondral ossification, as opposed to the direct intramembranous ossification of endogenous regeneration (Yu, et al., 2010).

In stark contrast to the regeneration response of P3, amputation mid-way though the adult mouse middle phalanx (P2) results in scar formation (Turner et al, 2010; Agrawal et al., 2011; Agrawal et al., 2012; Mu et al., 2013). Amputation mid-way through P2 transects the epidermis (containing hair follicles), dermis, bone, the marrow cavity, tendon, and ventral fibrocartilage. Earlier preliminary data consisting of histological samples and immunohistochemistry studies suggested the P2 bone healing response post amputation injury recapitulated that of bone development, i.e., with a cartilaginous intermediate. In accordance with this, the bone healing response of P2 is characterized by robust chondrocyte proliferation adjacent to the periosteal surface, followed by chondrocyte hypertrophy and matrix mineralization, woven bone formation, and secondary bone remodeling. The resulting bone displays a lack of patterning, presumably due to the direction of chondrocyte proliferation; post P2 amputation, chondrocyte proliferation occurs annularly along the periosteal surface of the bone stump, expanding perpendicular to the bone as opposed to distally, ultimately forming a perpendicular template for woven bone formation. Thus the amputated P2 bone does not show a significant increase in bone length post amputation injury, instead the amputation healing response culminates in an unpatterned bone stump.

Our model focuses on the perpendicular expansion and source of the chondrocytes, with several questions arising: How might we manipulate the proliferation of the chondrocytes to increase the template for P2 bone regeneration? How might we direct the chondrogenic component of P2 to a distal location, therefore increasing the length of the P2 bone post amputation? If we intend to target the chondrocytes, where do they arise from? And what growth factor(s) will these cells respond to in order to induce

the regeneration of the adult P2 digit? An earlier study had shown that neonate P2 digits respond to BMP2 treatment post amputation via the formation of a distal center of endochondral ossification, whereby BMP2-responsive chondrocytes proliferate, undergo hypertrophy, and ultimately form the template for bone regeneration (Yu et al., 2012). Importantly, it was also demonstrated that adult tissues respond to BMP2 treatment post amputation; the amputated mouse hindlimb treated with BMP2 showed a larger increase in length relative to controls, as well as a distal chondrogenic cap over the amputated bone stump presumably responsible for the distal bone regeneration response (Yu et al., 2012). Determining the source of the chondrocytes mediating both the endogenous healing response and the induced-regeneration response is essential to better targeting and enhancing the regeneration response of long bones.

The Development of Bone: Endochondral and Intramembranous Ossification:

P2 bone development generally follows that of the long bones; a coordinated series of events referred to as endochondral ossification. The commencement of endochondral ossification occurs through skeletal patterning, characterized by mesenchymal cell condensations throughout the developing embryo thereby forming an early template of the bone outline (Karsenty et al., 2003). At this early stage, the mesenchymal cells produce an extracellular matrix (ECM) rich in Collagen I (Col 1), and upon their differentiation into proliferating chondrocytes, begin the production of Collagen 2 (Col 2) (Karsenty et al., 2003). Mesenchymal cells at the margin of the structure do not undergo chondrocyte differentiation, instead they maintain Col I production and form the perichondrium, described as an enveloping structure which will ultimately become the periosteum (Karsenty et al., 2003). Chondrocytes in the center of

the cartilage template cease proliferation and undergo elongation, forming prehypertrophic chondrocytes, which subsequently form hypertrophic chondrocytes exhibiting a Collagen X (Col X)-rich ECM (Karsenty et al., 2003). Meanwhile, hypertrophic chondrocyte ECM mineralization occurs, with subsequent Matrix metalloproteinase (MMP)-mediated liberation of Vascular endothelial growth factor (VEGF) from the matrix thus enabling vascular invasion whereby vessels and preosteoblastic cells enter through the bone (Karsenty et al., 2003). Differentiation of these cells yield bone forming cells, termed osteoblasts, which migrate over the Col X matrix and secrete Col I in a pericellular random fashion, synthesizing woven bone (Karsenty et al., 2003; Shapiro, 2008). The woven bone formation described thus far, which occurs in a region of the growing bone called the diaphysis, replaces most of the cartilage template (Karsenty et al., 2003). Located at each end of the diaphysis, chondrocytes continue the ordered process of proliferation, elongation, and hypertrophy in a region between the epiphysis and metaphysis, referred to as the growth plate (Karsenty et al., 2003). The epiphyseal margin of the growth plate is comprised of parathyroid hormone (PTH) receptor-positive proliferating chondrocytes surrounded by Parathyroid hormone-related protein (PTHrP) expressing perichondrial cells (Kronenber, 2003). Proliferating chondrocytes also express PTHrP, and importantly, both sources act on pre and early hypertrophic chondrocytes to prevent hypertrophy (Karsenty et al., 2003; Kronenber, 2003). Concurrently, prehypertrophic chondrocytes located above the metaphyseal region express Indian hedgehog (IHH), a growth factor which functions to increase chondrocyte proliferation, differentiation, and to induce PTHrP expression in proliferating chondrocytes and subarticular perichondrium (Karsenty et al., 2003). The

ordered process of the growth plate enables longitudinal expansion of the bone, regulated in part by the columnar orientation of the chondrocytes, which ensures one row of chondrocytes will undergo hypertrophy and subsequent woven bone formation at a time. Diaphyseal radial growth, i.e. the increase in bone width, occurs through intramembranous bone formation-described as bone formation directly from a mesenchymal condensation without intermediate chondrocyte formation-by osteoblasts supplied by the cell-rich region of the periosteum, the inner cambial layer (Shapiro, 2008). Development of comparatively smaller bones, such as the mouse metatarsals and phalanges, including P2, initially occurs via similar mechanisms, i.e. endochondral ossification, however, the proximal and distal growth plates display unequal contribution to the overall length of the bone (Reno et al., 2006). Phalanges have been described to only contain the proximal growth plate, with the distal portion of the bone exhibiting unorganized cartilage and lacking a secondary ossification center (Reno, et al., 2006). And lastly, while endochondral ossification is the principal mode of bone formation, the bones of the vertebrate skull, the calvariae, a portion of the pectoral girdle, and sesamoid bones such as the patella, develop via intramembranous ossification (Franz-Odendaal, 2011).

Adult Fracture Healing:

As of 2013, upwards of 7.9 million bone fractures occurred in the United States annually (Sathyendra and Darowish, 2013). While a great proportion healed successfully, an estimated 10 percent of the fractures resulted in inadequate repair,

including non-union of the bone segments and delayed healing (Sathyendra and Darowish, 2013).

Adult fracture healing in the mouse and human is thought to closely follow the developmental events occurring during skeletogenesis (Ferguson et al., 1999; Vortkamp et al., 1998; Gerstenfeld et al., 2003). Therefore, the study of skeletogenesis will often yield insights into the mechanisms of fracture healing, both of which may prove useful in understanding bone healing and induced-regeneration post P2 amputation. However, there are two key differences between development and bone repair post fracture. Firstly, the mechanism in which bone undergoes fracture repair is reliant upon its environment; stabilized fractures (stabilized through the use of intra and extra-medullary rods or well positioned bone surfaces) heal through endosteal/marrow-derived intramembranous ossification with relatively low periosteal contribution, while non-stabilized fractures (characterized by movement and pressure at the fracture site) heal predominantly through endochondral ossification along the periosteal surface in conjunction with concomitant intramembranous ossification surrounding the periosteal callus (Shapiro, 2008; Ferguson et al., 1999; Vortkamp et al., 1998; Thompson et al., 2001; Colnot, 2008; Einhorn, 2005). Importantly, the endosteal/marrow compartment also undergoes intramembranous ossification during unstable fracture repair, yet the development of the medullary callus is delayed relative to the periosteal callus, presumably due to the instability of the environment (Merloz, 2011). Secondly, the initiation of fracture repair follows an initial inflammatory response at the site of bone injury, characterized by the expression of various cytokines and growth factors, including IL-1, IL-6, TGF-β, TNF-α, PDGF, and BMP2 (Al-Aql et al., 2008). Regardless of these differences, non-stable fracture repair is

the chief mode of bone healing and follows a specific series of events to ultimately rebuild the organ to its pre-fracture strength and morphology, and notably, without an increase in bone volume (Al-Aql et al., 2008; Einhorn, 2005). These bone healing events include (i) an initial inflammation stage, (ii) the formation of a cartilaginous "soft callus" along the periosteal surface analogous to the cartilage anlage in the developing embryo, (iii) subsequent formation of the "hard callus," consisting of boney material deposited in a woven irregular pattern by osteoblasts much the same way as during development, and (iv) remodeling of the primary bone into an organized secondary structure through the balance of bone resorption and bone deposition by osteoclasts and osteoblasts, respectively, ultimately forming strong, lamellar bone (Shapiro, 2008; Schindeler et al., 2008). The time course of unstabilized fracture repair in the adult mouse in a standardized model indicate (i) the fate of the cells localized to the periosteal surface has been determined (i.e. chondrocytes in unstabilized fracture repair, and osteoblasts in stabilized fracture repair) by 72-96 hours post fracture, (ii) the cartilaginous callus is readily apparent by 7 days post fracture (DPF), (iii) the cartilaginous callus is undergoing intense proliferation at 10 DPF, (iv) followed by bridging of the fracture gap and subsequent chondrocyte hypertrophy by 14 DPF, and (v) removal and replacement of the cartilaginous callus with a woven boney callus by 21 DPF (Thompson et al., 2001).

While the four bone healing events are sequential, they do have considerable overlap, and each step is equally important to rebuilding the fractured bone (Schindeler et al., 2008). We will focus on the soft callus step; our P2 model exhibits a significant cartilaginous callus, whereby chondrocytes develop along the periosteal surface and seemingly provide a template for the succeeding woven bone formation. In unstablized

fracture healing, mesenchymal progenitor cells differentiate into chondrocytes, found almost exclusively along the periosteal surface, and undergo proliferation to surround and bridge the immediate fracture site (Colnot, 2008; Al-Aql et al., 2008; Schindeler et al., 2008). The typically avascular chondrocytes progress to hypertrophy, undergo matrix mineralization, and finally die via programmed cell death (Al-Aql et al., 2008). The mineralized matrix they leave behind is degraded via osteoclasts, coupled with the deposition of new woven bone by osteoblasts along with simultaneous vascularization (Al-Aql et al., 2008; Shapiro, 2008). In accordance with this, transcripts of *Col 2*, *Ihh*, and *PTHrP* are localized to chondrocytes along the periosteal surface post fracture, with subsequent Col X, VEGF, and MMP 13 expression during soft callus remodeling (Ferguson et al., 1999; Vortkamp et al., 1998; Gerstenfeld et al., 2003; Thompson et al., 2001).

Our main goal is to look to discoveries made in the fracture healing field and apply that knowledge to advancing the regeneration response post mammalian long bone amputation injury. And conversely, discoveries made in the regeneration field may greatly benefit the field of fracture repair. In line with this, the axolotl, known for its outstanding capacity to regenerate missing structures, including the limb, also undergoes a fracture repair response analogous to humans and mice, albeit on a longer time scale (Hutchison et al., 2007). Following fracture of the axolotl radius or ulna, the bone shows no signs of repair by 15 DPF, yet by 45 DPF whole mount staining indicates a cartilaginous callus has bridged the fracture gap, with the cartilaginous callus remaining for several months, and the bone ultimately bridged with boney callus by 5 months post fracture (Hutchison et al., 2007). Since the axolotl is capable of mounting an

extraordinary regeneration response following amputation of the limb, the authors tested the axolotl's ability to heal critical gap fractures, thus bone repair in a gap too large to heal on its own, an injury no vertebrates have been shown to heal (Hutchison et al., 2007). Importantly, the axolotl was shown to not have the potential to heal critical gap fractures, with whole mount staining indicating the lack of cartilaginous growth at the severed bone surfaces, no increase in bone length, and no indication of bone repair at 7 months post fracture (Hutchison et al., 2007). Thus, the authors concluded the axolotl does not employ the regeneration process to heal bones post fracture of critical dimension (Hutchison et al., 2007). Accordingly, we must look to targeting cell population(s) known to play a critical role in successful bone repair, with the intentions of modulating their proliferation, aiding in their recruitment to the injury site, and ultimately patterning the cells to enable a robust regeneration response following amputation.

An area of debate regarding bone regeneration during fracture repair is the source of the mesenchymal cell population which will ultimately form the chondrogenic component of the fracture callus. Cellular contribution to fracture repair has been suggested to arise from the endosteum and marrow cavity, the cortical bone, the surrounding soft tissues, delivered via the vasculature, and from the cell dense region of the periosteum, the cambium layer (Shapiro, 2008; Colnot, 2008; Schindeler et al., 2008; Dwek, 2010). Elucidating the source of the chondrocytes which form the soft callus is of great importance due to their role in stabilization of the fracture site as well as providing a template for primary bone formation (Gerstenfeld et al., 2003).

An extensive amount of evidence suggests the periosteum as the main source of the chondrogenic, as well as osteoblastic, precursors in fracture repair (Ito et al., 2001;

Colnot, 2008; Dwek, 2010; Yu et al., 2010a). The periosteum covers all non-articular portions of the bone and is composed of two layers, an outer layer of predominantly fibrous tissue, referred to as the fibrous layer, and a highly vascularized, cell rich, inner layer, termed the cambium layer (Dwek, 2010; Ito et al., 2001). The cambium and the fibrous layers can be further divided into 3 zones; zone I comprises the cambium layer, the thinnest layer, made up of round cells primarily identified as mesenchymal stem cells that function to repair and build bone, zone II comprises the bulk of the fibrous layer and is the largest component of the periosteum, also termed the matrix layer, and is characterized by the presence of Sharpey's fibers (collagen structures), vasculature and associated perivascular cells, and lastly, zone III, the smaller component of the fibrous layer, also termed the fibroblastic/collagenous layer, is comprised of flattened fibroblastic cells (Chang and Knothe Tate, 2012; Colnot et al., 2012). The outer fibrous layer, due to its Sharpey's fibers and other extracellular matrix components, is responsible for the toughness and mechanical stability of the periosteum (Chang and Knothe Tate, 2012; Colnot et al., 2012). The cambium layer of the periosteum is thought to provide the osteoblastic cells responsible for the circumferential growth of long bones during development, with bone deposited in a direct fashion, without a cartilaginous intermediate (Shapiro, 2008; Chang and Knothe Tate, 2012). Importantly, the perichondrium (the structure preceding the periosteum, different only in that it envelops chondrocytes, while the periosteum envelops bone) has been shown to supply all of the osteoblasts that comprise the periosteum and the endosteum during long bone development (Colnot et al., 2004; Colnot et al., 2012). In contrast to the actions of the periosteum during the development of long bones, the periosteal surface is rich with

chondrocytes post unstabilized fracture (Colnot, 2008). The progenitor cells found within the periosteum may differentiate into chondrocytes and/or osteoblasts post injury, depending on the stabilization of the bone fragments (Wang et al., 2011). Moreover, studies have shown the periosteum, in comparison to the endosteal/marrow region, is the predominant contributor to the external fracture callus, providing both chondrocytes and osteoblasts (Colnot et al., 2012). Significant delay in fracture healing occurs after physical removal of the periosteal layer, apparently due to removal of cambium-derived cartilaginous progenitor cells, thus stressing their importance (Ferguson et al., 1999; Dwek, 2010). Indeed, it has been shown in-vitro in periosteal organ culture the proliferation of prechondrogenic cells and their subsequent differentiation into Col 2 expressing chondrocytes localized to the inner cambium layer of the periosteum (Ito et al., 2001). Using in vivo cell lineage tracing studies, β-gal labeled bone grafts placed within a non-stabilized fracture site yield β-gal positive chondrocytes along the periosteal surface of the graft (Colnot, 2008). Importantly, the endosteum/marrow compartment was removed prior to engraftment, therefore excluding the medullary cells as the source of the chondrocytes (Colnot, 2008). Furthermore, periosteal activation, characterized as periosteal-cell-derived-proliferation, has been shown in vivo to be essential for adequate bone repair; mice lacking periosteal activation exhibited complete absence of cartilaginous soft callus formation and non-union of the bone segments (Tsuji et al., 2006). However, recent findings challenge the notion of periosteal cells as the predominant source of chondrocytes involved in soft callus formation (Kitaori et al., 2009). Injection of murine BrdU-labeled bone marrow derived stromal cells post femoral bone grafting resulted in their incorporation within the soft callus, with 25% of the callus

composed of labeled chondrocytes (Kitaori et al., 2009). However, the study utilized the manipulation of a known chemoattractant signaling axis to recruit the injected BrdU-labeled bone marrow derived stromal cells to the injury site, thus their findings may not necessarily translate to the endogenous cartilaginous healing response following the fracture of long bones (Kitaori et al., 2009). Regardless, proliferating chondrocytes are essential for adequate bone healing post injury, and data suggests proliferating chondrocytes are essential for the induction of P2 regeneration, therefore it is crucial to determine their source post bone injury in order to successfully target them at the P2 stump (Yu et al., 2012).

Chapter One: Integration of Middle Phalanx Fracture Repair and

Amputation healing: Periosteal Chondrogenesis

I. Introduction

Mammals lack the extensive regenerative capacity of Urodele amphibians, capable only of partial regeneration of the terminal phalanx (P3), i.e., amputation midway through P3 results in essentially complete regeneration of the digit tip (Neufeld, 1992; Borgens, 1982; Han et al., 2008; Fernando et al., 2011; Rinkevich et al., 2011; Lehoczky et al., 2011). Conversely, amputation including and proximal to the P3 nail matrix results in scar formation. P3 undergoes regeneration post amputation, resulting in near perfect bone patterning, distal bone growth, and function (Han et al., 2008, Fernando et al., 2011). The P3 regeneration response is characterized by the formation of a blastema and subsequent direct osteoblast differentiation, forming bone through intramembranous ossification, thus differing from its development via endochondral ossification (Han et al., 2008). Unlike P3, the bone healing response of the regeneration-incompetent middle phalanx (P2) post amputation injury follows that of developmental mechanisms, i.e., the unpatterned bone regeneration attempt as well as the development of P2 occurs via endochondral ossification, therefore comprised of a cartilaginous intermediate(Agrawal, et al; 2011). Previous work has shown that while the neonatal P2

digit does not undergo a regeneration response post amputation injury, the digit is capable of induced regeneration post BMP2 treatment, and notably, the regeneration response is an endochondral event (Yu et al., 2012). Furthermore, amputation of the adult mouse regeneration-incompetent hindlimb is also receptive to BMP2-treatment vs. BSA controls, undergoing a regeneration response via endochondral ossification (Yu et al., 2012). Interestingly, we have found the adult mouse P2 endochondral ossification response post amputation is histologically reminiscent of unstabilized fracture repair, also mediated via endochondral ossification. Thus, identifying the cellular and molecular similarities between long bone fracture repair and P2 amputation injury healing, and namely, further understanding of the chondrogenic component, may help us gain insight into effectively inducing regeneration of bones at regeneration-incompetent levels.

Many of the cellular and molecular events of adult mouse and human long bone fracture healing recapitulate those of skeletogenesis (Ferguson et al., 1999; Vortkamp et al., 1998; Gerstenfeld et al., 2003). It is important to highlight that fracture healing differs from developmental mechanisms in several ways, i.e., fracture healing is characterized by an initial inflammatory response, and the mechanism in which bone regenerates post fracture is dependent upon its environment: stabilized fractures heal via intramembranous ossification whereby a boney periosteal and endosteal callus forms, with no apparent cartilaginous callus, and unstabilized fractures heal via endochondral ossification through the formation of an external cartilaginous and boney callus in addition to the formation of an endosteal boney callus (Shapiro, 2008; Ferguson et al., 1999; Vortkamp et al., 1998; Thompson et al., 2001; Colnot, 2008; Einhorn, 2005). Therefore, with the exception of the initial inflammatory response, the sequence of events

comprising unstabilized fracture healing are quite like that of endochondral bone development, including: (i) the formation of a cartilaginous "soft" callus along the periosteal surface of the bone, acting, in part, as a template for (ii) the subsequent formation of the boney "hard" callus whereby osteoblasts deposit Col I in an irregular pattern over the mineralized cartilaginous matrix, and followed with (iii) the ultimate remodeling of the woven bone into an organized lamellar structure through the balance of bone resorption and bone deposition by osteoclasts and osteoblasts, respectively (Shapiro, 2008; Schindeler et al., 2008). Indeed, similarities have been determined between skeletogenesis and the events of bone healing post fracture, lending much insight to be gained for both fields (Ferguson et al., 1999; Vortkamp et al., 1998; Gerstenfeld et al., 2003), however, questions remain: are all mechanisms of bone healing similar, regardless of injury type, such as amputation injury or fracture? What cell populations are essential for the successful union of fractured bones, and can we manipulate those same cell populations to induce regeneration of amputated bones?

Successful fracture healing rebuilds the bone to its pre-fracture strength and morphology, and the success of fracture healing lies largely in the initial and sustained periosteal response (Al-Aql et al., 2008; Einhorn, 2005; Tsuji et al., 2006; Wang et al., 2011). The periosteum is defined as the outer structure of the bones, covering all non-articular surfaces and composed of two layers: a cell rich inner layer, termed the cambium layer, and a relatively cell-poor outer layer, referred to the as the fibrous layer (Dwek, 2010, Ito et al., 2001). During bone development, periosteal-derived osteoblasts deposit collagen I along the bone surface, enabling the radial expansion of bones (Shapiro, 2008). Post unstabilized fracture healing, on the other hand, the periosteum has

been shown to supply not only osteoblasts, but also chondrocytes to the fracture callus, and many suggest it is ultimately responsible for the formation of the cartilaginous callus (Colnot, 2008; Tsuji et al., 2006; Ito et al., 2001; Dwek, 2009). It is this cartilaginous callus that stabilizes the fracture gap, and also creates a template for the subsequent woven bone formation, thus stressing its importance (Gerstenfeld et al., 2003). Several days post long bone fracture, periosteal activation, described as marked proliferation of periosteal cells, is a critical factor determining the overall success of bone union; bones lacking the activation lack the continued maintenance of BMP 2, 4, and 7 expression, as well as lacking the overall cartilaginous callus (Tsuji et al., 2006). Additionally, significant delay or inhibition of fracture healing occurs following physical removal of the periosteal layer, almost certainly due to the removal of periosteal-derived pre-chondrogenic cells (Ferguson et al., 1999). In line with this, we have found that the bone healing response post amputation of the adult mouse P2 digit exhibits a cartilaginous callus along the periosteal surface, which then is replaced by woven bone and eventually remodeled into lamellar bone, much like that of the P2 fracture healing response. Additionally, BMP2 has been shown to induce regeneration of the neonate P2 digit via an intermediate cartilaginous step, and importantly, BMP2 has been shown to specifically target periosteal cells to undergo chondrogenesis post bone injury (Yu et al., 2012; Yu et al, 2010a). Determining the source of the chondrogenic component, and furthermore, the potential contribution and role of periosteal cells in the P2 bone healing response post amputation injury may be critical to effectively inducing regeneration of the digit.

Here, we explored the histological, cellular, and molecular relationships between the amputation response and the fracture healing response of P2. We hypothesized that

the P2 bone healing response was analogous to one-half of the P2 fracture healing response, and therefore, the source of the chondrocytes post amputation arise from the same source as during long bone fracture, i.e., the periosteum. Importantly, our histology, immunohistochemistry, and MicroCT data suggests the P2 amputation response is much like that of the P2 fracture healing response. We also demonstrate the role of the P2 periosteum post amputation injury. Furthermore, through the use of bone grafting and transgenic mouse models we show for the first time the chondrogenic and osteogenic cell source(s) post P2 amputation injury. Our goal was to determine the potential similarities between the digit amputation response and the fracture repair response in order to apply the advances in fracture healing to digit regeneration. Moreover, we aimed to determine the critical cell populations and their behavior post P2 amputation in order to manipulate them and ultimately regenerate not only the P2 bone, but other long bones of the body.

II. Materials and Methods

Mice, P2 amputation, and P2 fracture

Mice used in this study, C57Bl/6, CD-1 wild-type, Actin-eGFP, and NOD-SCID were purchased from Jackson Labs. P2 amputations were carried out on hind limb digits two and four of 8 to 12-week-old adult female mice. Mice were anesthetized using Isofluorane, with an initial dose of 3% Isofluorane, and maintained at 2% Isofluorane. P2 amputations were performed using a scalpel to sever the digit at approximately the

second ventral fat pad indent. Fracture of the P2 bone was carried out by an initial micro-scissor incision, creating a small hole thus exposing the P2 bone, followed by fracture of the bone through the use of small surgery scissors. The open wound was closed through the use of Dermabond. The P2 bone was fractured at approximately the second ventral fat pad indent, coinciding with the P2 amputation level. All animal use and procedures were in compliance with Tulane University's Institutional Animal Care and Use Committee.

P2 Bone Grafting

Transgenic 8-week-old Actin-eGFP mice, which constitutively express the eGFP protein under the control of the CMV-Actin promoter, were used to trace periosteal and endosteal/marrow cell fate post P2 amputation. Mice were anesthetized, and portions of the P2 bone were harvested from unamputated hindlimb digits, and immediately grafted into newly fractured unlabeled NOD-SCID mice P2 digits. For determination of periosteal contribution post P2 amputation, we reamed the labeled bone marrow and scraped the endosteal surface with a sharp tungsten needle, leaving the periosteum intact, and grafted the bone into the P2 fracture region of a NOD-SCID host. Conversely, in some samples we removed the periosteum of the labeled bone via scraping the bone surface with a scalpel at the time of amputation, and immediately grafted the periosteum-free bone into the NOD-SCID host fractured P2 environment. As positive and negative controls, we grafted periosteum and endosteum/marrow intact labeled P2 bones, as well as periosteum and endosteum/marrow free bones (i.e., only cortical bone), respectively.

All samples were collected 11 days post grafting and fracture, when chondrogenesis was prevalent.

Histological Staining

Amputated P2, fractured P2, and labeled-graft digits were collected at various time points and fixed from 24-96 hours in Z-fix (Anatech, LTD) at room temperature. Digits were then decalcified using Decalcifier I (Surgipath) for at least 8 hours, and no more than 24 hours. Digits were processed using a graded ethanol series, xylenes, and immersed in paraffin wax. Digits embedded in paraffin wax were sectioned at 5 μm thickness. In order to analyze the whole callus, digits were sectioned completely, and serial sections were created. Mallory's Trichrome staining was performed to determine the relative amounts of cartilage and bone formation. In order to visualize cartilage formation specifically, Toluidine blue staining was performed. All samples were imaged using the Olympus DP72 microscope using DP2-BSW software.

Antibodies and Immunohistochemistry

Digits were harvested and treated as described in Histological Staining. Slides were incubated at 60 degrees Celsius for 45 minutes, followed by a 15 minute-96 hour incubation at 37 degrees Celsius. Antigen retrieval was performed using Proteinase K solution (Dako) and incubated at 37 degrees Celsius for 15 minutes, or heat retrieval performed in 1X citrate buffer solution (Dako). Slides were blocked using Protein Block for 30 minutes to 1 hour (Dako). Slides were incubated with primary antibody/antibodies over night at 4 degrees, washed in TBST solution and incubated in secondary

antibody/antibodies for 45 minutes at room temperature. Slides were subsequently incubated in DAPI solution, dried, and mounted with Prolong Gold (Invitrogen). Primary antibodies used include Mouse-Anti Collagen Type II (Acris) at a 1:200 concentration and Proteinase K retrieval, Rabbit-Anti Osterix, SP7 (Abcam) at a 1:400 concentration and heat retrieval, Rabbit-Anti Cathepsin K at a 1:100 concentration and heat retrieval, Rabbit-anti-Aggrecan (Millipore) at a 1:300 concentration using heat retrieval, and Chick-Anti GFP (Novus Biologicals) at a 1:1000 concentration using heat retrieval. Secondary antibodies used include Goat-Anti Rabbit 488 (Invitrogen), Goat-Anti Rat 568 (Invitrogen), Goat-Anti Chick 568 (Invitrogen), Goat-Anti Mouse 647 (Invitrogen), Goat-Anti Mouse 488 (Invitrogen), all at 1:500 concentration in antibody diluent (Invitrogen). All samples were imaged using the Olympus BX61 microscope, with the Slidebook software.

Microtomography Scans & Fiji

P2 digits were scanned from one day post amputation with intact periosteum or one day post amputation and periosteum removal and weekly thereafter for up to 4 weeks using the vivaCT 40 (SCANCO Medical, Wayne, PA) as described previously (Fernando, et al., 2011). Digits were scanned at 10.5µm voxel size and Energy 45 kVp and saved as dicom files. Using the boneJ Fiji plugin, 3-D reconstructed images were created in which bone volume was measured.

III. Results

Histology of the P2 Amputation and Fracture Healing Responses

In order to determine the potential bone healing relationship between the P2 amputation response and the P2 fracture healing response, we amputated digits at the P2 level, followed by harvesting the digits at various time points and completing histological staining. Post long bone fracture and the initial inflammatory response, studies have shown a cartilaginous callus develops along the periosteal surface, followed by woven bone formation over the mineralized cartilaginous matrix, and ultimately remodeling of the woven bone into a lamellar structure (Shapiro, 2008; Schindeler et al., 2008). In agreement with the abundant fracture healing literature, we harvest P2 amputated samples at time points specific to the initial inflammatory response at 1-3 days post amputation (DPA) (Fig. 1.1 A and B), formation of the cartilaginous callus at 9DPA (Fig. 1.1 C), woven bone hard callus formation at 15-19DPA (Fig. 1.1 D and E), hard callus remodeling at 28DPA (Fig. 1.1 F) and the completely remodeled lamellar bone at 45 and 90DPA (Fig. 1.1 G and H).

Our Mallory's stained samples show the P2 amputation inflammatory response is characterized by the infiltration of red blood cells and the subsequent swelling of the digit (Fig. 1.1 A and B). Soon after amputation, a large scab forms at the distal tip of the digit, plugging the marrow cavity (Fig. 1.1 B). At 9DPA, the digit displays a cartilaginous callus along the periosteal surface of the bone only, not within the marrow cavity, and not distal to the bone stump (Fig. 1.1 C, outlined). The wound has been closed by 9 DPA, with the scab removed and replaced with a large distal wound epidermis (Fig. 1.1, C). Histological evidence indicates the transient cartilaginous callus of the amputated digit has been largely replaced by woven bone including the formation of marrow spaces along the periosteal surface at 15DPA (Fig. 1.1 D). The woven boney callus adjacent to the

periosteal surface of the amputated digit appears denser at 19DPA, and has completely replaced the previous cartilaginous structure (Fig. 1.1 E). Post amputation of P2, the bone undergoes distal closure of the marrow space between 19-28DPA, and notably, without a cartilaginous intermediate and no distal elongation of the digit (Fig. 1.1 E and F). Unlike the 19 and 28DPA samples displaying the woven bone callus, the P2 amputation response shows signs of organized lamellar bone at 45 DPA (Fig. 1.1 G), with similarly remodeled bone at 90DPA (Fig. 1.1 H).

In an attempt to compare the P2 fracture healing response to the amputation response of P2, we fractured the digit at the P2 amputation level, followed by harvesting the digits at various time points and performing histological staining. Time points included consist of the initial inflammatory response 1-5 days post fracture (DPF) (Fig. 1.2 A and B), the formation and remodeling of the cartilaginous callus at roughly 11-28DPF (Fig. 1.2 C, D, E, and F), the woven bone hard callus stage at roughly 15-35DPF (Fig. 1.2 D, E, F, and G), and finally the completely remodeled bone, at 84DPF (Fig. 1.2 H).

Similar to the amputation response of P2, Mallory's staining shows the fractured digit is characterized by the infiltration of red blood cells followed by swelling during the inflammatory stage, yet lacking the large scab of the amputated digit (Fig. 1.2 A and B). Much like the cartilaginous callus post amputation, the fractured digit shows the presence of cartilage along the periosteal surface only and not within the marrow region, and notably, both the proximal and distal portions of the fractured digit show the presence of cartilage (Fig. 1.2, C, arrowheads). In contrast to the transient cartilaginous callus of the amputated digit, the fractured P2 digit displays a relatively continuous cartilage response,

1 DPA 3 DPA 9 DPA 15 DPA

19 DPA 28 DPA 45 DPA 90 DPA
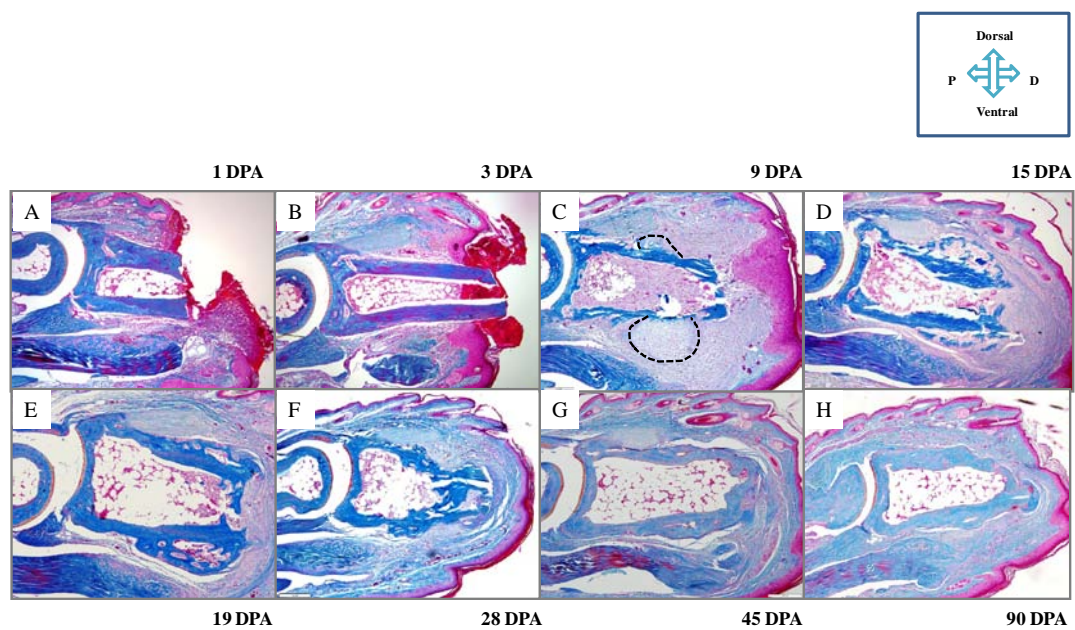
Figure 1.1- Dawson et al.

Fig. 1.1 Histological staining of the endochondral ossification healing response post P2 amputation. (A) Mallory's staining of the amputated P2 digit shows the infiltration of red blood cells at 1 DPA. (B) By 3 DPA, in addition to swelling of the digit, a scab has formed at the distal tip of the bone, plugging the marrow cavity. (C) By 9 DPA, a cartilaginous amputation callus has formed along the periosteal surface of the injured bone (outline), and importantly, no chondrocytes are present within the endosteal/marrow space or distal to the bone stump. (D) By 15 DPA, the cartilaginous callus has largely been removed and replaced with woven bone, including marrow spaces. (E) At 19 DPA, only the boney amputation callus remains on the periosteal surface, and the distal digit tip is showing signs of distal bone closure. (F) At 28 DPA, the amputated P2 bone is undergoing continued remodeling. (G and H) By 45 and 90 DPA, the bone has been remodeled into a lamellar structure, evident by the relatively smooth surface of the bone and the lack of marrow spaces in the amputation callus compared to earlier time points, and the distal marrow wound has been completely closed by bone formation. All images 100X. All digits sectioned at 5 μm.

with chondrocytes present 11-35DPF, as well as proximal and distal expansion of the cartilaginous callus, ultimately bridging the fracture gap (Fig. 1.2 C-G). Histological evidence suggests the cartilaginous callus of the amputated digit has been completely removed and replaced by woven bone at 19DPA (see Fig. 1.1 E), while the fracture model displays much overlap between the cartilaginous and boney calluses, from 15-35DPF (Fig. 1.2 D-G). Note the newly formed disorganized woven bone evident between 15-35DPF, replacing the cartilaginous callus (Fig. 1.2 D-G). Histological evidence shows the last stage of successful fracture healing, the remodeling of woven bone into an organized lamellar structure, has been completed by 84DPF (Fig. 1.2 H).

Immunohistochemistry of the P2 Amputation and Fracture Cartilaginous Callus

Our histological studies suggest bone healing similarities between the P2 amputation response and the P2 fracture healing response, whereby they both exhibit inflammation, a cartilaginous callus along the periosteal surface, the replacement of the cartilaginous callus by a woven boney callus, and ultimately remodeling of the bone into a lamellar structure. Immunohistochemistry was performed on digit samples displaying a prominent cartilage callus in order to elucidate the potential molecular relationships between the P2 amputation response and the P2 fracture healing response. As show via Aggrecan (Agc1) staining, a marker for chondrocytes, the 9DPA digit stump is positive for chondrocytes along the periosteal surface only, not within the marrow cavity nor distal to the amputation plane (Fig. 1.3 A). Accordingly, the proximal portion of the P2
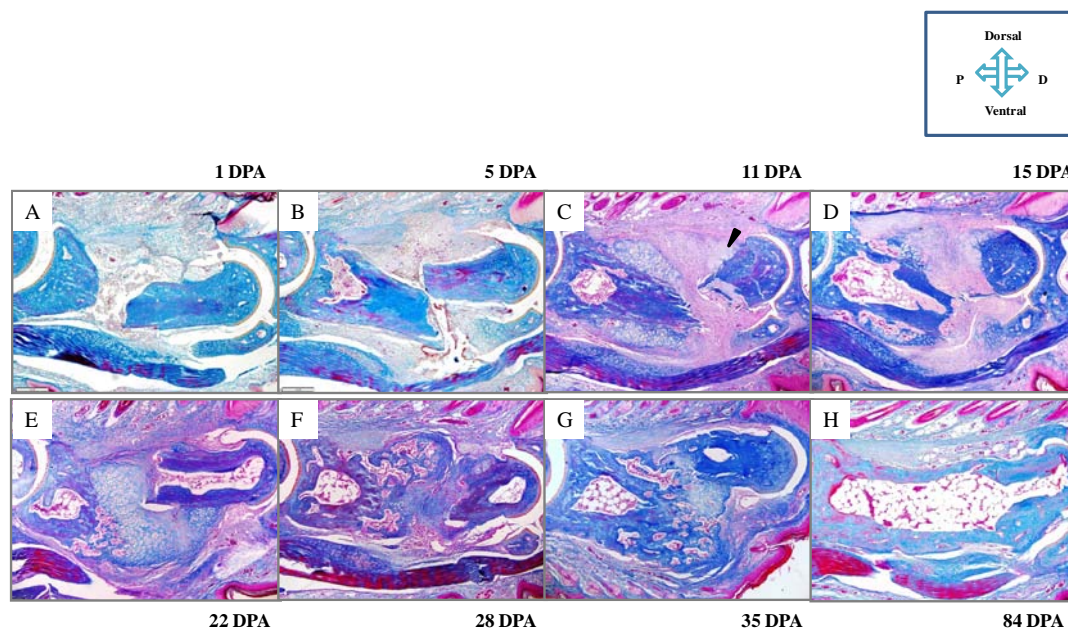
Figure 1.2 – Dawson et al.

Fig. 1.2 Histological staining of the endochondral ossification healing response post P2 fracture. (A) Mallory's staining of the fractured P2 digit shows infiltration of red blood cells localized to the fracture gap at 1 DPF. (B) At 5 DPF, the fractured digit is swollen and lacks chondrocytes on the periosteal surface. (C) By 11 DPF, the periosteal surface of the proximal and distal bone fragments shows large areas of chondrogenesis. (D) The cartilaginous fracture callus is still present on the 15 DPF digit, as well as signs of chondrocyte remodeling and new woven bone formation on the periosteal surface, complete with marrow spaces. (E) The 22 DPF histological sample shows the cartilaginous callus has bridged the fracture space, and the boney fracture callus is clearly present adjacent to the proximal bone fragment. (F) At 28 DPF, the soft callus persists, yet the fracture callus is predominantly boney by this time point, largely comprised of woven, irregularly patterned bone. (G). The 35 DPF callus is primarily comprised of woven bone, yet cartilage still joins the two bone pieces. (H) At the 84 DPF, the woven boney callus has been remodeled into a smooth lamellar structure, evident from the smooth continuous appearance of the bone. All images 100X. All digits sectioned at 5 μm.

fracture callus is immunopositive for Agc1 along the periosteal surface at 11DPF, also not within the marrow cavity, nor distal to the fracture gap (Fig. 1.3 D).

The chondrocytes which comprise the cartilaginous callus post bone fracture are thought to be encircled by a thin layer of osteoblasts, and both cell types have been shown to be periosteal-derived (Gerstenfeld, et al., 2003; Ito et al., 2001; Colnot, 2008). Indeed, the cartilaginous callus of the fractured P2 digit at 11DPF is surrounded by osterix, OSX, (a transcription factor involved in osteoblast differentiation) positive cells, as well some immunopositive cells within the fracture callus (Fig. 1.3 E). Additionally, cells lining the fractured endosteum test immunopositive for OSX at 11DPF (Fig. 1.3 E), coinciding with published reports (Colnot, 2008). Immunohistochemistry for OSX positive cells in the 9DPA digit localizes osteoblasts to comparable locations, i.e., surrounding and within the fracture callus and within the endosteal/marrow region, thus indicating a similar bone healing organization between the fractured P2 digits and the amputated digits (Fig. 1.3 B). Lastly, the fracture cartilaginous callus undergoes matrix mineralization and is replaced by woven bone, all while undergoing degradation mediated via osteoclasts (Schindeler et al., 2008). In line with this, osteoclasts, visualized through the osteoclast-marker, Cathepsin K (CpsK), are present lightly within the amputation cartilaginous callus (arrowheads), within the cortical bone (arrow), and within the endosteal/marrow region (Fig. 1.3 C). Similarly, the fracture cartilaginous callus shows light immunostaining osteoclasts (arrowheads), CpsK immunostaining within the cortical bone (arrow), and within the endosteal/marrow region (Fig. 1.3 F).
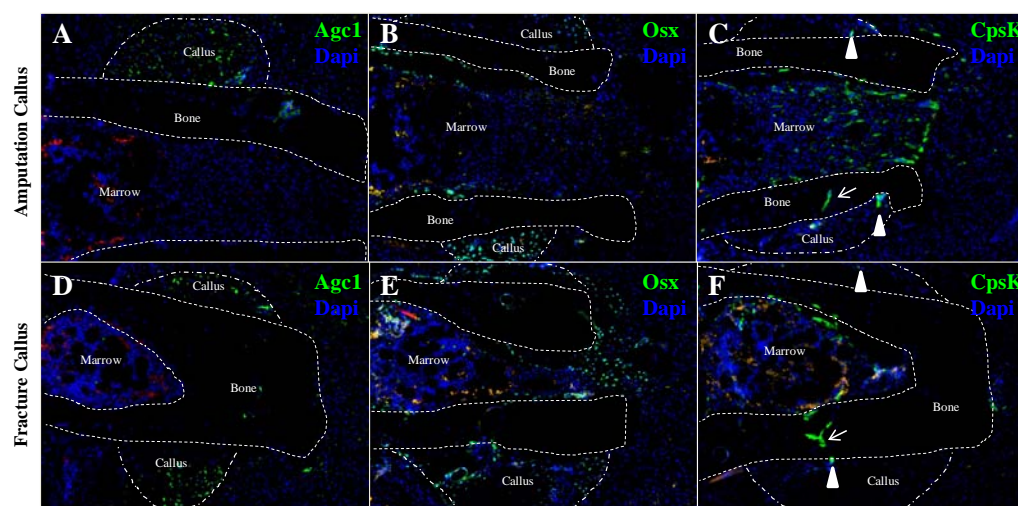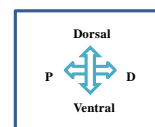
Figure 1.3 – Dawson et al.

Fig 1.3 Immunohistochemical analysis of the P2 amputation and fracture soft cartilaginous callus indicates a similar bone healing response post injury. (A and D) Immunohistochemistry probing for Agc1 positive chondrocytes reveals a similar distribution of immunostaining in the cartilaginous callus of the 9 DPA digit and the 11 DPF digit, with chondrocytes localized only along the periosteal surface, not within the endosteal/marrow cavity or distal to the bone. (B) Osx immunohistochemistry shows osteoblasts localized to the periosteal amputation callus and within the endosteal/marrow region at 9 DPA. (E) Osx-immunopositive cells are localized to periosteal fracture callus, within the endosteal/marrow region, and distal to the bone stump at 11 DPF. (C and F) Both the amputation and fracture injuries show CpsK-immunopositive osteoclasts in comparable locations, including lightly with the periosteal callus (arrowheads), within the cortical bone (arrows), and within the endosteal/marrow space. All images 100X. All digits sectioned at 5 μm, D-F serial sectioned.

Immunohistochemistry of the P2 Amputation and Fracture Woven Bone Callus

We then explored the molecular components of the woven bone callus stage of the P2 amputation and fracture digits. Probing the 24 DPA amputated digit for chondrocytes using the Agc1 antibody shows no staining within the callus region of the digit, but positive signal within the articular cartilage (arrow), indicating the cartilaginous amputation callus has been removed by this time point (Fig. 1.4, A). The 22 DPF fractured digit tests immunopositive for Agc1, displaying a large mass of chondrocytes bridging the fracture gap between the proximal and distal bone fragments (Fig. 1.4, D). Portions of the fracture callus adjacent to the proximal bone fragment do not test immunopositive for Agc1 (Fig. 1.4, D). Importantly, we performed immunostaining probing for osteoblasts on a serial section of the fractured digit, which revealed Osx-positive cells within the fracture callus adjacent to the proximal bone fragment, analogous to the portion that did not test immunopositive for chondrocytes (Fig. 1.4, E). Using a serial section again, we probed for osteoclasts via the CpsK antibody, finding positive cells within the portion of the fracture callus that did not test positive for chondrocytes, but did test positive for osteoblasts, indicating remodeling of the new bone formation (Fig. 1.4, F). Immunostaining for osteoblasts and osteoclasts in the 24 DPA digit revealed a comparatively broader staining region than the fracture callus; the amputation callus as well as distal to the bone stump stained immunopositive for Osx, indicating new bone formation capping the stump, and CpsK immunostaining showed osteoclasts localized to the periosteal boney callus, the cortical bone, and within the endosteal/marrow region (Fig. 1.4, B and C). Overall, our immunostaining shows both

the fracture and amputation calluses are formed via endochondral ossification in a similar spatial orientation.

Elucidation of the Chondrogenic Cell Source (Periosteal Contribution) Post P2 Amputation

Our ultimate goal is to induce regeneration of the adult P2 digit post amputation, yet what cells must be targeted in order to induce regeneration is unclear. Based on earlier work in the regeneration field, and the fact that chondrocytes act as a template for bone formation post bone fracture, chondrocytes may be a great target for induced regeneration of P2 (Yu et al., 2010a; Yu et al., 2012; Gerstenfeld et al., 2003; Schindeler et al., 2008). Our histological and immunohistochemistry results suggest the amputated P2 bone stump chondrocytes may be analogous to the proximal portion of the fractured P2 bone cartilaginous callus, therefore the amputation chondrocytes may be periosteal derived, as suggested post bone fracture (Colnot, 2008). In an effort to determine the periosteal contribution post P2 amputation, we amputated adult mouse digits at the P2 level, immediately pulled back the skin and surrounding soft tissues, and scraped the periosteum off the bone using a scalpel, followed by pulling the skin back in place, and closing the wound with Dermabond. Control digits were treated the same except without periosteal scraping. Digits were tracked over time using the MicroCT and harvested at various time points for histological processing and immunohistochemistry.

At 9DPA, Mallory's staining reveals the control P2 bone stump with periosteum intact is surrounded by chondrocytes on the lateral portions of the bone, yet with a lack of chondrocytes located distally as well as no cartilage within the endosteal/marrow cavity
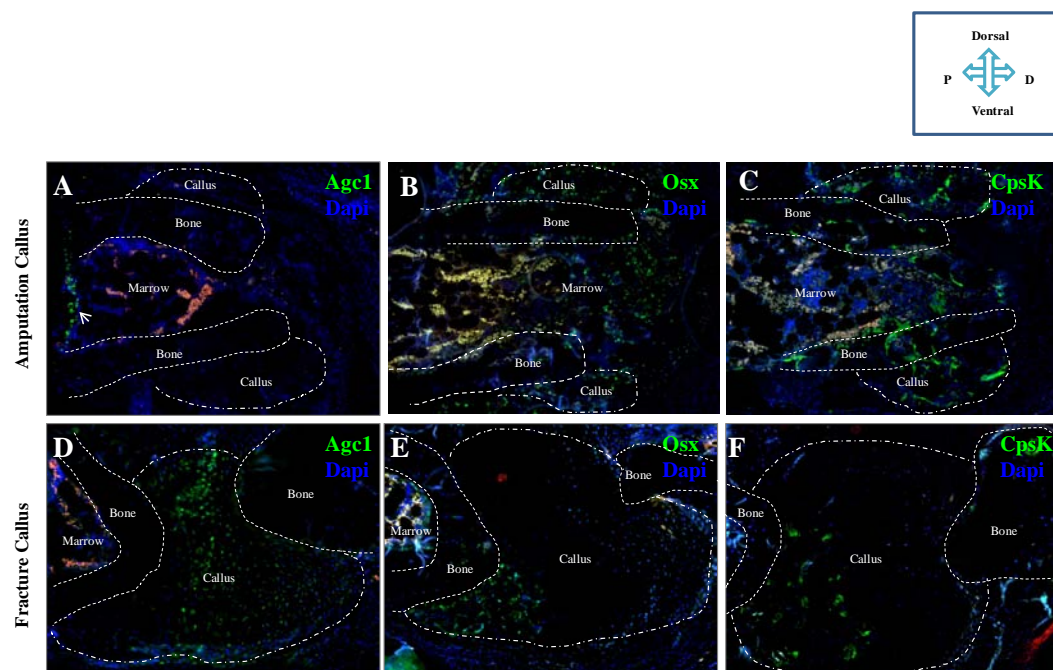
Figure 1.4 – Dawson et al.

Fig. 1.4 Immunohistochemical analysis of the P2 amputation and fracture hard boney callus indicates a similar bone healing response post injury. (A) Agc1 immunohistochemistry shows a lack of chondrocytes within the boney amputation at 24 DPA, yet positive cells within the articular region (arrow). (D) Agc1 immunohistochemistry of the fracture callus at 22 DPF shows a much broader region of cartilaginous staining, with chondrocytes in the fracture space linking the proximal and distal bone fragments. (B) Osx immunohistochemistry confirms the 24 P2 amputation periosteal callus is comprised of osteoblasts, yet also shows staining within the endosteal/marrow region and distal to the bone stump. (E) Osx immunostaining of the 22 DPF callus shows osteoblasts localized to the ventral region of the proximal bone fragment, comparable to region in image D lacking Agc1 immunostaining. (C) CpsK immunostaining shows osteoclasts are present within the amputation periosteal callus, the endosteal/marrow region, and within the cortical bone, indicating extensive bone remodeling. (F) CpsK immunostaining shows osteoclasts are localized to the proximal portion of the fracture callus at 22 DPF, comparable to the region positive for osteoblasts in image E. All images 100X. All digits sectioned at 5 μm, A-C serial sectioned, and D-F serial sectioned.

(Fig 1.5 A). We specifically harvested the 9DPA P2 time point due to the consistent and relatively large amount of chondrogenesis. Importantly, the 9DPA P2 bone stump without the periosteum intact (removed at the time of amputation), lacks the annular cartilaginous growth, however all other portions of the digit remain intact, including the P2 bone itself, the soft fibroblastic connective tissue, the dorsal tendon, the ventral fibrocartilaginous tissue, the marrow compartment, as well as the epithelial tissue (Fig 1.5 E). Furthermore, Toluidine blue staining, which has been shown to target and stain cartilaginous tissue, coincides with the Mallory staining; the periosteum intact digit shows great toluidine blue staining both in the articular cartilage region as well as the cartilaginous callus region on the exterior of the bone, and the periosteum removed tissue lacks a cartilaginous callus surrounding the lateral portions of the bone, while still staining the articular cartilage (thus control cartilaginous staining) (Fig. 1.5 B and F).

Immunohistochemistry was performed to confirm our histological findings whereby in the absence of the P2 periosteum, the cartilaginous callus did not form. We probed the periosteum-intact and periosteum-removed digits for the presence of proliferating chondrocytes, as well as newly formed osteoblasts, with the Collagen 2 (Col2) antibody and the Osx antibody, respectively (Fig 1.5 C, G, D, H). The periosteum-intact digit tested immunopositive for Col2 along the periosteal surface, displaying proliferating chondrocytes localized to the lateral portions of the bone, yet not within the marrow/endosteal compartment nor distal to the bone stump (Fig. 1.5 C). Conversely, the periosteum-removed digit tests immunonegative for Col2 along the periosteal surface, as well as lacking staining within the endosteal/marrow compartment and distal to the bone stump (Fig. 1.5 G).

Literature suggests the periosteum, in addition to yielding chondrocytes, may also give rise to osteoblasts post bone fracture, and in particular, the periosteal-derived osteoblasts encircle the cartilaginous component of the fracture callus, both directly adjacent to the bone surface as well as surrounding the proliferating chondrocytes (Gerstenfeld et al., 2003; Ito et al., 2001; Colnot, 2008). In an effort to determine if bone cells were present in the soft callus post P2 amputation and subsequent periosteum removal, we performed immunohistochemistry for Osx at 9DPA and compared those findings to control digits with the periosteum intact (Fig. 1.5 D and H). The periosteum-intact digits tested immunopositive for Osx both adjacent to the bone surface (arrow), as well as within and surrounding the cartilaginous component of the amputation callus (Fig. 1.5 D). Furthermore, the periosteum-intact digit showed Osx positive cells within the endosteal/marrow region (Fig. 1.5 D). In samples lacking the periosteum, the 9DPA P2 digit tested immunonegative for Osx in the periosteal compartment, yet importantly, tested immunopositive for Osx in the endosteum/marrow cavity (Fig. 1.5 H).

In the absence of the periosteum post P2 amputation, the histological and immunohistochemistry data point to the lack of external callus formation, i.e., the lack of a bone regeneration response. In order to explore this further, we tracked amputated P2 digits with the periosteum intact or the periosteum removed at various time points for changes in form and volume using the MicroCT. Digits lacking periosteum and digits with intact periosteum were scanned beginning at 1 DPA, and weekly thereafter for four weeks total. MicroCT 3-D reconstructed images show no indication of periosteal bone growth in digits with an intact periosteum or digits lacking the periosteum at 1 and 7 DPA (Fig. 1.6, A, B, F, and G). Notably, digits with an intact periosteum show a
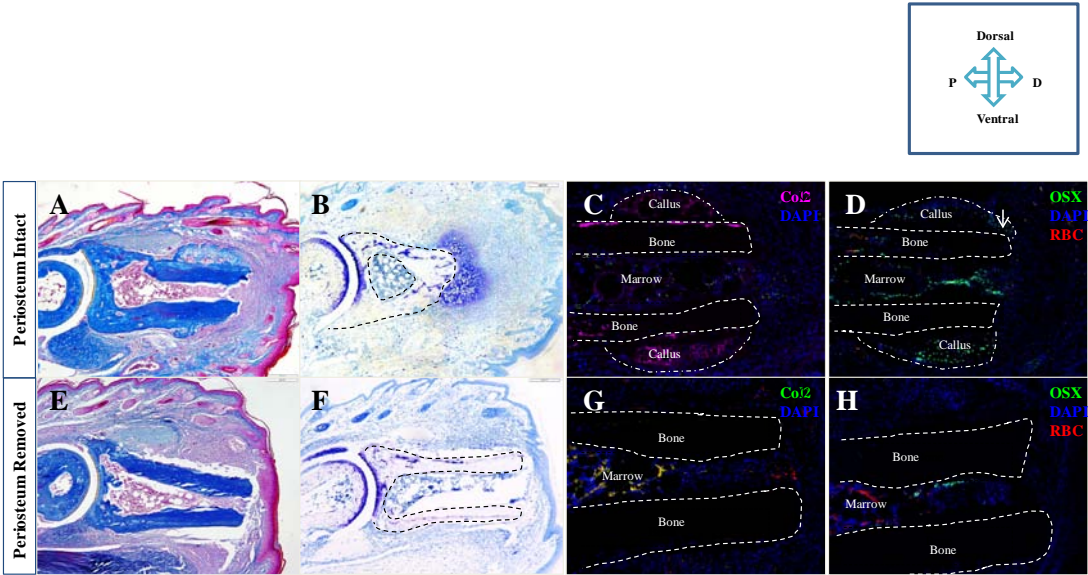
Figure 1.5 – Dawson et al.

Fig. 1.5 Chondrocytes and osteoblasts are not present along the periosteal surface in amputated 9 DPA P2 digits lacking the periosteum. (A and B) Mallory's and Toluidine Blue staining of the amputated P2 bone at 9 DPA with intact periosteum shows cartilaginous growth adjacent to the periosteal surface, not within the endosteal/marrow space or distal to the bone stump. (E and F) Mallory's and Toluidine Blue staining of the amputated P2 bone at 9 DPA with periosteum removed at the time of amputation shows no chondrogenesis adjacent to the periosteum. (C and G) Col2 immunohistochemistry probing for proliferating chondrocytes shows the 9 DPA periosteal amputation callus is comprised of Col2-positive cells in digits with an intact periosteum, yet no Col2 immunostaining is present in 9DPA digits without intact periosteum. (D) Immunostaining for Osx reveals osteoblasts within the 9 DPA amputation periosteal callus and within the endosteal/marrow space of digits with intact periosteum. (H) Osx immunostaining in 9 DPA digits lacking the periosteum shows no positive cells along the periosteal surface, yet positive immunostaining within the endosteal/marrow space. All images 100X. All digits sectioned at 5 μm.

decrease in bone volume at 7 DPA, statistically different from the periosteum-removed

digits (Fig. 1.6, K. $p < 0.05$). By 14 DPA, the digits with an intact periosteum display a

broad band of new bone formation, coinciding with an increase in bone volume, located

along the periosteal surface and proximal to the bone stump (Fig. 1.6, C and K).

Periosteum-removed digits, conversely, showed no new bone formation along the

periosteal surface at 14 DPA and no change in bone volume (Fig. 1.6, H and K). 21 DPA

digits with an intact periosteum showed continued bone growth along the periosteal

surface, while 21 DPA digits lacking the periosteum remained virtually unchanged from

the previous time points (Fig. 1.6, D and I). By the end of our study at 28 DPA,

periosteum-intact digits show signs of continued bone growth and remodeling, evident

from the relative lack of pitting on the bone surface, while 28 DPA periosteum-removed

digits remain unchanged, exhibiting no sign of new bone formation along the periosteal

surface (Fig. 1.6, E and J). In line with the 3-D images, periosteum-intact digits exhibited

increases in bone volume at 21 and 28 DPA, increasing overall to 125% the starting bone

volume, while digits lacking the periosteum showed a slight overall decrease in bone

volume at the end our study, decreasing to approximately 90% the starting bone volume,

with differences in volume between the two groups statistically significant at 21 and 28

DPA (Fig. 1.6, K. $p < 0.05$). Importantly, bone formation still occurred in the

endosteal/marrow region of the digits lacking the periosteum, effectively closing the open

marrow space at the distal bone stump by 3 to 4 weeks post amputation (not shown).

Studies in which we remove the periosteum at the time of P2 amputation hint that

the periosteum is the source of the chondrogenic component of the bone healing

response, however, the periosteal cells could be responsible for recruiting circulating pre-
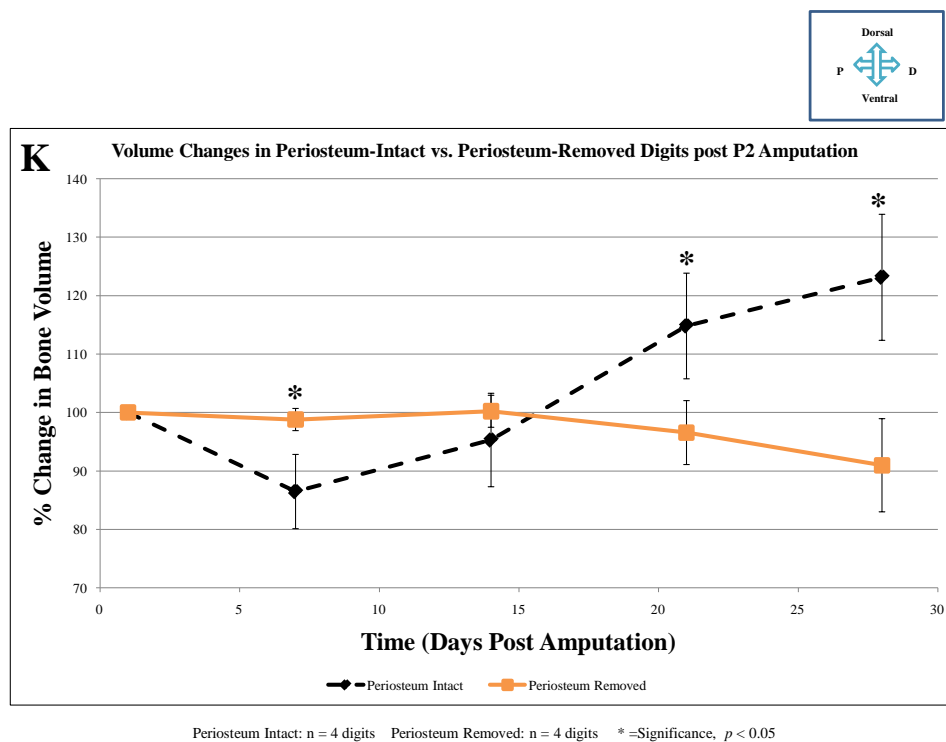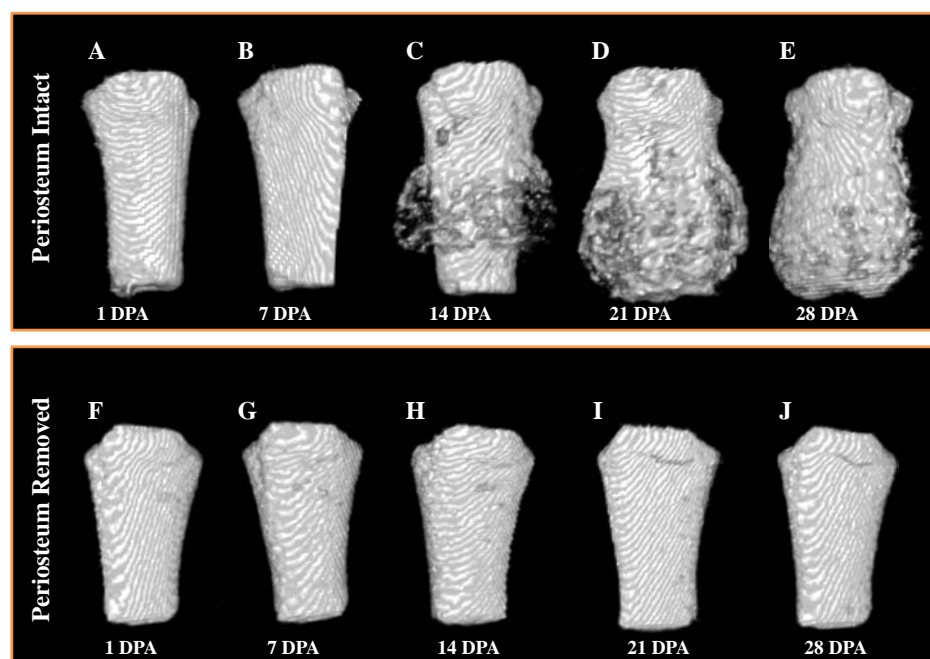
Figure 1.6 – Dawson et al.

Fig. 1.6 Lack of external callus formation in P2 digits without intact-periosteum.
Adult mouse P2 digits were amputated, had their periosteum immediately removed (or left intact for control digits), and tracked using the MicroCT from 1 DPA and weekly thereafter for 4 total weeks, ending at 28 DPA. (A, B, F, G, and K) P2 digits with intact-periosteum or removed-periosteum initially show no growth at 1 and 7 DPA, yet the periosteum-intact digits show a significant decrease in bone volume at 7 DPA compared to digits lacking the periosteum ($p < 0.05$). (C, H, and K) At 14 DPA, digits with intact-periosteum show evidence of a boney callus extending perpendicular to the bone, while periosteum-removed digits show no periosteal growth, yet there are no significant differences in bone volume changes between the two groups ($p < 0.05$). (D, I, and K) By 21 DPA, the boney callus of the periosteum-intact digit has increased substantially in size and appears denser than the previous time point, while the digit lacking the periosteum does not show any boney growth along the periosteal surface, coinciding with the large difference in bone volume changes between the two groups, whereby periosteum-intact digits are increasing in volume, periosteum-removed digits are slightly decreasing ($p < 0.05$, significant). (E and J) At 28 DPA, the digit with intact-periosteum shows signs of bone growth and remodeling, while the digit lacking the periosteum is unchanged from the previous time points. (K) The changes in bone volume between the periosteum-intact digits, increasing overall to approximately 125%, and the digits lacking the periosteum, decreasing overall to roughly 90%, are significantly different from each other by the end of our study at 28 DPA ($p < 0.05$). Student's *t*-test was used to calculate *P* value, bars specify standard error.

chondrogenic cells to the bone stump post amputation injury. In order to definitely establish the chondrogenic cell source post P2 amputation injury, we utilized bone grafting techniques whereby we grafted Actin-GFP labeled P2 bone into the fractured P2 bone environment of unlabeled NOD-SCID mice, and harvested the digits 11 days post grafting and fracture when chondrogenesis is prominent. Importantly, several grafting designs were implemented to trace specific cellular compartments of the bone: 1) as a positive control to trace both the periosteal cellular contribution as well as the endosteal/marrow compartment, we grafted the labeled bone with all compartments intact, 2) to trace solely the periosteal contribution post P2 amputation, we grafted P2 labeled bones with the endosteal/marrow compartment reamed with a sharpened tungsten needle, 3) to trace solely the endosteal/marrow compartment post P2 amputation, we grafted P2 bones with the endosteal/marrow compartment intact, yet with the periosteum removed via stripping the tissue away with a scalpel, and 4) as a control for cortical bone contribution post amputation, we removed the periosteum as well as reamed the endosteal/marrow compartment of the labeled grafted bone.

In order to visualize the effectiveness of the grafting procedure, we harvested tissues and processed them for histological studies. We specifically aimed to visualize if the grafted bone was alive, determined by intact chondrocytes/osteoblasts within their lacunae. At 11 days post grafting and fracture, Mallory's Trichrome staining revealed a large area of new cartilaginous growth (outlined) adjacent to the periosteal surface of the GFP-labeled grafted bone (with the periosteum and endosteum/marrow compartment intact), as well as large cartilaginous callus formation on the proximal and distal portions of the fractured unlabeled host bone (Fig. 1.7, A). Note the absence of cartilaginous

growth within the endosteal/marrow region of the graft, yet the presence of fatty marrow, indicating an intact marrow cavity (Fig. 1.7, A). Histological samples of the labeled graft containing only the periosteum and the cortical bone (with the endosteum/marrow region reamed) also show chondrogenesis adjacent to the periosteal surface of the graft (outlined), and importantly, do not show the presence of a fatty marrow, suggesting the absence of the endosteal/marrow region (Fig. 1.7, B). In samples lacking the periosteum yet with the endosteal/marrow portion intact, no cartilaginous growth was present adjacent to the labeled bone graft, instead, only the host bone showed cartilaginous growth adjacent to the bone surface (Fig. 1.7, C). The labeled graft without periosteum displayed a fatty marrow cavity, indicating the presence of the endosteal/marrow compartment (Fig. 1.7, C). Lastly, histological analysis of the GFP-labeled graft with periosteal and endosteal/marrow compartments removed showed no bone formation along either the periosteal or endosteal/marrow bone surfaces, indicating the cortical bone does not contribute to the P2 amputation injury milieu (not shown).

To explore the periosteal cellular contribution further, we performed immunohistochemistry specifically probing for GFP, to trace the cells of the labeled graft, and Agc1, to determine if the labeled periosteum gave rise to chondrocytes (Fig. 1.8). In samples with the periosteum and endosteal/marrow compartments intact, a large proportion of the cells tested immunopositive for Agc1, indicating the presence of chondrocytes (Fig. 1.8, A). Importantly, the GFP-labeled bone graft displayed a large amount of cells adjacent to the bone in the periosteal region, all of which tested immunopositive for GFP, indicating that the graft was both viable and gave rise to a localized population of cells (Fig. 1.8, B). The merged image reveals a great many cells

A — Periosteum Intact &
Endosteum/Marrow Region Intact

B — Periosteum Intact &
Endosteum/Marrow Region Reamed

C — Periosteum Removed &
Endosteum/Marrow Region Intact

Figure 1.7 – Dawson et al.

Fig. 1.7 Elucidation of the chondrogenic cell source post P2 amputation: Histology of the Actin-GFP labeled P2 bone grafted into the unlabeled host P2 injury milieu. Actin-GFP P2 bone segments (with various bone compartments intact or removed) were grafted into the 0 DPF P2 fracture milieu of NOD-SCID mice, harvested 11 days later, and processed for histology. (A) Mallory's stained section of Actin-GFP bone graft with periosteum and endosteal/marrow region intact shows chondrogenesis along the periosteal surface (outlined) and a fatty marrow. (B) Mallory's stained section of Actin GFP bone graft with periosteum intact and endosteal/marrow region reamed shows cartilaginous growth along the periosteal surface (outlined) and the lack of a fatty marrow. (C) Mallory's stained section of Actin GFP bone graft lacking periosteum, yet with an intact endosteal/marrow region, shows no chondrocytes directly adjacent to the periosteal surface, and the presence of a fatty marrow region. All images 100X. All digits sectioned at 5 μm.

double labeled for GFP and Agc1, showing the presence of periosteal derived chondrogenic cells adjacent to the labeled bone graft (Fig. 1.8, C). Note: 1) that not all GFP-positive cells tested immunopositive for Agc1, indicated a mixed cell population stemming from the labeled bone graft, and 2) that not all Agc1 positive cells tested immunopositive for GFP, indicating the host cellular contribution to the injury environment (Fig. 1.8, C).   No Agc1 positive cells were found within the endosteal/marrow compartment of the graft (not shown). Next, we probed for Agc1 and GFP positive cells in samples with the periosteum intact, yet with the endosteal/marrow compartment reamed (Fig. 1.8, D-F). Many cells tested immunopositive for Agc1, indicating the presence of chondrocytes, and GFP, indicating the presence of labeled-graft derived cells (Fig. 1.8, D and E). When merged, we noted the presence of a large amount of GFP and Agc1 double labeled cells, and as show in image C, not all GFP-positive cells tested positive for Agc1, indicating a mixed graft-derived cellular contribution, and not all Agc1-positive cells were GFP labeled, indicating host-derived chondrocytes (Fig. 1.8, F). Lastly, probing for Agc1-positive cells in the samples lacking the periosteum, yet having the endosteal/marrow compartment intact, reveals a large area of chondrocytes, however a complete lack of chondrocytes associated with the labeled bone graft (Fig. 1.8, G). In line with this, probing for GFP revealed the greatest amount of staining associated with the endosteal/marrow compartment, and several positive cells along the periosteal surface and within the cortical bone (Fig. 1.8, H). Probing for GFP and Agc1 double labeled cells revealed no GFP positive cells were labeled with Agc1, indicating the endosteal/marrow compartment of the labeled bone graft did not give rise to chondrocytes (Fig. 1.8, I).
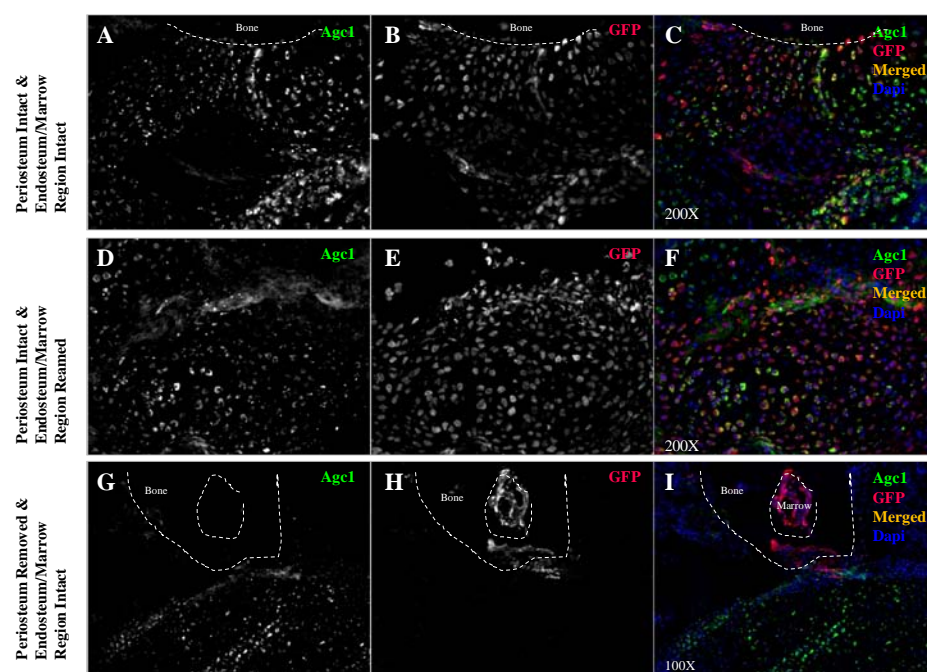
Figure 1.8 – Dawson et al.

Fig. 1.8 Elucidation of the chondrogenic cell source post P2 amputation: Agc1 immunohistochemistry of the Actin-GFP labeled P2 bone grafted into the unlabeled host P2 injury milieu. Actin-GFP P2 bone segments (with various bone compartments intact or removed) were grafted into the 0 DPF P2 fracture milieu of NOD-SCID mice, harvested 11 days later, and processed for immunostaining. (A-C) In grafts with the periosteum and endosteal/marrow region intact, immunostaining for Agc1 shows a large area of chondrocytes adjacent to the bone graft (A), immunostaining for GFP shows many graft-derived cells adjacent to the bone graft (B), and when merged, most GFP-positive cells test immunopositive for Agc1, indicating the GFP bone graft gives rises to chondrocytes. (D-F) In bone grafts with the periosteum intact, yet with the endosteal/marrow region reamed, immunostaining for Agc1-postive chondrocytes (D) and GFP-positive graft derived cells (E) shows most GFP-positive cells are Agc1, indicating that in the absence of the endosteal/marrow region, the periosteum still gives rise to chondrocytes in the P2 injury milieu. (G-I) In bone grafts lacking the periosteum, yet with the endosteal/marrow region intact, immunostaining for Agc1 shows many positive cells, yet no chondrocytes directly associated with the bone graft (A), and accordingly, GFP immunostaining for GFP positive cells associated with the endosteal/marrow region and the cortical bone (H), and when merged, no chondrocytes are double-labeled with GFP, indicating the endosteal/marrow region does not give rise to chondrocytes in the P2 injury milieu. A and B images 200X, C 100X. All digits sectioned at 5 μm.

As previously noted, the periosteum has also been shown to give rise to osteoblasts post long bone fracture (Colnot, 2008). To investigate the periosteal contribution of the amputated P2 bone further, we probed the 11 days post grafting GFP-labeled bone grafts for osteoblasts using the Osx antibody. In grafted samples with both the periosteal and endosteal/marrow compartments intact, we found Osx-positive cells along the endosteal surface of the graft, as well as several cells adjacent to the periosteal surface of the graft (Fig. 1.9, A). The GFP-labeled bone graft displayed a large amount of GFP-positive cells along the periosteal surface of the bone, as well as GFP-positive cells within the endosteal/marrow compartment (Fig. 1.9, B). When probing for both Osx and GFP double labeled cells, not only did we observe double-labeled periosteal cells, we also observed the presence of GFP labeled Osx-positive cells within the endosteal/marrow compartment of the graft (Fig. 1.9, C). We also detected Osx-positive cells not labeled with GFP, indicating host cellular contribution to the injury environment (Fig. 1.9, C, arrow). Next we probed grafted samples with the periosteum intact, yet with the endosteal/marrow compartment reamed (Fig. 1.9, D-F). Osx-positive cells were present throughout the sample, as well as GFP-positive cells (Fig. 1.9, D and E). Importantly, Osx-positive cells were also labeled for GFP, indicating the periosteum of the injured P2 bone gives rise to osteoblasts (Fig. 1.9, F, arrowheads). Lastly, we probed samples lacking the periosteum, yet with the endosteal/marrow compartment intact, for osteoblasts and graft-derived cells (Fig. 1.9, G-I). Osx-positive cells were found not associated with the bone graft, indicating host cellular contribution, and within the endosteal/marrow compartment of the graft (Fig. 1.9, G). Note the relatively small cellular contribution from the graft, with GFP-positive cells predominantly localized to
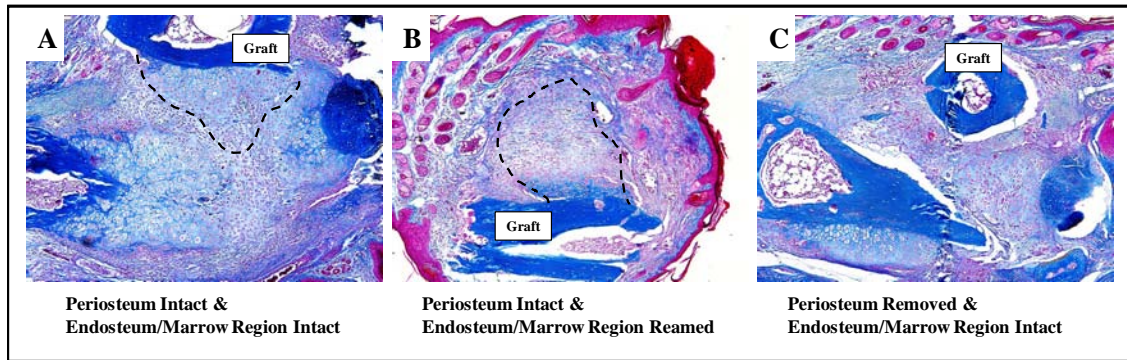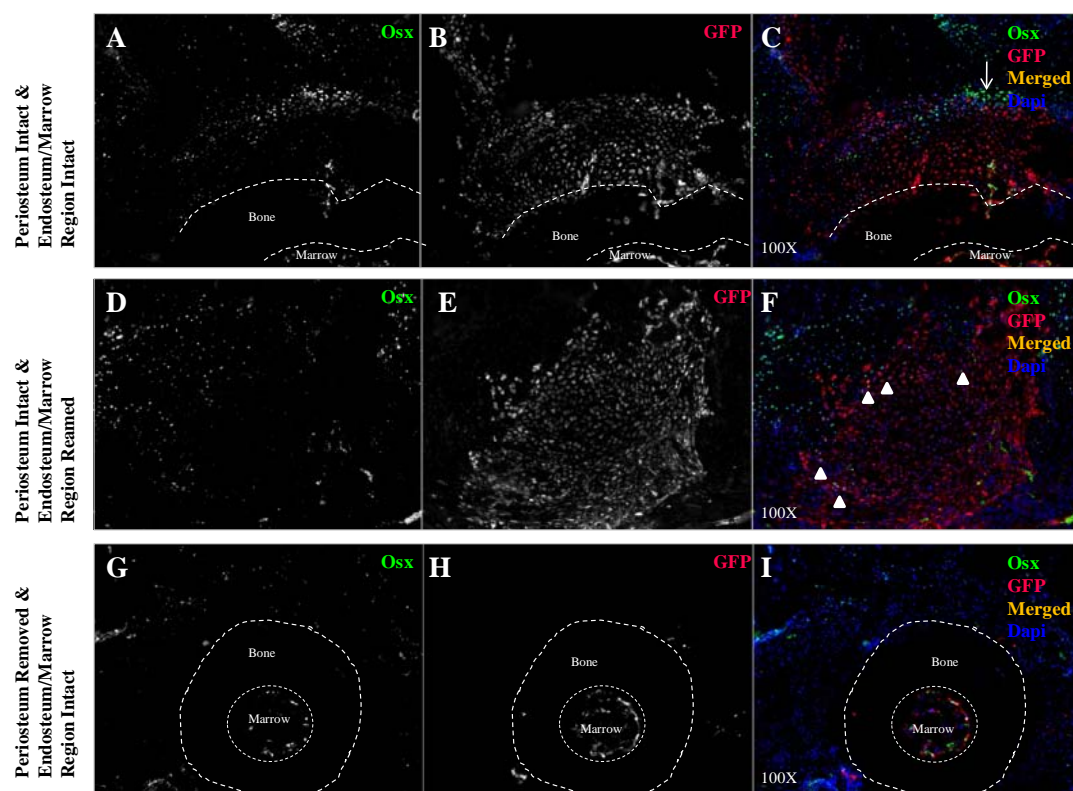
Figure 1.9 – Dawson et al.

Fig. 1.9 Elucidation of the osteogenic cell source post P2 amputation: Osx immunohistochemistry of the Actin-GFP labeled P2 bone grafted into the unlabeled host P2 injury milieu. Actin-GFP P2 bone segments (with various bone compartments intact or removed) were grafted into the 0 DPF P2 fracture milieu of NOD-SCID mice, harvested 11 days later, and processed for immunostaining. (A-C) In bone grafts with the periosteum and endosteal/marrow region intact, immunostaining for Osx shows osteoblasts associated with the grafted bone, including the endosteal/marrow region, and throughout the sample (A), while GFP immunostaining reveals a much broader staining pattern (B), and double labeling of Osx-GFP shows several double positive cells within the endosteal/marrow region, and several within the periosteal compartment (C). (D-F) In grafts with intact periosteum and reamed endosteal/marrow region, Osx positive cells where found within the injury milieu (D), yet a much broader region of GFP-positive were cells present (E), and double-labeling of the cells showed several GFP-positive osteoblasts stemming from the periosteum of the graft (arrowheads indicate areas of several cells each) (F). (G-I) In grafts lacking the periosteum, yet with intact endosteal/marrow region, Osx immunostaining is present through the sample, including the endosteal/marrow region of the graft (G), while GFP-positive cells are predominantly localized to endosteal/marrow region of the graft (H), and when merged, Osx-GFP-double-labeled cells are localized to the endosteal/marrow region of the bone graft, not the periosteum (I). All images 100X. All digits sectioned at 5 μm.

the endosteal/marrow region (Fig. 1.9, H). When probing for Osx and GFP double labeled cells, we observed double-positive cells lining the endosteal surface of the bone (Fig. 1.9, I).

IV. Discussion

Earlier studies have shown the P2 digit does not undergo regeneration post amputation, instead, it results in scar formation without elongation of the bone stump (Neufeld and Zhao, 1993; Yu et al., 2012). However, it has been demonstrated that the neonate P2 bone is capable of induced regeneration post BMP2 treatment, and importantly, the induced bone elongation is mediated via a cartilaginous intermediate (Yu et al., 2012). Furthermore, the same study showed the amputated adult mouse hindlimb undergoes BMP2-induced regeneration, again through endochondral ossification, suggesting similar cartilaginous regeneration methods are utilized between long bones (Yu et al., 2012). In line with this, it has been established that long bone fracture healing predominantly occurs via endochondral ossification (Einhorn, 2005). Due to the cartilaginous response acting as the predominant mediator of induced regeneration, we used the adult mouse P2 digit as a model to further study the endogenous cartilaginous healing response post long bone amputation injuries. In particular, we focused on the potential link between the cartilaginous response of P2 fracture healing and the cartilaginous response post P2 amputation.

Our histological and immunological data indicates definite similarities between the cartilaginous and osteogenic components of the fracture healing response of P2 and the bone healing response post amputation of P2. Here, we show the amputated bone

healing response of P2 is analogous to one-half of the fracture healing response, i.e., the P2 amputation response represents the proximal fragment of the fractured P2 bone. Our data reveal that post fracture of P2, and following the initial inflammatory response, an annular chondrogenic callus forms along the periosteal surface of the bone adjacent to the fracture gap. Published reports confirm the presence of cartilaginous callus formation post long bone fracture, indicating the cartilaginous response of the fractured P2 bone does not differ from that of other long bones (Shapiro, 2008; Ferguson et al., 1999; Vortkamp et al., 1998; Thompson et al., 2001; Colnot, 2008; Einhorn, 2005). Similarly, the amputated P2 bone stump also undergoes an initial inflammatory response and subsequent chondrogenesis along the periosteal surface in an annular fashion, suggesting a comparable healing mechanism to the fracture event. Both models display robust chondrogenesis positive for Aggrecan within the soft callus adjacent to the periosteal surface. In agreement with the literature, chondrocytes are found preferentially on the periosteal surface, not within the endosteal/marrow region (Gerstenfeld et al., 2003; Colnot, 2009). The fracture cartilaginous callus extends beyond the gap in order to bridge the fragments, while the amputation callus is relatively unpatterned and very rarely extends beyond the amputation plane, instead extending perpendicular to the bone. Earlier studies utilizing in-vitro methods suggest the periosteum supplies chondrocytes to the fracture callus in a specific organization (Ito et al., 2001). In line with this, both the cartilaginous callus of the P2 amputation and fracture response are organized whereby the less differentiated cells are adjacent to the fibrous layer of the periosteum, and the cells undergoing hypertrophy are neighboring the bone surface, thus providing evidence the

cells along the periosteum are behaving similarly between the amputation and fracture models.

Following long bone fracture and cartilaginous callus formation, the mineralized callus is replaced with woven bone through the actions of osteoblasts and osteoclasts, complete with marrow formation (Shapiro, 2008; Schindeler et al., 2008). Here, we show the P2 fracture and amputation cartilaginous calluses undergo remodeling into a woven bone structure, evident in both models by 15 days post injury. Our immunohistochemical data reveals the cartilaginous matrix is remodeled via osteoclasts in both the amputation and fracture models, concomitant with new bone formation, ultimately forming the boney callus. Overlapping with the woven bone callus, the P2 fracture callus remains chondrogenic considerably longer than the amputation callus, presumably due to the instability of the fracture milieu, thus creating an environment in which chondrogenesis is favored (Shapiro, 2008). While the chondrogenesis timeline between the P2 amputation and fracture models may differ, the spatial organization of the cells and the equivalent sequential remodeling of the chondrogenic component into a boney callus provides evidence the two models are comparable. Our histological sections indicate further analogies in that the P2 amputation and fracture woven callus is remodeled into a lamellar structure, ultimately completing the healing process.

Our model focuses predominantly on the chondrogenic component of the amputation and fracture callus, due to the potential of modulating the chondrogenic callus to create a patterned template for bone formation during bone regeneration (Yu et al., 2012). In order to manipulate the non-regenerative P2 bone response into a potentially regenerating system, it is essential to determine what cells, and their origin, to target for

the induced-regeneration response. Previous studies suggest chondrocytes arise from the cambium layer of the periosteal compartment post long bone injury (Ito et al., 2001; Dwek, 2010; Colnot, 2009; Tsuji et al., 2006). Indeed, successful fracture healing is dependent upon the periosteal response adjacent to the fracture gap (Einhorn, 2005; Tsuji et al., 2006; Wang et al., 2011). The initial periosteal cell proliferation, essential for sustained BMP production, and the subsequent cartilaginous bridging of the fracture gap, are integral to rebuilding the bone to its pre-fracture strength and morphology (Al-Aql et al., 2008; Einhorn, 2005; Tsuji et al., 2006; Wang et al., 2011).

Here, we report for the first time that the periosteal derived cells of the amputated P2 bone contribute almost exclusively to the external cartilaginous callus, parallel to what has been discovered in mouse long bone fracture healing (Colnot, 2009). In the absence of the local periosteum, the formation of the P2 amputation cartilaginous callus is not delayed; instead, it will not form, thus suggesting that non-local periosteal and non-periosteal tissues will not compensate for the loss of the local periosteum. While removal of the periosteum and subsequent inhibition of callus development suggests the periosteum is the source of the cells which give rise to the callus, this experimental design does not definitively determine cell source. In particular, it does not control for periosteal derived cells playing a role in the recruitment of chondrogenic cells to the amputation site. In order to track periosteal cell fate post P2 amputation, we utilized eGFP-labeled bone grafting techniques, probing for labeled chondrocytes using immunohistochemistry. Labeled bone grafts either contained an intact periosteum and endosteal/marrow region, to trace all bone components in the injury milieu, intact periosteum with endosteal/marrow region removed, to trace solely the periosteal

contribution, bone grafts lacking the periosteal tissue yet with an intact endosteal/marrow region, to trace solely the cellular contribution of the endosteal/marrow region, and bone grafts lacking both the periosteum and the endosteal/marrow, to control for cortical bone contribution in the P2 injury milieu. In labeled-bone grafts with periosteum and endosteal/marrow region intact, the graft showed GFP positive chondrocytes adjacent to the periosteal surface, yet not within the marrow cavity. In labeled-bone grafts with intact periosteum, yet with the endosteal/marrow region removed, we again found GFP-labeled chondrocytes adjacent to the periosteal surface, not within the endosteal/marrow region. Conversely, in grafts lacking the periosteum, yet with an intact endosteal/marrow region, the bone grafts did not exhibit any GFP-positive chondrocytes, nor did they exhibit any positive cartilaginous staining within the endosteal/marrow region. Lastly, in grafts with the periosteum and the endosteal/marrow regions removed, we observed no cartilaginous growth on the bone surface. Taken together, the cell tracing data suggests the local P2 periosteum gives rise to chondrocytes in the P2 injury milieu, with or without the presence of an intact endosteal/marrow region, and the endosteal/marrow-derived cells do not have the potential to form chondrocytes in the P2 injury milieu. Thus, the chondrogenic component post P2 amputation, analogous to fracture repair, is periosteal derived.

In the absence of the periosteum, not only did the chondrogenic callus not form, the boney amputation callus of the P2 stump did not form, and likewise, the overall bone volume decreased post amputation. Regeneration of bone, as opposed to bone repair, has been described as an increase in bone volume (Al-Aql et al., 2008). Therefore, while the P2 bone does not grow in length post amputation, and lacks lateral patterning, the lateral

bone growth which results in an increase in bone volume can be thought of as an attempted regeneration response. In line with this, in the absence of the periosteal-derived cells, the P2 bone regeneration attempt is inhibited, suggesting the periosteal-derived cells are essential for the P2 bone regeneration response. Our data suggests that since the boney callus did not form in the absence of the periosteum, non-local periosteal cells and marrow derived cells do not compensate for the periosteum in its absence. An earlier in-vivo study, using GFP-positive marrow cells transplanted into wild type mice, proposed that marrow derived cells migrate outside the medullary cavity and ultimately comprise the boney callus along the periosteal surface post bone injury (Taguchi et al., 2005). In correlation with others, our GFP labeled bone grafting studies indicated the periosteal tissue could indeed form osteoblasts, yet our grafting studies were not carried out long enough to determine if the entire boney callus would be comprised of graft-derived cells, thus further studies must be performed to definitely elucidate the source of the periosteal boney callus post P2 amputation (Colnot, 2009)

While our studies do not show endosteal/marrow derived cells contributing to the external callus post P2 amputation, our work instead suggests that local endosteal/marrow derived cells contribute to the local medullary callus. At the time of P2 amputation, the endosteal surface and within the marrow cavity tests immunopositive for osteoblasts, however, our histological and immunological data shows that intramembranous bone formation is not occurring within the marrow space prior to amputation. In this way, our data suggests medullary intramembranous bone formation occurs post amputation, much like how it occurs in the medullary cavity post bone fracture (Einhorn, 2005; Colnot, 2008; Shapiro, 2008; Merloz, 2011). Using in vivo GFP grafting techniques, we found

GFP/Osx double positive cells within the endosteal/marrow space of the GFP-positive bone graft. Importantly, the periosteum was removed in these samples at the time of amputation, suggesting the periosteum did not give rise to the medullary callus, conversely, the endosteum/marrow cavity served as the cellular origin. Additionally, the lack of periosteal tissue, yet presence of medullary callus, demonstrates that the medullary callus would not compensate for the periosteum in its absence. Indeed, it is thought that the endosteal/marrow cavity and the periosteal tissue house distinct populations of stem cells, and they are not necessarily interchangeable (Colnot, 2009). Grafting studies, in which the periosteal portion of the bone is inverted, therefore oriented toward the marrow space, report that chondrocytes and osteoblasts still form along the periosteal surface post bone injury, indicating the marrow does not inhibit chondrogenesis, and that the periosteum can give rise to osteoblasts and chondrocytes in other environments (Colnot, 2009). Likewise, grafting studies in which the endosteal/marrow portion of the bone is oriented toward the periosteal surface post bone injury show that endosteal/marrow derived cells do not form cartilage in this environment, instead they form bone through intramembranous ossification (Colnot, 2009). These findings suggest that the cell populations within the periosteum and endosteal/marrow cavity are distinct from one another, therefore lending support to our findings of endosteal/marrow derived cells not compensating for periosteal tissue in its absence (Colnot, 2009).

Overall, our studies show the bone healing response, in particular the chondrogenic component, following amputation of the adult mouse P2 bone is analogous to the fracture healing response of P2 and other long bones of the body. Therefore, the

vast amount of progress in the fracture healing field may be translated to long bone amputation studies, thus enhancing regeneration studies with techniques and ideas not previously considered. Our work is proof of that concept, in that recent fracture healing studies have shown the periosteum to predominantly contribute to the chondrogenic component of the fracture callus, and we have shown the P2 periosteum is essential for, and gives rise to, the chondrogenic callus post P2 amputation. Earlier reports characterizing the BMP-induced-regeneration response have shown the necessity for a cartilaginous template to precede the regeneration of bone following the amputation of digit tips and long bones at regeneration-incompetent levels, therefore, determining the source of the endogenous chondrogenic component post amputation may help enable us to better target and enhance future regeneration studies (Yu et al., 2010; Yu et al., 2012).

Chapter Two: Optimization and Characterization of BMP2-Induced

Regeneration of the Adult Mouse Amputated Middle Phalanx

I.   Introduction

As demonstrated in Chapter One, the unpatterned bone healing response post adult mouse middle phalanx (P2) amputation is analogous to one half of the non-stabilized fracture healing response, i.e., the amputated P2 bone represents the proximal portion, relative to the fracture gap, of the long bone fracture. Due to the similarities between the healing response of the amputated and fractured P2 bone, we may gain additional insight by investigating the vast array of fracture healing literature with the specific intent to induce regeneration of the amputated P2 bone.   In particular, investigating the previously reported affects of exogenous BMP2 application post long bone fracture, and applying those findings to the P2 amputation response. Importantly, BMP2 and 7 have shown great potential for bone regeneration following the amputation of mouse digits (Han et al., 2003; Yu et al., 2010; Yu et al., 2012). An earlier study of fetal mouse digit tip regeneration showed BMP signaling is essential for a successful regeneration response following amputation (Han et al., 2003). Studies have shown that post amputation of the proximal portion of the distal phalanx (P3), BMP2 and 7 induce regeneration of the digit, and interestingly, the regeneration response occurs via

endochondral ossification, thus differing from the intramembranous ossification of endogenous P3 regeneration (Yu et al., 2010; Han et al., 2008). BMP2 has also been determined to induce regeneration of the amputated P2 stump in neonatal studies, characterized by the accumulation of BMP2-responsive proliferating mesenchymal cells adjacent to the BMP2 source, and the subsequent formation of an endochondral ossification center consisting of proliferating and hypertrophic chondrocytes (Yu et al., 2012). The BMP2-induced endochondral center is further replaced by bone, resulting in a P2 digit comprised of non-ectopic bone and 88% the length of an unamputated P2 digit at a similar developmental stage (Yu et al., 2012). Furthermore, this study demonstrated the effectiveness of exogenous BMP2 treatment on adult tissues post amputation, specifically the adult mouse hindlimb, showing greater distal elongation of the amputated limb stump relative to controls, as well as the formation of an endochondral ossification center (Yu et al., 2012). Thus, it is intuitive that we integrate the fields of fracture healing and regeneration, and specifically BMP2-involvement in both, to aid our efforts in regeneration of limbs post amputation injury.

BMPs, members of the transforming growth factor β (TGF-β) super family of signaling molecules, have long been known to play crucial roles in ectopic bone formation (Urist, 1965), and more recently shown to be critical mediators of chondrocyte condensation, proliferation, and survival during bone development (Rosen, 2009). Studies in which mice exhibit limb specific deletion of BMP2 demonstrate that the growth factor is not essential for the development of long bones (Tsuji et al., 2006). It is thought that other BMPs present within the growing limbs compensate for the loss of BMP2; these mice exhibited normal skeletal-limb-patterning, as well as proper

endochondral ossification of the limb bones (Tsuji et al., 2006). On the other hand, as the mice lacking limb BMP2 aged, they experienced multiple spontaneous fractures of the long bones, and importantly, the fractures did not undergo proper healing (Tsuji et al., 2006). Post femoral fracture, mice with limbs deficient in BMP2 lacked periosteal cell proliferation, i.e. periosteal-derived chondrogenesis and osteogenesis, and subsequently lacked the maintenance of BMP 2, 4, and 7 expression in the periosteal compartment, resulting in the complete absence of cartilaginous soft callus formation and non-union of the bone segments (Tsuji et al., 2006; Wang et al., 2011). The periosteum is the cell rich outer covering of the bones, enveloping all non-articular bone surfaces, and has been shown to give rise to the chondrocytes comprising both the long bone fracture and P2 amputation calluses (Colnot, 2009; Dwek, 2010; Chapter One). Recent studies suggest that periosteal-cell-derived BMP2 initiates the healing response of long bones post fracture, and is required for mesenchymal cell differentiation into cartilage and bone during fracture healing (Wang et al., 2011). In line with this, studies tracking the mRNA expression of *BMP2* over the course of fracture repair report an initial spike in expression 1 day post fracture, with high expression levels maintained over the duration of the inflammatory response (Cho et al., 2002). While the expression levels of BMP2 do decrease post inflammation, moderately high levels of *BMP2* mRNA remain constant over the course of the cartilaginous response, woven bone formation, and secondary bone remodeling (Cho et al., 2002). Later studies revealed the immunolocalization of BMP2 differed with respect to the mRNA expression domains during unstabilized fracture repair, i.e. the inflammation stage exhibited weak BMP2 immunostaining, whereas the cartilaginous and woven bone callus stages displayed relatively high levels of BMP2 (Yu

et al., 2010b). Of particular importance to our P2 model, the proliferating, prehypertrophic, and hypertrophic chondrocytes of the fracture callus tested immunopositive for the BMP effectors pSmad 1/5/8 (Yu et al., 2010b). The foremost study using BMP2 in fracture healing indicated exogenous BMP2 increased the size and volume of the periosteal boney callus post goat tibial fracture (Welch et al., 1998). Recent fracture healing data in the mouse has revealed that exogenous BMP2 acts specifically on periosteal-derived cells, not endosteal-marrow-derived cells, to undergo chondrogenesis (Yu et al., 2010a, Minear et al., 2010). Instead, endosteal/marrow-derived cells respond to exogenous BMP2 application in conflicting ways; either via intramembranous bone formation (Yu et al., 2010a) or no bone formation at all (Minear et al., 2010). Taken together, endogenous BMP2 function is essential for successful fracture healing, and exogenous application of BMP2 may particularly target periosteal-derived cells to undergo chondrogenesis. However, until now, whether BMP2 targets the periosteal derived cells of the amputated adult mouse P2 bone to undergo chondrogenesis and ultimately induce regeneration of the digit has not been investigated.

Importantly, studies using BMP2 have not all shown consistent or beneficial results. Using a standardized bone growth technique in rabbits, it was shown that after addition of various concentrations of BMP2, there was an overall decrease in new bone formation vs. controls (Jeppsson and Aspenberg, 1996). Interestingly, the same BMP2 sample was shown to be effective in inducing bone formation in rats, indicating potential animal model-related differences (Jeppsson and Aspenberg, 1996). Furthermore, animal models utilizing BMP2 and 7 do not necessarily translate to human fracture models; while deleterious effects may not occur, more often than not, the effects are not

statistically different from traditional healing interventions in humans (e.g. autologous bone grafting and intramedullary nailing) (Gautschi et al., 2007). Large scale human fracture healing studies have shown, however, statistically significant differences in the speed of wound healing and less infections in fractures treated with standard care and BMP2 vs. standard care alone (Govender, et al., 2002). Due to the possibility for inconsistent or deleterious effects of the bone healing response post BMP2 treatment, further studies are warranted to ensure the best possible outcomes.

Here, we use the adult mouse amputated P2 digit as a model system to investigate the temporal response and cellular contribution to BMP2-induced bone regeneration. We hypothesized that the BMP2-induced endochondral regeneration response of P2 specifically targets periosteal derived cells to create a chondrogenic template for bone formation. In our investigation, not only did we discover the predominant cellular contribution to the cartilaginous template, but we also discovered that BMP2 treatment has specific temporal responses within the amputated P2 stump. Here, we show for the first time, that BMP2 treatment can consistently hinder, induce, or have no effect on bone growth of the amputated P2 digit, all of which evidence suggests is dependent on the timing of treatment. Furthermore, through optimization of temporal BMP2 application in the P2 digit stump, we report BMP2 treatment can consistently induce the regeneration of relatively new amputation injuries, but more importantly, older amputation injuries can be modified to respond to BMP2 treatment and undergo distal bone elongation.

II. Materials and Methods

Mice, P2 amputation

C57Bl/6 and CD-1 wild-type mice were purchased from Jackson Labs. P2 amputations were carried out on hind limb digits two and four of 8 to 12-week-old adult female mice. Mice were anesthetized using Isofluorane, with an initial dose of 3% Isofluorane, and maintained at 2% Isofluorane. P2 amputations were performed using a scalpel to sever the digit at approximately the second ventral fat pad indent and allowed to heal on their own. All animal use and procedures were in compliance with Tulane University's Institutional Animal Care and Use Committee.

Treatment Groups (BMP2 and BSA sol-gel treatment, periosteum removal, and re-amputation)

Various combinations of P2 amputation(s) and BMP2 or BSA treatment were performed in this study.

The 8 DPA BMP2/BSA treatment group consisted of digits amputated at the P2 level, followed by allowing the digits to heal for 8 days. At 8 days post amputation (DPA), mice were anesthetized once more and received either 0.500µg/µl BMP2 sol-gel or 0.1% BSA sol-gel treatment. As a delivery system for BMP2 and BSA, we used a sol-gel derived carrier. We added BMP2 or BSA to the room temperature sol-gel solution as previously described (Santos et al., 1999). The sol-gel containing BMP2 or BSA was allowed to air-dry several hours, and subsequently stored at -20 degrees until used. To implant the sol-gel, micro-scissors were used to create a small space within the distal portion of the digit (between the bone stump and wound epidermis or scab), the sol-gel was implanted within the space, and the wound was closed using Dermabond.

The 9 DPA BMP2/BSA treatment group consisted of digits amputated at the P2 level, followed by allowing the digits to heal for 9 days. At 9 DPA, mice were anesthetized once more and received either 0.500μg/μl BMP2 sol-gel or 0.1% BSA sol-gel treatment, with the same implantation method as outline above.

The second 9 DPA BMP2/BSA treatment group consisted of digits amputated at the P2 level followed by removal of the periosteum at the time of amputation. P2 digits were amputated, and the skin and surrounding soft tissues were pulled back, thus exposing the bone, and the periosteum was stripped off the bone surface using a scalpel. The soft tissues and skin were pulled forward, and the distal wound was closed with Dermabond. The periosteum removed digits were allowed to heal for 9 days. At 9 DPA, mice were anesthetized once more and received either 0.500μg/μl BMP2 sol-gel or 0.1% BSA sol-gel treatment, with the same implantation method as outline above.

The 24 DPA BMP2/BSA treatment group consisted of digits amputated at the P2 level, followed by allowing the digits to heal for 24 days. At 24 DPA, mice were anesthetized once more and received either 0.500μg/μl BMP2 sol-gel or 0.1% BSA sol-gel treatment, with the same implantation method as outline above.

The 24 DPA/Re-amputated 9 DPA BMP2/BSA treatment group consisted of digits amputated at the P2 level, followed by allowing the digits to heal for 24 days. At 24 DPA, mice were anesthetized again and the P2 digits were re-amputated, removing the distal portion of the digit tip (the fibrous scar) and the very tip of the bone, thus exposing the marrow cavity. At 9 days post re-amputation, mice were anesthetized once more and received either 0.500μg/μl BMP2 sol-gel or 0.1% BSA sol-gel treatment, with the same implantation method as outline above

The 21 weeks post amputation (WPA)/Re-amputated 9 DPA BMP2/BSA treatment group consisted of digits amputated at the P2 level, followed by allowing the digits to heal for 21 weeks (5 months). At 21 WPA, mice were anesthetized again and the P2 digits were re-amputated, removing the distal portion of the digit tip (the fibrous scar) and the very tip of the bone, thus exposing the marrow cavity. At 9 days post re-amputation, mice were anesthetized once more and received either 0.500μg/μl BMP2 sol-gel or 0.1% BSA sol-gel treatment, with the same implantation method as outline above

Histological Staining

BMP2-treated and BSA-control digits were collected at various time points and fixed from 24-96 hours in Z-fix (Anatech, LTD) at room temperature. Digits were then decalcified using Decalcifier I (Surgipath) overnight, and no more than 24 hours. Digits were processed using a graded ethanol series, xylenes, and immersed in paraffin wax. Digits embedded in paraffin wax were sectioned at 5 μm thickness. In order to analyze the whole digit, digits were sectioned completely, and serial sections were created. Mallory's Trichrome staining was performed to determine the relative amounts of regenerated cartilage and bone formation. In order to visualize woven and lamellar bone, Picro Sirius Red staining was performed. All samples were imaged using the Olympus DP72 microscope using DP2-BSW software.

Antibodies and Immunohistochemistry

Digits were harvested and treated as described in Histological Staining. Slides were incubated at 60 degrees Celsius for 45 minutes, followed by a 15 minute-96 hour

incubation at 37 degrees Celsius. Antigen retrieval was performed using Proteinase K solution (Dako) and incubated at either room temp for 12 minutes, or heat retrieval performed in 1X citrate buffer solution (Dako). Slides were blocked using Protein Block for 30 minutes to 1 hour (Dako). Slides were incubated with primary antibody/antibodies over night at 4 degrees, washed in TBST solution and incubated in secondary antibody/antibodies for 45 minutes at room temperature. Slides were subsequently incubated in DAPI solution, dried, and mounted with Prolong Gold (Invitrogen). Primary antibodies used include Mouse-Anti Collagen Type II (Acris) at a 1:200 concentration and Proteinase K retrieval at room temp, Rabbit-Anti Osterix, SP7 (Abcam) at a 1:400 concentration and heat retrieval, Rabbit-Anti Cathepsin K at a 1:100 concentration and heat retrieval, and Rabbit-anti-Aggrecan (Millipre) at a 1:300 concentration using heat retrieval. Secondary antibodies used include Goat-Anti Rabbit 488 (Invitrogen), Goat-Anti Rat 568 (Invitrogen), Goat-Anti Mouse 647 (Invitrogen), Goat-Anti Mouse 488 (Invitrogen), all at 1:500 concentration in antibody diluent (Invitrogen). All samples were imaged using the Olympus BX61 microscope, with the Slidebook software.

Microtomography Scans & Fiji

P2 digits were scanned from one day post amputation or BMP2/BSA treatment, and weekly thereafter for up to 8 weeks using the vivaCT 40 (SCANCO Medical, Wayne, PA) as described previously (Fernando, et al., 2011). Digits were scanned at 10.5μm voxel size and Energy 45 kVp and saved as dicom files. Using the boneJ Fiji plugin, 3-D reconstructed images were created in which bone volume, length, width, and relative bone thickness were measured.

III. Results

MicroCT studies reveal BMP2 implanted at 8 DPA decreases P2 bone length vs BSA controls

Our earlier studies have demonstrated the important link between the chondrogenic component of the P2 bone healing response post amputation and the fracture healing response of long bones. In particular, we showed the chondrocytes of the injured P2 bone are predominantly derived from the periosteum of the local environment. Furthermore, our lab has also shown the BMP-induced-regeneration response of the amputated neonate P3, P2, and adult mouse hindlimb occurs via a cartilaginous template, thus patterning the bone healing response (Yu et al., 2010; Yu et al., 2012). Significantly, it has been demonstrated in mouse long bone fracture healing studies that exogenous BMP2 targets periosteal cells preferentially to undergo an endochondral response (Yu et al., 2010a). Our previous unpublished studies using BMP2 to induce regeneration of the amputated adult P2 digit suggested an increase in bone length post growth factor application, yet quantification of the previous studies were not preformed. To explore this further, our initial efforts to induce regeneration of the amputated adult mouse P2 bone included implantation of 0.500 μg/μl BMP2 sol-gel into the distal digit tip of 8 DPA digits and tracking changes in bone volume, length, and width via the MicroCT.   Control digits received sol-gel implants containing 0.1% BSA at 8 DPA. Digits were scanned one day post treatment and weekly thereafter for 4 weeks total. We chose to treat digits with BMP2 or BSA at 8 DPA due to the presence of cartilage along the periosteal surface. We implanted the sol-gel under the distal wound scab or wound epidermis of the P2 bone. Importantly, not all P2 digits had undergone complete wound

closure by 8 DPA, instead, of the four 8 DPA digits harvested and assayed for wound closure, 50% still contained the scab without the underlying epidermis capping the distal bone stump (not shown).

MicroCT 3-D reconstructions at 1 day post implantation (DPI) reveal BMP2-treated digits (n = 8) do not show an initial difference in length vs. BSA-treated control digits (n = 4) (Fig. 2.1, A). The BMP2-treated digit shows signs of remodeling compared to the BSA control digit, evident from the open marrow space, yet this response was not consistent between samples at this time point. The 8DPI BMP2-treated digits display a large decrease in bone length compared to BSA control digits (arrowheads, amputation plane indicated by blue line), with an average statistically significant decrease of approximately 73% the initial bone length (Fig. 2.1, K. $p < 0.005$), corresponding to a lack of increase in the bone volume compared to BSA treated control digits (Fig. 2.1, L. $p < 0.05$). The increase in bone volume in BSA treated samples at 8DPI corresponds to the formation of an external boney callus, indicating active bone growth along the periosteal surface (Fig. 2.1, D and L). Note the extensive new boney growth along the periosteal surface of the BMP2-treated digit, yet the lack of bone volume change, suggesting the amount of new bone growth was equivalent to the amount of bone loss (i.e., bone loss due to the decrease in length) (Fig. 2.1, B and L). At 15DPI, the BMP2-treated digit has not shown a substantial increase in bone length, increasing an average 7% from the week prior, to approximately 80% the initial bone length (Fig. 2.1, K), yet the BMP2-treated samples show no statistically significant differences in bone volume compared to BSA-treated digits, indicating an equivalent amount of bone growth between the two groups (Fig. 2.1, L. $p < 0.05$). The 3-D reconstructions and the graphical data of the BSA-treated

samples show the changes in bone length have been minimal to none from 1-15DPI (Fig. 2.1, F-H, and K). The graphical data does show an average increase in bone width in BMP2-treated digits compared to BSA-treated digits, statistically significant at 15DPI only (Fig. 2.1, M. $p < 0.05$), indicating greater periosteal lateral expansion in BMP2-treated samples. The 3-D reconstructions of both the BMP2 and BSA-treated samples at 22 and 28 DPI show the bone is less trabecular than earlier time points, evident from a more uniform appearance (Fig. 2.1, D and I). At both 22 and 28 DPI, no average change in length since the previous time point is evident from the graphical data in the BMP2-treated samples; however the overall bone length remains less than BSA-treated digits (Fig. 2.1, K). Note the volumes of both groups are similar at 22 and 28 DPI, with an overall percent change of approximately 175% the initial starting bone volume (Fig. 2.1, L). The graphical data also indicates the average bone widths between the two groups are not statistically significantly different (presumably due to variability between digits), yet the trend of the BMP2-treated digits suggests the digits are wider than the BSA control group (Fig. 2.1, M. $p < 0.05$). Taken together, MicroCT data shows BMP2 treatment at 8 DPA leads to an approximate 20% reduction in bone length compared to BSA control samples, thus not only is BMP2 treatment not inducing regeneration of the amputated bone, it also creates a truncated bone stump shorter than the original amputation level.

Studies employing BMPs to induce a bone healing response have reported conflicting results; reports of BMP2 used in conjunction with a standardized bone growth technique in a rat model and BMP2 application in fracture repair in mouse, goat, and human studies suggest BMPs greatly aid the healing response, while others using BMP2 in conjunction with a standardized bone growth technique in a rabbit model as well as
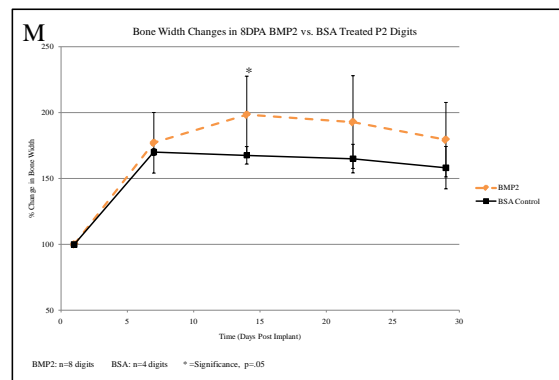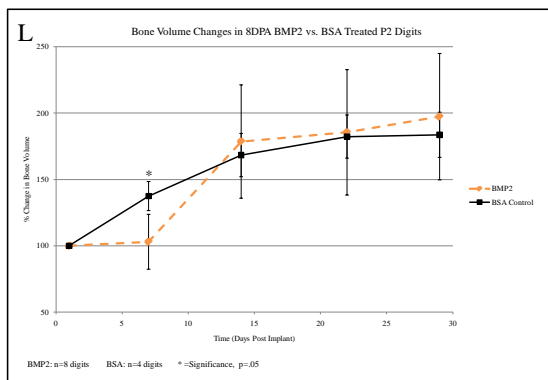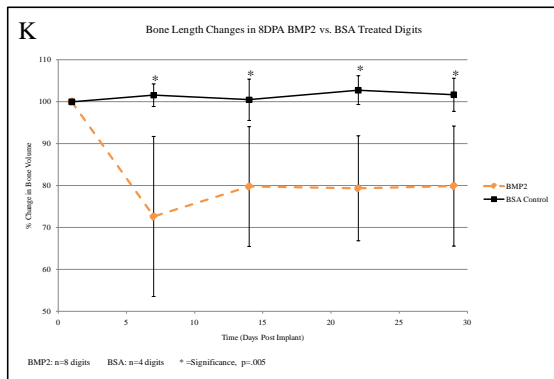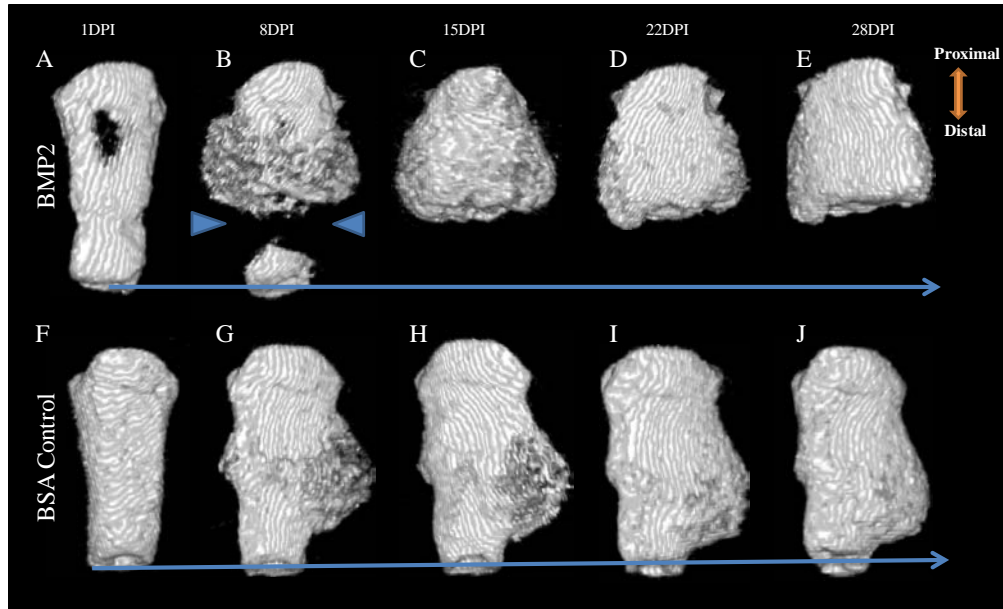
Figure 2.1 – Dawson et al.

Fig. 2.1 Lack of induced regeneration and decrease in bone length in 8 DPA BMP2-treated digits vs. BSA control digits. (A-E) MicroCT 3-D reconstructed images show BMP2 treatment at 8 DPA results in a decrease in bone length by 8 DPI (B), compared to BSA control digits (F-J). Note, the BSA control digits do not increase in bone length. (K) The percent decrease in bone length of BMP2-treated digits is statistically significant from BSA control digits over the duration of the study after week one ($p < 0.005$). (L) Percent changes in bone volume are significantly different at 8 DPI between the BMP2 and BSA control digits, yet no other times show significance ($p < 0.05$). Percent changes in bone width are insignificant at all time points except 15 DPI ($p < 0.05$). Student's *t*-test was used to calculate *P* value, bars specify standard error. Amputation plane indicated by blue line.

other human fracture repair studies suggest BMPs hinder the healing response, or have no significant effect, respectively (Jeppsson and Aspenberg, 1996, Welch et al., 1998, Govender et al., 2002, Yu et al., 2010a, Gautschi et al., 2007). Our findings indicate that addition of BMP2 at 8 DPA does not lead to an enhancement of bone length, but rather an overall reduction in length resulting in a bone shorter than the original amputation level. In line with this, reports have shown an increase in osteoclast numbers (Yu et al, 2010a) and an increase in the production of the osteoclast stimulator RANKL with a concomitant decrease in the osteoclast antagonist OPG post BMP2 treatment and bone fracture (Minear et al., 2010). To investigate the potential involvement of osteoclasts post BMP2 treatment in our P2 model, we utilized the MicroCT to create bone thickness 3-D models, thus elucidating the bone remodeling response, as well as immunohistochemistry for Cathepsin K, a marker for osteoclasts, in 8DPA BMP2 treated digits vs. BSA controls. At 8 DPI, bone thickness 3-D models of the BMP2 and BSA treated digits indicate the BMP2-treated samples have undergone extensive remodeling and increased degradation compared to the BSA controls, evident from the blue and purple colors as well as the open marrow space, respectively (Fig. 2.2, A and B). Note the lack of thick lamellar bone (white and yellow colors) in the bone shaft of the BMP2-treated digit, resulting in a digit comprised primarily of trabecular bone (Fig. 2.2, A). Conversely, the BSA control digit is largely comprised of thick lamellar bone, with trabecular bone found within the woven callus surrounding the lateral portions of the bone, indicating an area of localized bone remodeling (Fig. 2.2, B).

The decrease in bone length and the extensive degradation evident from the thickness model in the BMP2-treated digits indicates enhanced osteoclast activity or an

increase in cell number. We probed the 8 DPI BMP2 treated digits (n = 3) and the 8 DPI BSA control digits (n = 3) for osteoclast cell staining using immunohistochemistry for Cathepsin K (CpsK). Surprisingly, while the graphical trend suggests more osteoclast immunostaining in BSA control digits, CpsK immunostaining divided by total cell count revealed no significant difference in osteoclast numbers between BSA and BMP2 treated digits at 8DPI (Fig. 2.2, C. $p < 0.05$). BSA treated digits showed CpsK staining in both the periosteal and endosteal-marrow compartments, as well as distal to the bone stump, while the BMP2 treated digits showed CpsK positive cells localized primarily to the periosteal and endosteal/marrow compartments, yet not distal to the bone stump (not shown).

Histological Samples and Immunohistochemistry of the 8DPA BMP2-treated P2 Digit reveal the lack of Distal Chondrogenic Cap Formation

Earlier studies utilizing BMPs to induce regeneration post neonate digit amputation and adult mouse hindlimb amputation injury show a cartilaginous cap forms distal to the bone stump in the BMP-treated samples (Yu et al., 2010; Yu et al., 2012). Furthermore, the cartilaginous cap is responsible for creating the template for the induced regeneration of the amputated tissues (Yu et al., 2010; Yu et al., 2012). In order to further explore the lack of distal BMP2-induced bone formation in the 8DPA P2 digit, we harvested BMP2 and BSA treated samples at 8 DPI to probe for cartilaginous tissue capping the bone stump. A series of samples were collected for both BMP2 and BSA groups and processed for histology and immunohistochemistry. Histological sections
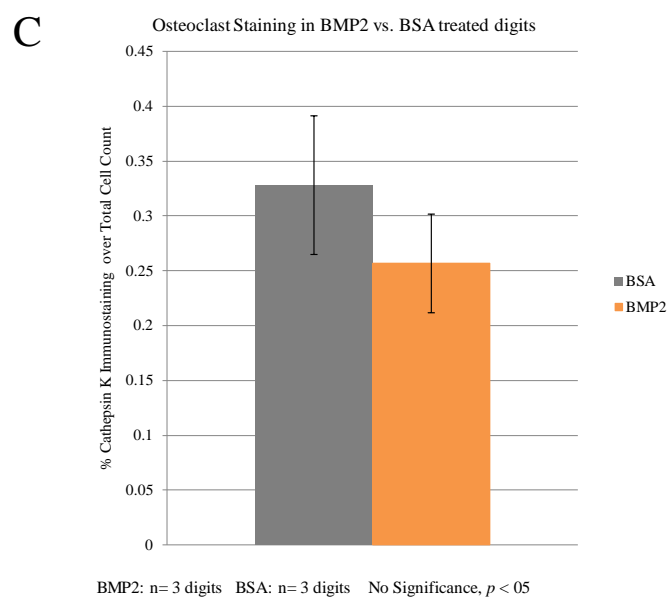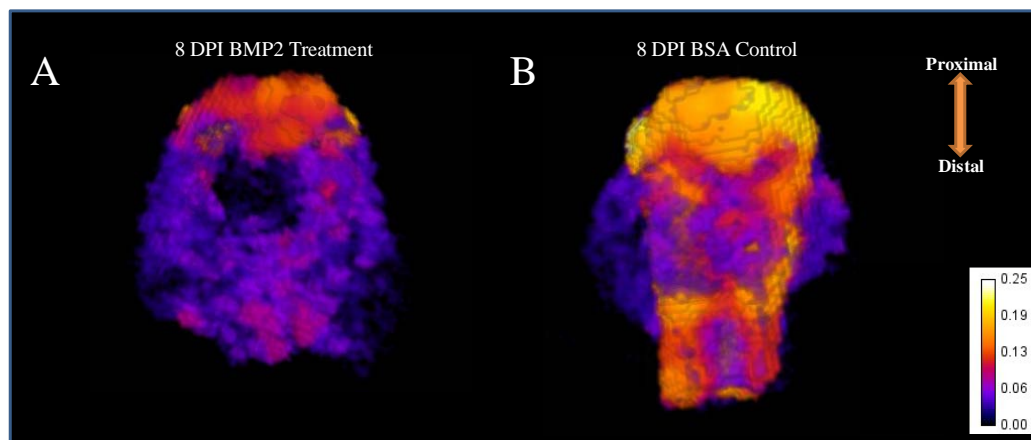
Figure 2.2 – Dawson et al.

Fig. 2.2 Analysis of bone remodeling between 8 DPA BMP2-treated digits and BSA control digits at 8 DPI. (A and B) MicroCT 3-D bone thickness images reveal the BMP2-treated digit is comprised primarily of thin woven bone (blues and purples) (A), while the BSA control digit is comprised of thick lamellar bone (yellow), with a thin woven callus surrounding the digit (blues and purples) (B). (C) Immunohistochemistry probing for osteoclasts using the Cathepsin K antibody (CpsK) show no significant difference in amount of immunostaining between BMP2 (n = 3) and BSA (n =3) digits at 8 DPI ($p < 0.05$). Student's t-test was used to calculate P value, bars specify standard error.

stained with Mallory's Trichrome suggest no cartilaginous formation distal to the bone stump has formed in the BMP2 treated digits (n = 3) (Fig. 2.3, A-C) or the BSA-control digits (n = 3) (Fig. 2.3, D-F) at 8 DPI (Fig. 2.3). Note the presence of the lateral periosteal hypertrophic cartilaginous callus in some samples, both in BMP2-treated digits (Fig. 2.3, A and B) and BSA-control samples (Fig. 2.3, D and F), indicating that while cartilage is not present distally, it is located laterally in some samples. The BMP2-treated samples appear to have truncated bones relative to the BSA-treated digits, and importantly, a distal bone fragment still visible (Fig. 2.3, A, black arrowhead), as well as a portion of the bone seemingly undergoing degradation (note the osteoclasts adjacent to the bone, green arrowhead) (Fig. 2.3, C), implying the bones of the BMP2-treated samples had been longer at one point, yet had become truncated via degradation.

We next probed the BMP2-treated digits using immunohistochemistry for Collagen 2 (Col2), a marker for proliferating chondrocytes, testing to confirm the absence of chondrocytes distal to the bone stump. The BMP2-treated digit does exhibit some Col2 staining, with articular cartilage staining immunopositive as well as light staining within the ventral hypertrophic callus (arrowhead) (Fig. 2.3, G, 100X). A view under greater magnification (boxed) indicates the distal portion of the cartilaginous callus does not test immunopositive for Col2, further providing evidence that chondrocytes are not present distal to the bone stump post BMP2 treatment (Fig. 2.3, H, 200X).

MicroCT studies reveal BMP2 implanted at 9 DPA increases P2 bone length vs BSA controls
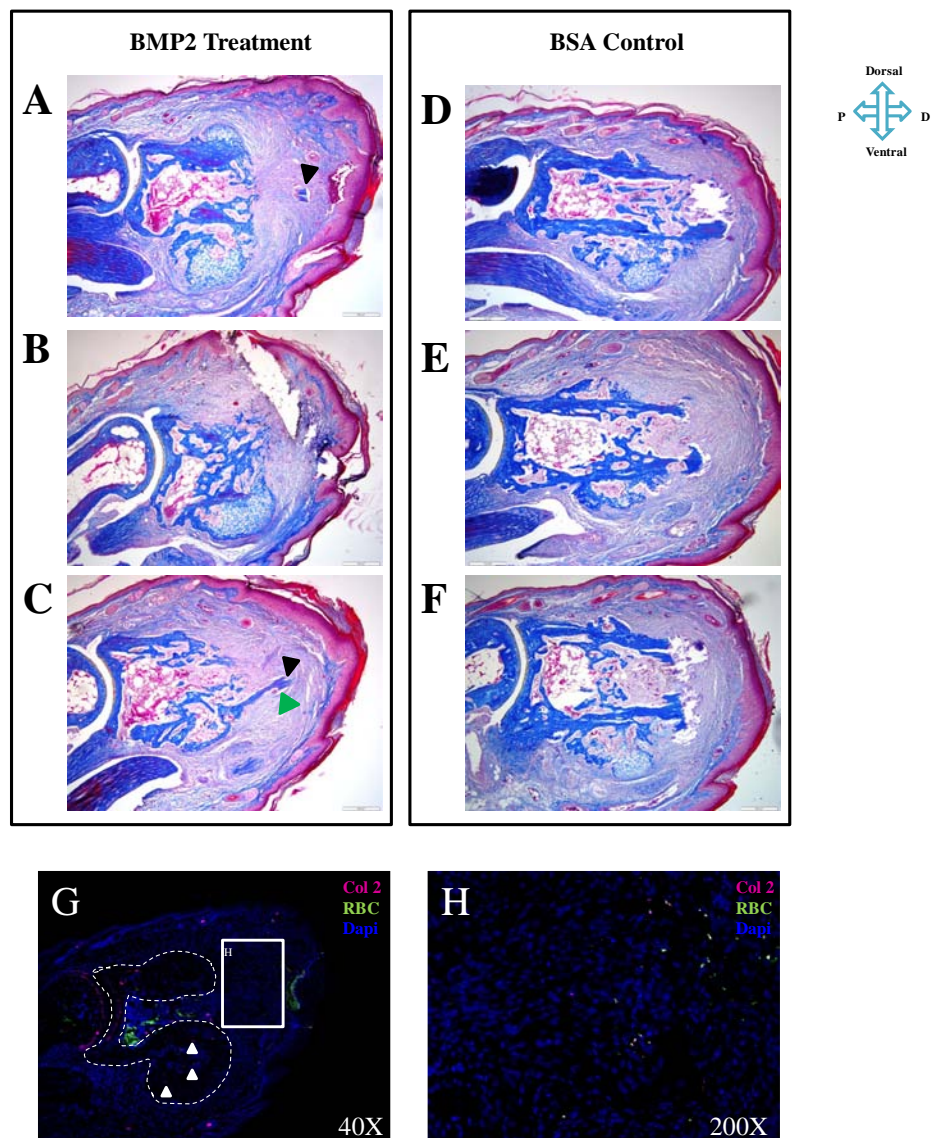
Figure 2.3 – Dawson et al.

Fig. 2.3 Histology and Immunohistochemistry reveals lack of distal chondrogenic cap in 8 DPA BMP2-treated digits. (A-F, 100X) Mallory's staining of 8 DPA BMP2-treated (n = 3) and BSA control digits (n = 3) at 8 DPI shows the truncated bone in BMP-treated digits (A-C), as well as distal remnants of bone (black arrowheads, A and C) compared to no evidence of bone truncation in BSA control digits. (C) An osteoclast is adjacent to the BMP2-treated distal bone fragment (green arrowhead). (A-F) Note, in all digits, the lack of distal chondrogenic cap, with chondrocytes localized only to the periosteal (lateral) regions of the bone. (G) Col2 immunostaining shows immunopositive cells within the articular cartilage and ventral periosteal callus (arrowheads), and no immunostaining distal to the bone stump (40X). (H) An inset of G indicates no Col2 immunostaining distal to the bone stump (200X). All digits sectioned at 5 μm.

Our ultimate goal is to regenerate lost appendages post amputation injury, therefore we made another attempt to induce regeneration of the amputated adult mouse P2 bone through the use of BMP2, yet implanted at a later time point, 9 DPA. At 9 DPA, the P2 bone shows robust chondrocyte proliferation along the periosteal surface, not within the endosteal/marrow cavity, nor distal to the bone stump (Chapter 1), and of 4 digits assayed for wound closure, only one digit exhibited a scab without underlying epidermal tissue capping the marrow space, while the others displayed a large wound epidermis (not shown). To induce regeneration of P2, we implanted 0.500 µg/µl BMP2 sol-gel (n = 3) into the distal digit tip of 9 DPA digits and tracked changes in bone volume and length via the MicroCT. Control digits received sol-gel implants containing 0.1% BSA (n = 4) at 9 DPA. Digits were scanned one day post treatment and weekly thereafter for 4 weeks total.

MicroCT 3-D reconstructions at 1 DPI indicate no periosteal callus has formed on the BMP2 treated digit, while the BSA sample does show some slight remodeling to the bone, exposing the marrow cavity, however this result was not consistent between samples at this time point (Fig. 2.4, A and F). By 8 DPI, both samples showed bone growth along the periosteal compartment, yet the BMP2-treated sample displayed growth not only localized central to the shaft, as in BSA-control samples, but bone growth nearly covering the whole periosteal surface in addition to some bone growth distal to the amputation plane (Fig. 2.4, B and G, amputation plane = yellow line). Surprisingly, while the 3-D model suggests more bone growth in the BMP2-treated sample than the control sample, the average bone volume of the BMP2-treated samples, while increasing since

the previous time point, is statistically significantly smaller than the average volume increase of BSA samples (Fig. 2.4, K, $p < 0.05$). The average percent change in bone length for both treatment groups indicates the length has not increased by 8 DPI (Fig. 2.4, L). At 15 DPI, the 3-D model of the BMP2-treated digit shows extensive distal elongation compared to the unchanged BSA control digit, with an average percent change in bone length of 167% (Fig. 2.4, C, H, and L, $p < 0.005$). Importantly, the distal bone growth is contiguous with the bone stump, not ectopic. There is, however, no significant difference in average bone volume between the two groups at this time point (Fig. 2.4, K, $p < 0.05$). At time points 22 and 29 DPI, the BMP2-treated digit continues to exhibit growth distal to the original amputation level (yellow line), with an average percent change of approximately 172 and 175%, respectively, differing greatly from the BSA-control digit which did not show noteworthy distal bone growth, with an average percent change of 103 and 109%, respectively (Fig. 2.4, D, E, I, J, and L, $p < 0.005$). Note the average change in bone volume is increasing at 22 and 29 DPI in the BMP2-treated digits compared to BSA controls, yet the change is not statistically different, presumably due to the large volume variability in BMP2 samples (Fig. 2.4, K, $p < 0.05$, note error bars).

Histological Samples and Immunohistochemistry of the 9 DPA BMP2-treated P2 Digit reveal Cartilaginous Growth Distal to the Amputation Plane

MicroCT data showing the significant increase in bone length in 9 DPA BMP2-treated digits provides much evidence that addition of the growth factor induces bone regeneration. Previous studies in which BMPs were utilized to induce a regeneration
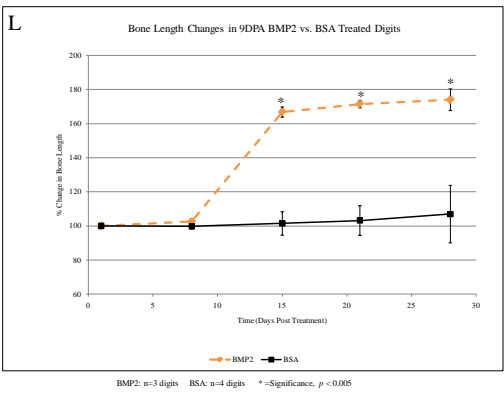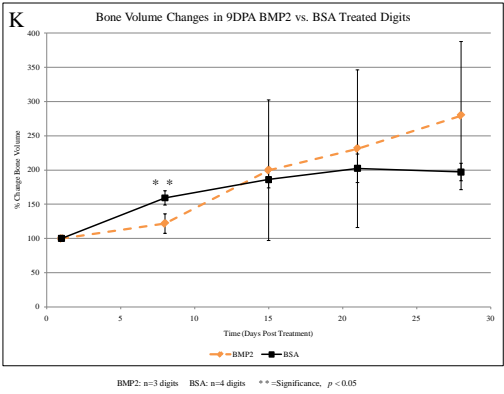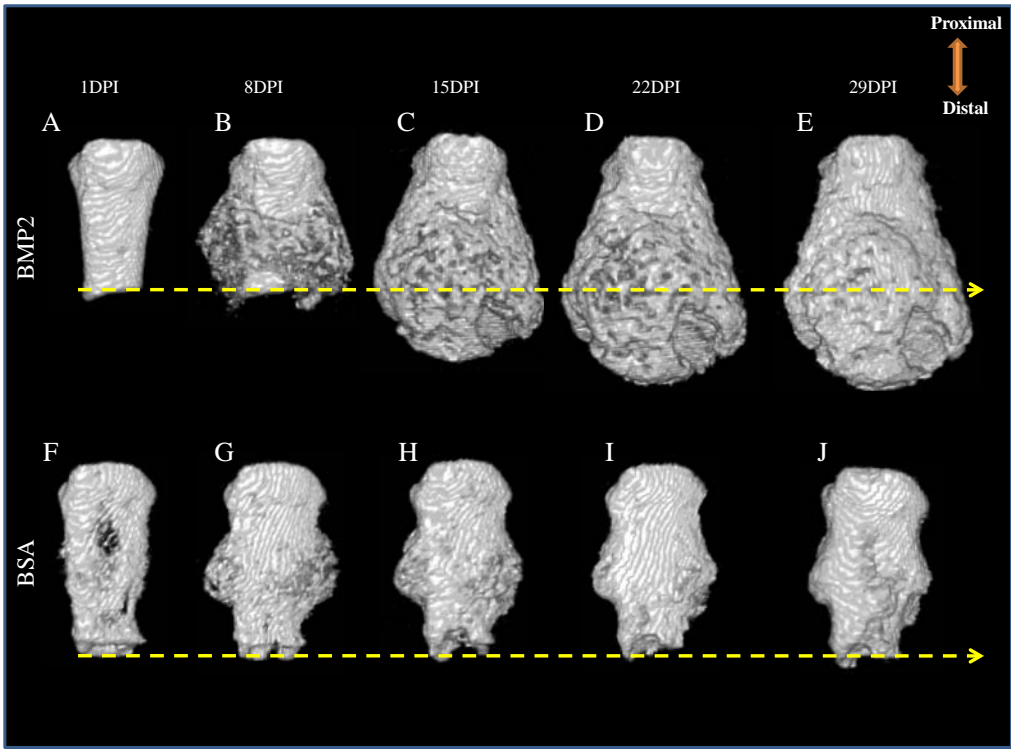
Figure 2.4 - Dawson et al.

Fig. 2.4 Induced regeneration and increase in bone length in 9 DPA BMP2-treated digits vs. BSA control digits. (A-E) MicroCT 3-D reconstructed images show BMP2 treatment at 9 DPA results in a robust increase in bone length compared to BSA control digits (F-J). The marked increase in bone of BMP2-treated digits is apparent at 15 DPI (C and L). (F-J) Note the BSA control digits do not show an increase in bone length. (L) The percent increase in bone length of BMP2-treated digits is statistically significant from BSA control digits at 15, 22, and 29 DPI ($p < 0.005$). (K) Percent changes in bone volume are significantly different at 8 DPI between the BMP2 and BSA control digits, yet no other times show significance ($p < 0.05$). Student's t-test was used to calculate P value, bars specify standard error. Amputation plane indicated by yellow line.

response post amputation injury show the bone regenerates via an endochondral pathway, whereby a chondrogenic cap forms distal to the bone stump, creating a template for subsequent bone formation (Yu et al., 2010; Yu et al., 2012). To elucidate whether the bone regenerates via an intramembranous (no cartilage intermediate) or endochondral pathway post BMP2 treatment, we harvested BMP2 and BSA-treated digits at various time points and performed histological staining and immunohistochemistry.

Mallory's Trichrome staining of 9 DPA BMP2 treated digits harvested at 8 DPI shows the more proximal portions of the periosteal callus have undergone cartilaginous matrix mineralization and replacement with woven bone and marrow spaces, yet the distal/lateral periosteal compartment (boxed) and distal to the amputation plane (dotted line) shows active chondrogenesis, indicating an endochondral healing mechanism (Fig. 2.5, A). By 15 DPI, the BMP2-treated digit no longer exhibits chondrogenesis, yet shows large amounts of woven bone formation distal to the amputation plane (dotted line), complete with marrow spaces (Fig. 2.5, B). The newly formed woven bone is contiguous with the bone stump, and also encases the distally located BMP2 sol-gel, evident from bone formation on both sides of the sol-gel (Fig. 2.5, B). By 64 DPI, the BMP2-treated digit has undergone bone remodeling into a lamellar structure, made apparent by the seamless bone appearance and the few marrow spaces within the regenerated bone, and the sol-gel has completely dissolved (Fig. 2.5, C).

In an effort to further investigate the BMP2-induced regeneration response, we performed staining and immunohistochemistry on serial sections of BMP2-treated digits (the same digit shown in Fig. 2.5, A) and BSA-control digits, harvested at 8 DPI. Histological results of the BSA-control digit reveal the lack of periosteal

8 days post BMP2 Treatment   15 days post BMP2 Treatment   64 days post BMP2 Treatment
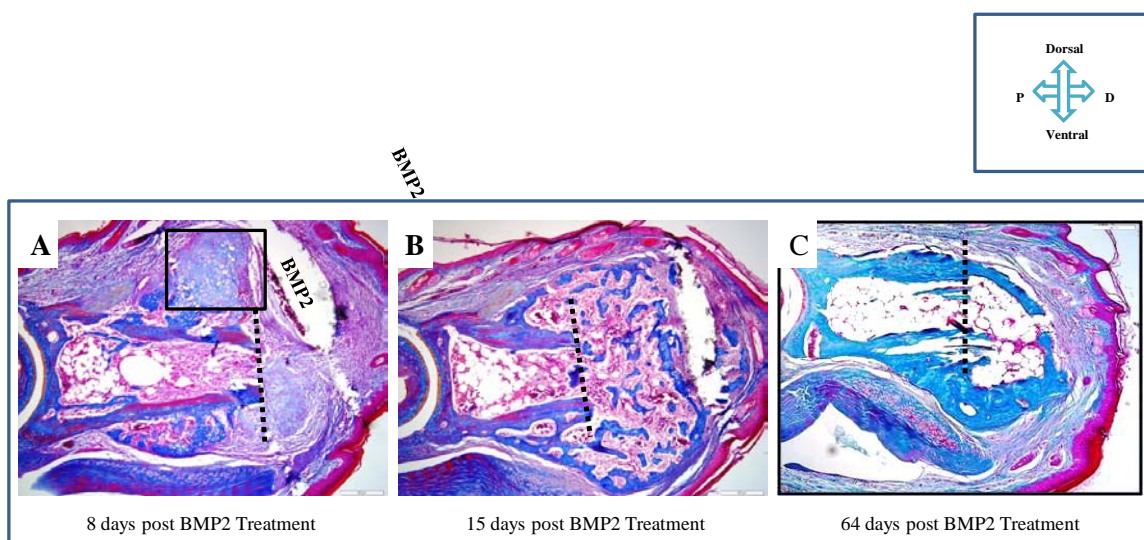
Figure 2.5 - Dawson et al.

Fig. 2.5 Histology of the 9 DPA BMP2-induced regeneration response indicates endochondral ossification distal to the amputation plane. (A) Mallory's staining of the 9 DPA BMP2-treated digit harvested at 8 DPI shows active chondrogenesis along the distal/dorsal periosteal surface (boxed) and distal to the amputation plane. (B) By 15 DPI, the cartilaginous response has been largely replaced by woven bone, complete with marrow spaces, extending far beyond the original amputation plane. (C) At 64 DPI, the regenerated bone distal to the amputation plane has been remodeled from a woven structure into lamellar bone. Amputation plane indicated by dotted black line. All digits sectioned at 5 μm, images at 100X.

chondrogenesis and no chondrogenesis distal to the amputation plane (Fig. 2.6, D). The transient cartilaginous callus of the BSA sample has been replaced by woven bone and marrow spaces, yet the BMP2-treated sample shows signs of continued chondrogenesis, both distal to the amputation plane, and adjacent to the periosteum, as previously mentioned (Fig. 2.6, A and D). In line with this, the 9DPA BMP2-treated sample tested immunopositive for Col2 staining along the dorsal/distal periosteal surface (boxed B), while the BSA-control digit did not test immunopositive for Col2 (boxed E), indicating the lack of chondrocytes in the control digit (Fig. 2.6). Furthermore, immunostaining for Osterix (Osx), a marker for osteoblasts, shows positive staining in the BMP2-treated sample within the endosteal/marrow region, periosteal compartment, distal to the amputation plane (dotted line), and surrounding the BMP2-sol-gel (Fig. 2.6, C). The BSA-treated sample tested immunopositive for Osx within the periosteal and endosteal/marrow compartments, but not distal to the bone stump, indicating the lack of distal bone growth (Fig. 2.6, F).

Elucidating Periosteal Contribution to the P2 9DPA BMP2-Induced Regeneration Response: Lack of BMP2-Induced Regeneration Response in the Absence of the local Periosteum

Our earlier studies focusing on the endogenous bone healing response post adult P2 amputation have suggested the P2 chondrocytes forming the cartilaginous callus are predominantly derived from the locally injured periosteal compartment (Chapter One). Following amputation of P2, periosteal chondrocytes proliferate to create an unpatterned
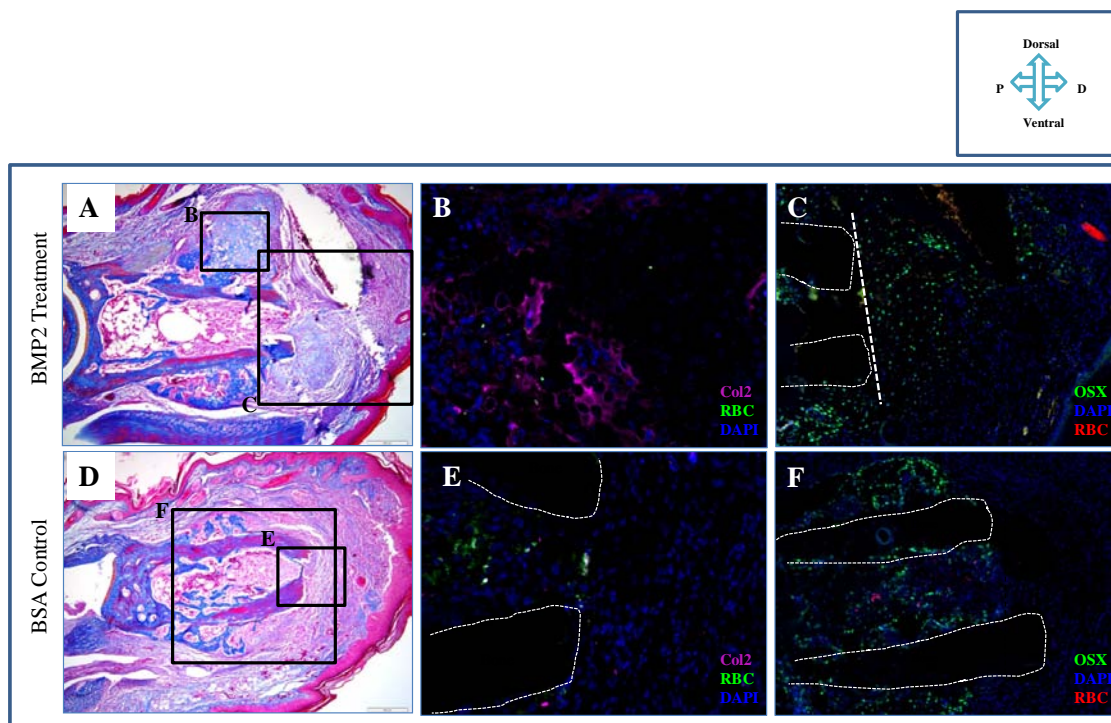
Figure 2.6 - Dawson et al.

Fig. 2.6 Histology and Immunohistochemistry shows distal chondrogenesis and osteoblasts in the 9 DPA BMP2-treated digits at 8 DPI. (A) Mallory's staining of the 9 DPA BMP2 digit harvested at 8 DPI shows chondrocyte proliferation along the dorsal/distal periosteal surface and distal to the bone stump (100X). (B) Col2 immunostaining shows the presence of proliferating chondrocytes in the BMP2 treated sample (200X). (C) Osx immunostaining shows osteoblasts distal to the amputation plane (dotted line) and surrounding the BMP2 sol-gel (100X). (D) Mallory's staining of the 9 DPA BSA control digit shows the periosteal chondrocytes have been replaced with woven bone, and no cartilage is distal to the bone stump (100X). (E) Col2 immunostaining shows no chondrocytes distal to the bone stump in the BSA control digit (200X). Osx immunostaining of the BSA control digit shows osteoblasts lining the periosteal callus and within the endosteal marrow space, yet not distal to the bone stump (100X). All digits sectioned at 5 μm.

annular cartilaginous callus proximal to the amputation plane, forming a template for subsequent woven bone formation, and importantly, the cartilaginous and woven bone calluses do not form in the absence of the local periosteum (Chapter One). Here, we show BMP2-induced regeneration of P2 occurs via endochondral ossification, i.e. with a cartilaginous template, indicating the injured periosteum may contribute to the regenerate.   Furthermore, studies have shown that BMP2 specifically targets the periosteum to induce a chondrogenic response, not the endosteal/marrow region (Yu et al., 2010, Minear et al., 2010). To test the periosteal contribution to the regenerating P2 digit post BMP2 treatment, we removed the periosteum immediately following amputation of the digit. After amputation, the P2 skin and surrounding soft tissues were gently pulled back, exposing the bone, and the periosteum was scraped off the bone surface using a scalpel. The skin and soft tissues were pulled forward following removal of the periosteum, and the distal wound was closed with Dermabond. 9 days post amputation and periosteum removal, 0.500 µg/µl BMP2 or 0.1% BSA sol-gel was implanted into the distal digit tip. We implanted BMP2 or BSA at 9 DPA due to the optimal regeneration response. Digits were tracked using the MicroCT beginning 1 day post BMP2 or BSA treatment, and each week after for 4 total weeks.

MicroCT 3-D reconstructions indicate that P2 digits lacking the periosteum and treated with BMP2 or BSA do not exhibit a boney periosteal response at 1 DPI, coinciding with 9 DPA BMP2-treated digits with the periosteum intact (Fig. 2.7, A and F, see Fig. 2.4, A). By 7 DPI, digits lacking the periosteum showed no evidence of periosteal growth in BMP2-treated or BSA-control samples, as well as no significant difference in bone volume or length between the two groups (Fig. 2.7, B, G, K, and L, *p*

< 0.05). Both BMP2-and-BSA-treated samples showed signs of bone degradation by 15 DPI, evident from the open marrow space in the BMP2-treated sample and the periosteal remodeling in the BSA-control sample, thus matching the slight dip in bone volume from 7 DPI (Fig. 2.7, C, H, and K, $p < 0.05$, no significance). Importantly, the BMP2-treated digits lacking the periosteum showed no increase in bone length at 15 DPI (Fig. 2.7, C, H, L, $p < 0.05$, no significance). At 22 and 28 DPI, both BMP2 and BSA-treated samples showed signs of periosteal remodeling, yet no periosteal growth expanding perpendicular to the bone, as well as no significant differences in bone volume or length between the two groups (Fig. 2.7, D, E, I, J, K, and L, $p < 0.05$.). Of the seven BMP2-treated digits assayed via MicroCT, 3 samples showed a small ectopic bone growth evident by 22 DPI, however the new bone growth was not contiguous with the amputated stump at this time point (not shown).

MicroCT Studies, Histology, and Immunohistochemistry Indicate BMP2 Treatment of P2 at 24 DPA does not induce a Regeneration Response

Collectively, these data suggest that the P2 regenerative potential post BMP2 treatment is time-dependent, i.e. digits treated at 8DPA resulted in significantly shorter bones than BSA treated control digits, and digits treated at 9 DPA resulted in significantly longer bones than BSA treated control digits of the same time point. In this study and in our earlier studies, we have only applied BMPs within a specific window post amputation injury, usually coinciding with wound epidermis formation (Yu et al., 2010; Yu et al., 2012). Here, we show the injured bone milieu is dynamic during these
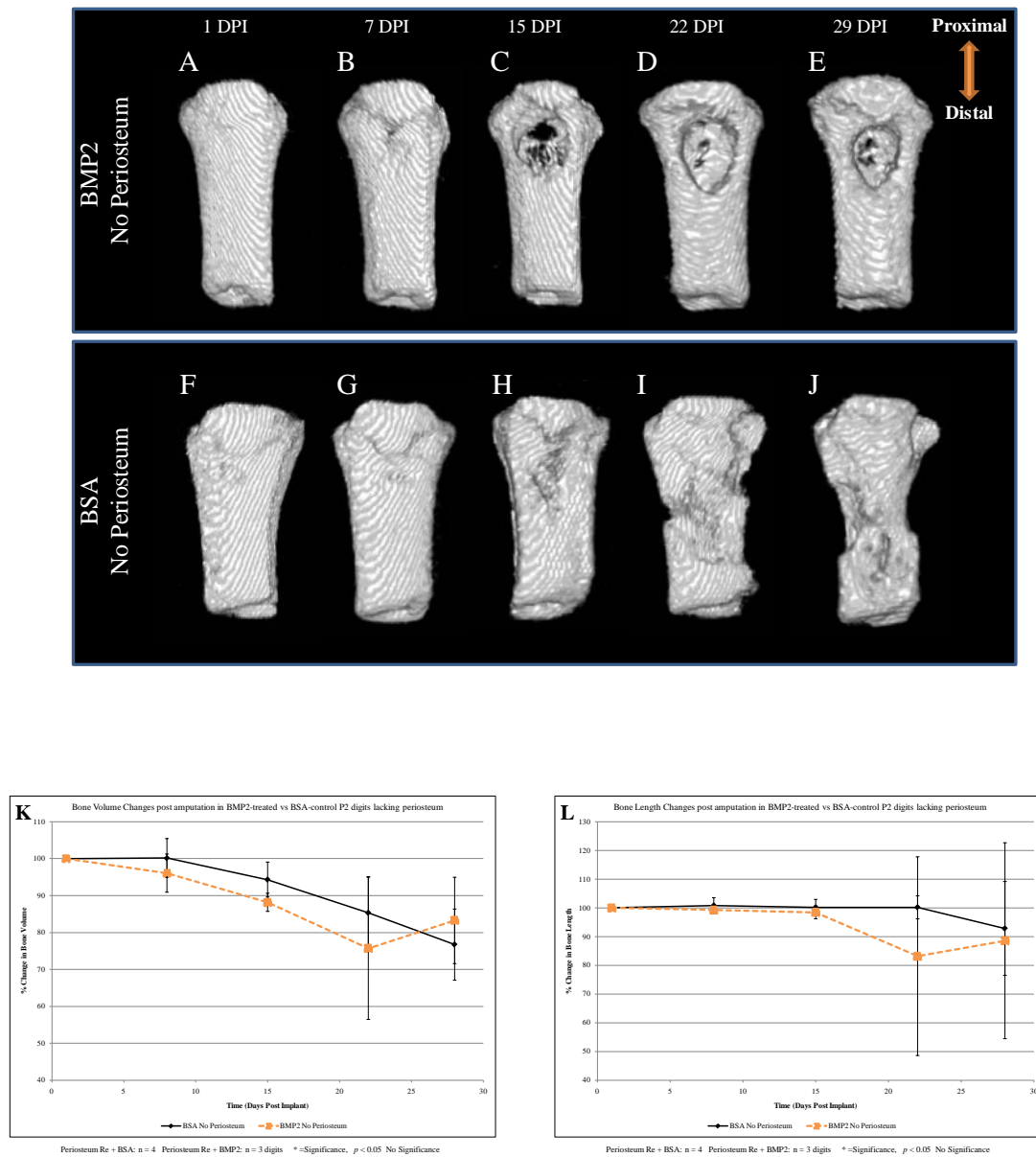
Figure 2.7 - Dawson et al.

Fig. 2.7 Lack of BMP2-Induced Regeneration Response in the Absence of the local Periosteum. (A-E) MicroCT 3-D reconstructed images show BMP2 treatment at 9 DPA does not induce a regeneration response in digits lacking the local periosteum, with no evidence of periosteal bone growth. (F-J) BSA control digits lack periosteal bone growth. (K) The percent change in bone volume between both groups was insignificant at all time points ($p < 0.05$). (L) The percent change in bone length between both groups was insignificant at all time points ($p < 0.05$). Student's t-test was used to calculate P value, bars specify standard error.

early stages and BMP2 can either facilitate or impair the regeneration response, but what is not clear is the effect of BMP2 at later healing stages post amputation injury. Importantly, our efforts to regenerate amputated digits/limbs, both in mice and humans, must encompass the new injuries (i.e., that window of time in which BMP2 is shown to induce a regeneration response, 9 DPA), and the injuries that have occurred months and years before. In an effort to further investigate the time-dependent BMP2 regeneration response in P2 digits, we amputated digits at the P2 level and allowed the digits to heal for 24 days, a full two weeks beyond wound closure, and added 0.500 μg/μl BMP2 or 0.1% BSA to the distal digit tip. These digits will be termed 24 DPA BMP2 or BSA-treated. Digits were scanned 1 DPI and weekly thereafter for 4 total weeks. Importantly, by 24 DPA, the P2 cartilaginous callus has been completely removed and replaced with woven bone and marrow, thus BMP2 was added at a time lacking chondrocyte proliferation.

3-D reconstructed images of both 24DPA BMP2 and BSA treated digits indicate that by 1 DPI, both digits have previously undergone a great amount of remodeling, as seen by the large boney periosteal callus (Fig. 2.8, A and F). By 7 DPI, both treatment groups do not show bone growth distal to the bone stump; the only evident bone growth appears to be some remodeling of the periosteal callus (Fig. 2.8, B and G). Furthermore, graphical data shows that percent changes in bone volume, width, and length have varied little from the previous time point, and BMP2-treated samples (n = 4) do not show significant differences from BSA-treated digits (n = 4) (Fig. 2.8, K, L, and M, $p < 0.05$). One week later, by 14 DPI, both treatment groups again do not show bone growth distal to the plane of amputation, yet bone remodeling of the periosteal callus is clearly seen,

evident from the decrease in bone marrow spaces and the smoother texture of the bone (Fig. 2.8, C and H). In line with this, both groups show an increase in percent change in bone volume, increasing by approximately 15% on average from the previous time point, yet 24 DPA BMP2-treated digits and 24DPA BSA-control samples lack statistically significant differences in bone volume (Fig. 2.8, K, $p < 0.05$). At 14 DPI, we observed no statistical significant differences between the width of the 24 DPA BMP2-treated digits and the BSA controls, yet did note an overall small sloping of the trend line, indicating the width of both groups was decreasing slightly each week (Fig. 2.8, L, $p < 0.05$). Interestingly, we noted a statistical difference in the bone length at 14 DPI (yet no other time points), indicating that 24 DPA BSA-control digits were slightly longer than 24 DPA BMP2-treated digits at the same time point (Fig. 2.8, M, $p < 0.05$). 3-D reconstructed images of 24 DPA BMP2-treated and BSA-control digits at 22 and 29 DPI show no increases in distal bone growth (orange line), and no significance between either group at both time points in percent change in bone volume, width, or length (Fig. 2.8, D, E, I, J, K, L, and M, $p < 0.05$).

We have already shown that by 24 DPA, the cartilaginous growth along the periosteal surface of the P2 bone has been replaced with a woven boney callus (Chapter One). The woven boney callus at this time is beginning the remodeling process from a relatively disorganized composition to an organized lamellar structure, mediated via the actions of osteoblasts and osteoclasts. Due to our 9 DPA BMP2 studies indicating that the chondrogenic component of the regenerating tissue is an integral part of the process, we harvested 24 DPA BMP2-treated and BSA-control digits at 9 DPI to probe for the presence of cartilaginous growth distal to the amputation plane
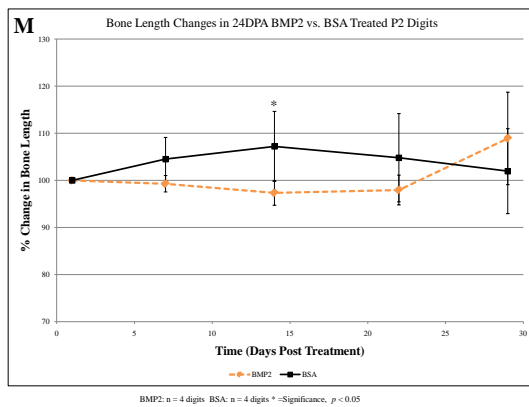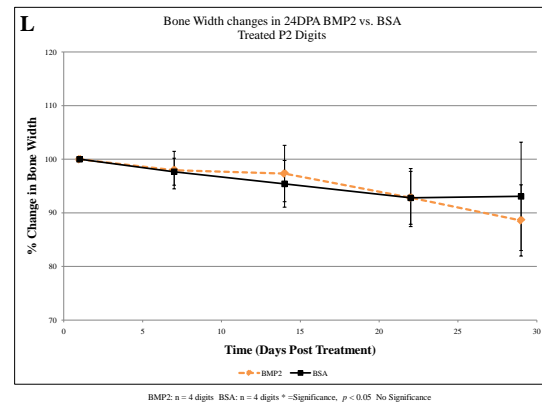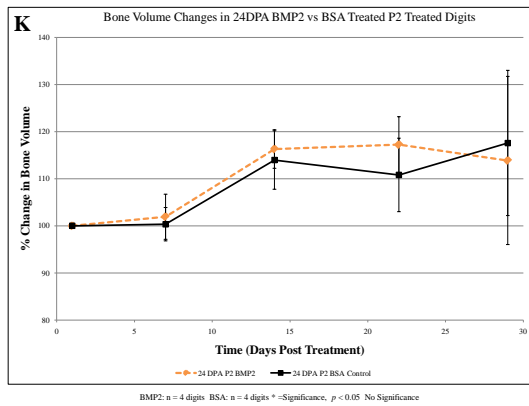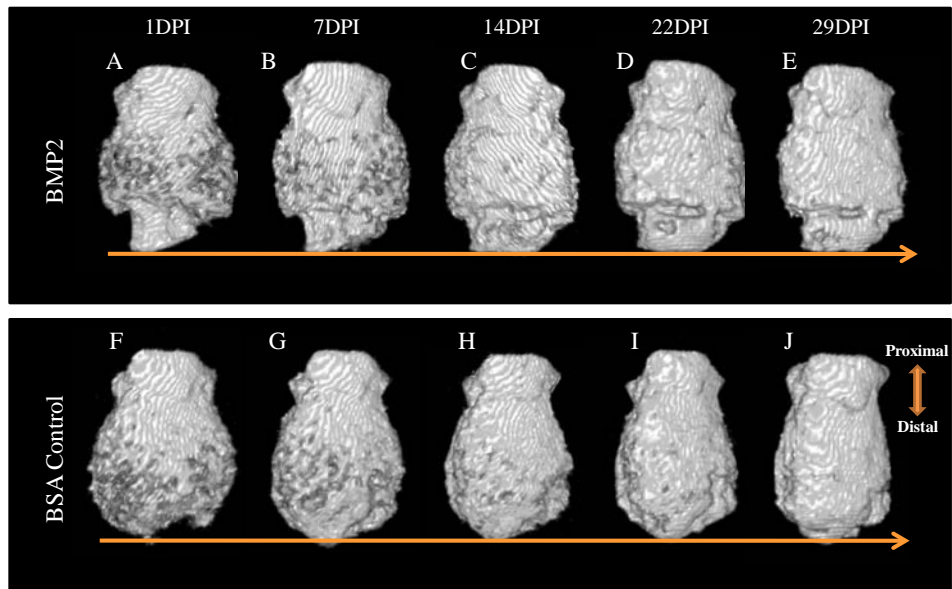
Figure 2.8 – Dawson et al.

Fig. 2.8 BMP2 does not induce regeneration of the 24 DPA digit. (A-E) MicroCT 3-D reconstructed images show BMP2-treatment does not induce distal elongation of the P2 digit if implanted at 24 DPA. (F-J) Note the MicroCT 3-D reconstructed images of BSA control digits also do not show an increase in bone length. (K) The percent change in bone volume between both groups was insignificant at all time points ($p < 0.05$). (L) The percent change in bone width between both groups was insignificant at all time points ($p < 0.05$). (M) The percent change in bone length between both groups was insignificant at all time points, except 14 DPI, indicating BSA control digits were longer than BMP2-treated digits at that time point ($p < 0.05$). Student's *t*-test was used to calculate *P* value, bars specify standard error. Amputation plane indicated by orange line.

using histology and immunohistochemistry (Fig. 2.9). Histological staining of the 24DPA BMP2-treated digit shows the bone stump has undergone much remodeling of the periosteal callus, yet does show signs of a small amount of chondrogenesis along the distal dorsal portion of the periosteal callus and a small cluster of chondrocytes at the distal tip of the bone (Fig. 2.9, A, arrowheads). Immunostaining for Col2 on a serial section reveals a small area of positive immunostaining coinciding with the cluster of chondrocytes at the distal tip of the bone (Fig. 2.9, B, boxed. Bone is outlined). Osx immunostaining shows positive signal within the endosteal/marrow region, the periosteal callus, and at the amputation plane, yet no positive immunostaining distal to the bone stump (Fig. 2.9, C). Histological staining of the 24 DPA BSA-control digit also shows a large amount of bone remodeling within the periosteal callus, yet no indication of cartilaginous growth (Fig. 2.9, D). Moreover, immunostaining for Col2 does not show any definitive areas of positive signal, indicating a lack of proliferating chondrocytes (Fig. 2.9, E). One of the two 24 DPA BSA-control samples harvested at 9 DPI did show a small area of chondrogenesis, comparable to the amount and location of the 24 DPA BMP2-treated digits, indicating that perhaps the bone suffered injury, and thus underwent remodeling, due to the sol-gel implantation (not shown). Immunostaining for Osx reveals a similar localization of osteoblasts as the BMP2-treated sample, showing staining in the endosteal/marrow region, the periosteal callus, and at the amputation plane, yet no positive immunostaining distal to the bone stump (Fig. 2.9, F). Taken together, our results indicate BMP2 does not induce a regeneration response in the 24 DPA P2 digit.
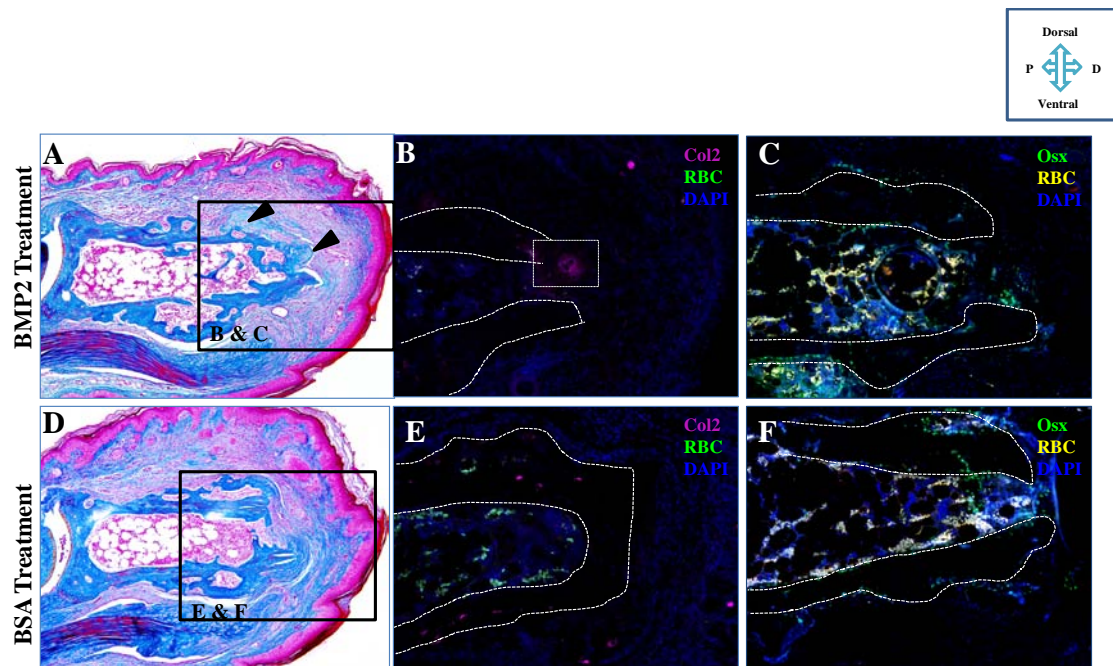
Figure 2.9 – Dawson et al.

Fig. 2.9 Histological staining and immunostaining indicates BMP2 does not induce a regeneration response at 24 DPA. (A) Mallory's staining of the 24 DPA BMP2-treated digit harvested at 9 DPI indicates the cartilaginous callus has largely been replaced with woven bone, with two areas of chondrocytes remaining (arrowheads). (B) Col2 immunostaining of the BMP2-treated sample shows one area positive for chondrocytes (boxed) (100X). (C) Osx immunostaining of the same digit shows in osteoblasts within the periosteal and endosteal/marrow spaces, yet not distal to the bone stump (100X). (D) Mallory's staining of the 24 DPA BSA control digit harvested at 9 DPI shows the cartilaginous callus has been replaced by woven bone. (E) No cells test immunopositive for Col2 in the BSA control sample (100X). (F) Immunostaining for Osx reveals positive cells within the periosteal and endosteal/marrow spaces, yet not distal to the bone stump (100X). All digits sectioned at 5 μm.

BMP2 Treatment of re-amputated 24 DPA P2 Digits induces a Regeneration Response

Our 9 DPA BMP2 studies in which the periosteum is removed indicate that BMP2 targets the periosteal tissue to induce a distal endochondral template for bone growth. Importantly, the 24 DPA P2 digit treated with BMP2 is largely healed by this time point, lacking chondrocytes and consisting of woven remodeling bone within the periosteal callus (Chapter One). In an effort to induce chondrogenesis within the remodeling 24 DPA P2 digit, and thus create a chondrogenic target for BMP2, we amputated digits at the P2 level and allowed the digits to heal for 24 days. At 24 DPA, the same digits were re-amputated at the distal portion of P2, making sure to remove the distal fibrous scar and epidermis, as well as to injure the bone ensuring the marrow cavity was exposed. We allowed the digits to heal for 9 days, harvested the digits and assayed for chondrocyte formation using histology and immunohistochemistry (Fig. 2.10). The Mallory's stained sample indicates the 24 DPA re-amputated digit has undergone bone remodeling both within the endosteal/marrow region and the periosteal region, as well as chondrocyte formation along the periphery of the periosteum, showing cartilage formation adjacent to the new bone formed from the original amputation injury (Fig. 2.10, A and B). Note the open marrow cavity, and the lack of chondrocytes within this region (Fig. 2.10, A). Immunostaining for Acg1 indicated chondrocytes comprised the periosteal callus of the re-amputated bone, with chondrogenesis extending perpendicular to the bone, not distal to the stump, suggestive of the re-amputation healing response recapitulating the cartilaginous response of the initial amputation injury (Fig. 2.10, C). Accordingly, Osx immunostaining showed osteoblasts within the re-amputation callus,

again suggestive of a recapitulation of the original bone healing response post P2 amputation (Fig. 2.10, D).

In order to induce regeneration of the 24 DPA P2 bone, we re-amputated the bone and allowed the digit to heal for 9 days. At 9 days post re-amputation, we implanted 0.500 μg/μl BMP2 (n = 8) or 0.1% BSA (n = 5) into the distal digit tip and tracked the changes in bone growth via the MicroCT, beginning at 1 DPI and scanning weekly for 5 total weeks. Here, we show two examples each of BMP2-treated and BSA-control digits. 3-D reconstructed images at 1 DPI indicate the BMP2-treated and BSA-control digits have undergone prior extensive periosteal bone remodeling, evident from the increased width of the digits, the many marrow spaces, and pitting on the bone surface (Fig. 2. 11, A and G). Note, however, some re-amputated digits have a relatively smooth periosteal surface, yet appear very short, indicating extensive bone degradation prior to the implantation of either BMP2 or BSA (Fig. 2. 11, M and S). At 8 DPI, the percent change in bone volume has increased for both BMP2-treated samples and BSA-controls (Fig. 2.11, Y, $p < 0.05$, no significance) and all digits appear to show some increase in bone length (amputation plane = orange dashed line), yet BMP2-treated digits show a greater percent increase in bone length than BSA-controls (Fig. 2. 11, B, H, N, T, and Z, $p <$ 0.05). By 15 DPI, the 3-D reconstructed images show extensive distal bone elongation in both BMP2-treated samples compared to the BSA-control digits, with the newly formed bone contiguous with the bone stump and resulting in an average percent increase in bone length of approximately 37% (Fig. 2. 11, C, I, O, U, and Z, $p < 0.005$). BSA-control digits also show evidence of distal bone growth at 15 DPI, yet this observation was not consistent between samples and the newly formed bone appeared localized to one area
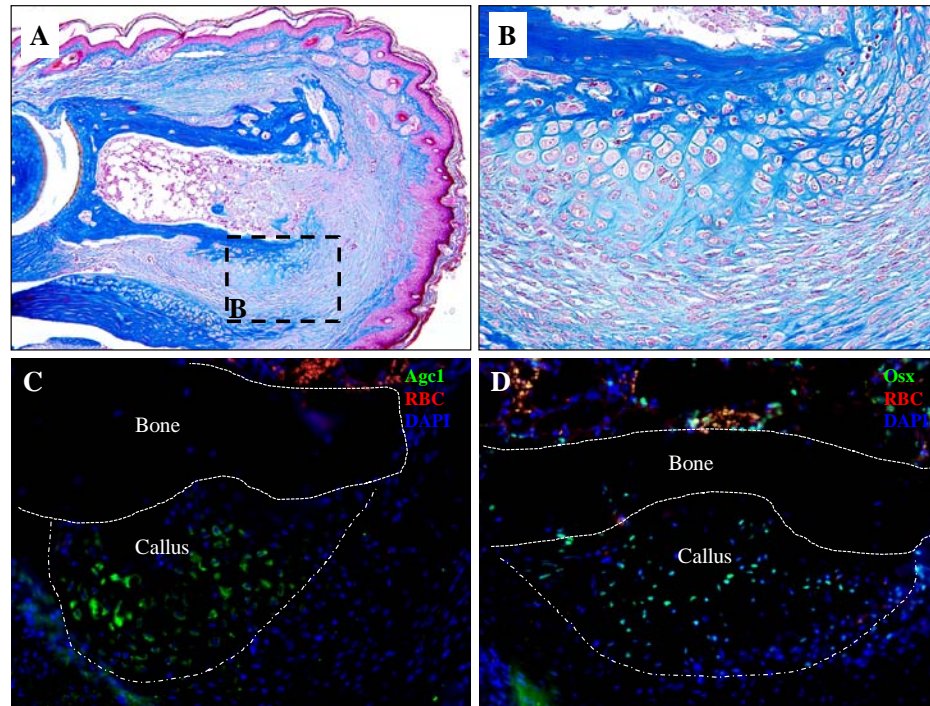
Figure 2.10 – Dawson et al.

Fig. 2.10 Histological staining and immunostaining of the cartilaginous periosteal callus following re-amputation of the 24 DPA digit. (A) Mallory's staining of the 24 DPA re-amputated digit harvested at 9 days post re-amputation shows cartilaginous growth along the ventral periosteal surface (boxed), not within the endosteal/marrow space nor distal to the bone stump (100X). (B) Higher magnification view of (A) showing greater detail of the 9 days post re-amputation cartilaginous callus comprised of proliferating and hypertrophic chondrocytes (200X). (C) Agc1 immunostaining shows the periosteal callus is comprised of chondrocytes (200X). (D) Osx immunostaining reveals the osteoblasts within the periosteal callus. All digits sectioned at 5 μm.

(arrowhead) (Fig. 2. 11, I). At 22 DPI, the newly formed bone in the BMP2-treated digits shows signs of continued distal bone growth and remodeling compared to BSA-control samples (Fig. 2. 11, D, J, P, V, and Z, significant, $p < 0.005$). BMP2-treated samples also show an average increase in bone volume at time points between 15-35 DPI, yet the change is not significant between BMP2- and BSA-control digits, presumably due to the large volume variability between all samples (Fig. 2. 11, Y, $p < 0.05$). At time points 28 and 35 DPI, BMP2-treated digits show signs of bone remodeling and have essentially halted distal growth, yet maintain the length of the regenerated bone (Fig. 2. 11, E, F, Q, R, and Z, $p < 0.005$).

To investigate the BMP2-induced bone regeneration response of the re-amputated 24 DPA P2 digit, we harvested samples at 10 days post BMP2 or BSA implantation and processed them for histology and immunohistochemistry. Histological sections demonstrate that 10 days post BMP2-treatment, large areas of cartilage are present along the distal periphery of the woven bone, near the BMP2 sol-gel (boxed) (Fig. 2. 12, A). The newly formed cartilage is organized with the large hypertrophic chondrocytes adjacent to the bone surface, and the smaller flatter proliferating chondrocytes comprising the periphery of the chondrogenic masses (Fig. 2. 12, A). Immunohistochemistry for Agc1 shows immunopositive cells along the periphery of the bone, coinciding with the cartilage shown in the histological sample, extending towards the BMP2 implant (Fig. 2.12, B). Osx immunostaining reveals a large area of osteoblasts distal to the bone stump and adjacent to the BMP2 implant (Fig. 2.12, C). Notably, the osteoblasts are sandwiched between the two areas of cartilaginous growth in the BMP2-treated sample, indicating the regeneration response of the re-amputated digit is a relatively unpatterned

Figure 2.11 – Dawson et al.

Y **Bone Volume Changes in 24DPA Re-amputated BMP2 vs. BSA Treated P2 Digits**

BMP2: n = 8 digits   BSA: n = 5 digits   * = Significance, $p < 0.005$, * * $p < 0.05$

Z **Bone Length Changes in 24DPA Re-amputated BMP2 vs. BSA Treated P2 Digits**

BMP2: n = 8 digits   BSA: n = 5 digits   * = Significance, $p < 0.005$, * * $p < 0.05$
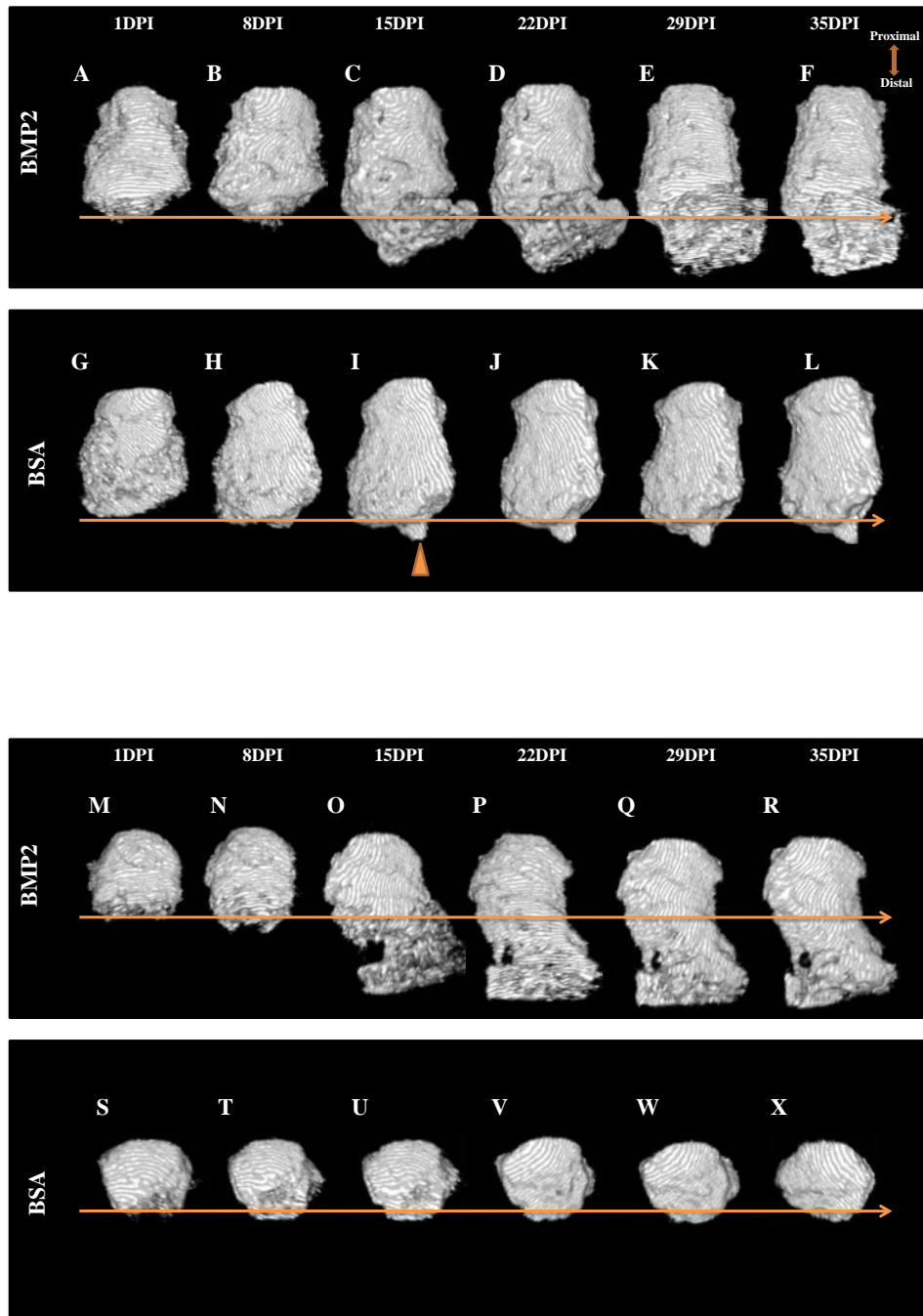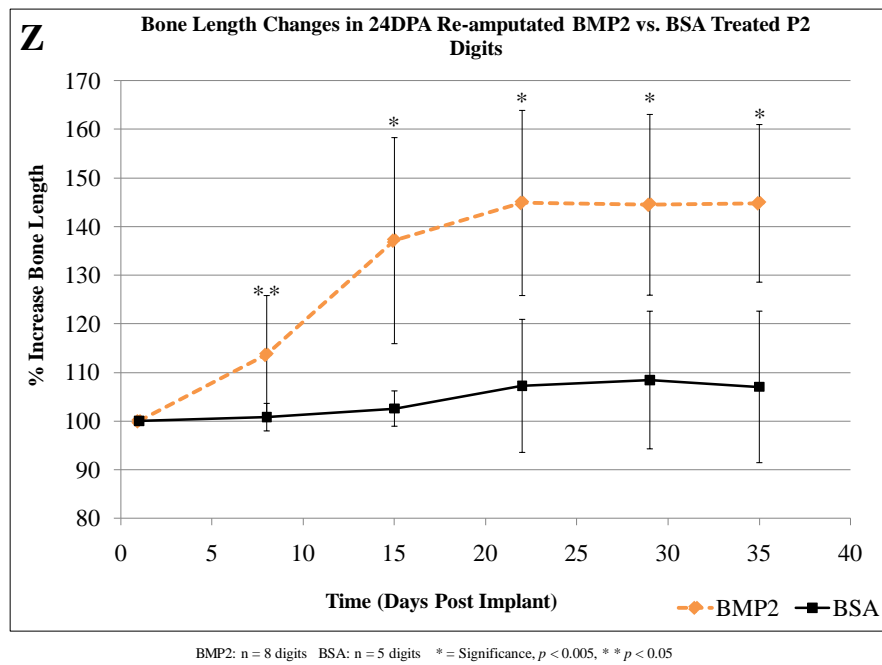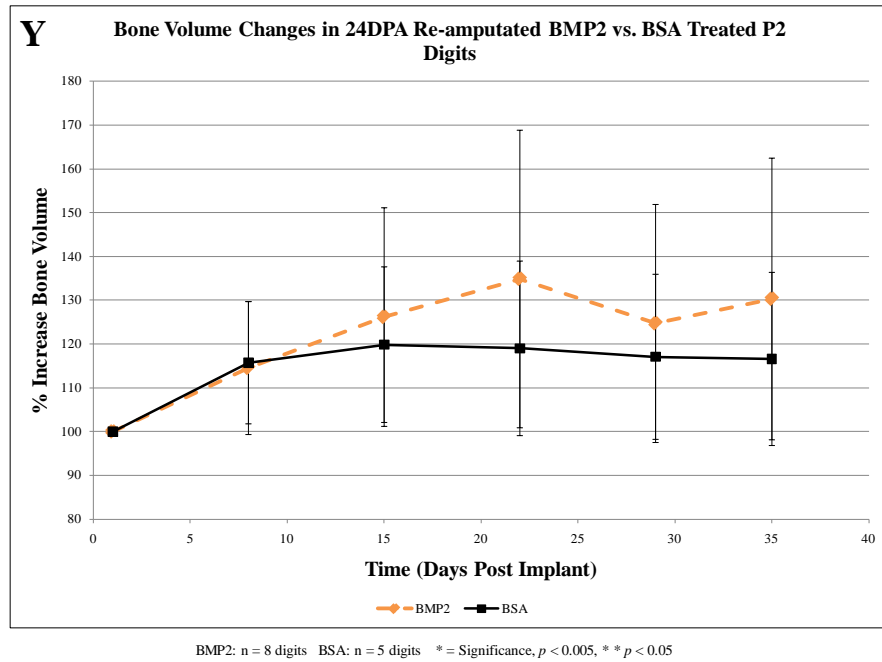
Figure 2.11 – Dawson et al.

Fig. 2.11 Induced regeneration and increase in bone length in re-amputated 24 DPA BMP2-treated vs. BSA control digits. (A-F) MicroCT 3-D reconstructed images of a re-amputated 24 DPA P2 digit shows BMP2-treatment induces a robust regeneration response vs. a BSA control digit of comparable starting length (G-L). (M-R) MicroCT 3-D reconstructed images of another re-amputated 24 DPA P2 digit shows BMP2-treatment induces a robust regeneration response vs. a BSA control digit of comparable starting length (S-X). (Y) Percent changes in bone volume are not significantly different between the two groups at any time point ($p < 0.05$). (Z) The percent increase in bone length of BMP2-treated digits is statistically significant from BSA control digits at 8 ($p < 0.05$), 15, 22, 29 and 35 DPI ($p < 0.005$). Student's t-test was used to calculate P value, bars specify standard error. Amputation plane indicated by orange line.

endochondral event (Fig. 2.12, B and C). BSA-control samples do not show cartilage formation near the implanted BSA sol-gel (dashed box), yet a small cluster of hypertrophic chondrocytes are present on the ventral lateral surface of the bone (Fig. 2. 12, D, boxed). Immunostaining for Agc1 shows no immunopositive chondrocytes, and Osx immunostaining shows osteoblasts associated only with the bone stump, not distal to the amputation level, indicating the BSA-control digit is not undergoing a regeneration response (Fig. 2.12, E and F).

Our earlier studies have shown that the amputated P2 bone undergoes a remodeling response characterized by initial woven bone and marrow space formation over the cartilaginous template, followed by continued remodeling of the woven bone into a relatively smoother lamellar structure (Chapter One). The remodeling of bone post injury is essential in that lamellar bone is comparatively much stronger than woven bone, and thus able to withstand greater loads (Shapiro, 2008). In order to investigate the remodeling response of the newly formed bone induced by BMP2-treatment, we tracked changes in bone thickness over time using the MicroCT. Bone thickness maps indicate less thick bone in blue and purple shades (presumably the newly formed woven bone or areas undergoing extensive remodeling) and the yellows and whites indicate thicker bone, i.e., lamellar bone. The dorsal and ventral views of the BMP2-treated 24 DPA re-amputated bone (the same bone shown in Fig. 2.11, A-F) show large areas of purple bone along the periosteal surface of the original bone stump and within the newly formed bone distal to the amputation plane at 14 DPI (green line) (Fig. 2. 13, A and D). Interestingly, the newly formed bone also showed signs of thickness dorsally, evident by the areas of yellow and select few punctuate white spots (Fig. 2.13, A). By 22 DPI, the regenerated
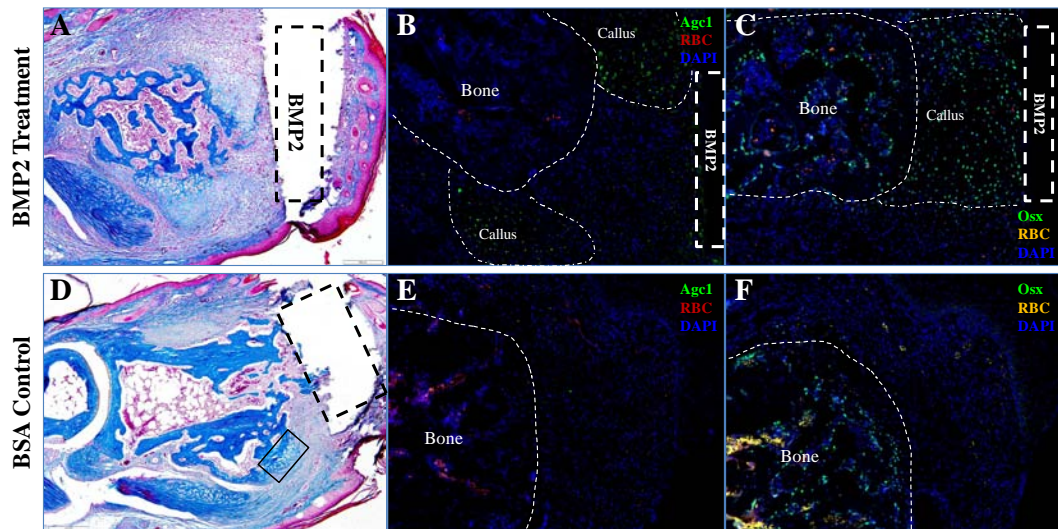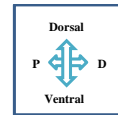
Figure 2.12 – Dawson et al.

Fig. 2.12 Histology and immunohistochemistry shows the re-amputated 24 DPA P2 digit treated with BMP2 regenerates via endochondral ossification. (A) Mallory's staining of the re-amputated BMP2-treated P2 digit harvested at 10 DPI shows cartilaginous growth along the periphery of the distal portion of the bone, corresponding to the periosteum (100X). (B) Agc1 immunostaining shows chondrocytes distal to the bone stump and proximal to the BMP2 sol-gel (100X). (C) Osx immunostaining shows osteoblasts within the bone stump and extending distal to the bone within the boney callus (100X). (D) Mallory's staining of the re-amputated BSA-control P2 digit harvested at 10 DPI shows the periosteal callus has largely been remodeled into woven bone, with chondrocytes present on within a small region of the ventral callus (boxed) (100X). (E) Agc1 immunostaining shows no chondrocytes distal to the bone stump in the BSA control digit (100X). Osx immunostaining of the BSA control digit shows osteoblasts within the bone stump, yet not distal to the bone stump (100X). All digits sectioned at 5 μm.

bone distal to the amputation level is showing an increased area of purple, indicating bone remodeling, and, coupled with the increase in bone length from the previous time point, suggestive of new bone formation (Fig. 2. 13, B and E). The 3-D reconstructed thickness model at 56 DPI shows large areas of white and yellow coloring within the newly formed bone, most notably in the ventral view, indicating relatively thick bone within the regenerated region (Fig. 2. 13, C and F).

To explore the remodeling of the regenerated bone further, we harvested the same digit we assayed for bone thickness, and processed it for histological staining. Mallory's staining of the 56 DPI 24 DPA re-amputated BMP2-treated digit shows the lamellar bone proximal to the re-amputation plane (arrowheads), the newly formed bone distal to the amputation plane, and the large marrow cavity spanning the entire digit (Fig. 2. 13, G). Studies have shown differences between woven and lamellar bone can be determined via Picro Sirius Red histological staining and assaying the passage of light, using polarized light microscopy, through the bone fibers; woven bone, due to its less organized composition relative to lamellar bone, will not allow light to pass through a section due to the random arrangement of collagen fibers blocking the light, yet lamellar bone will allow the light to pass through the sample more readily due to the organized pattern of the collagen fibers (Shapiro, 2008). A serial section was stained with Picro Sirius Red and haematoxylin, shown in polarized light (Fig. 2.13, H) and bright field (Fig. 2.13, I). Polarized light imaging shows an area of the regenerate comprised of woven bone (yellow arrowhead), evident from dark areas within the red and yellow stained collagen matrix (Fig. 2.13, H). Note the brightly colored yellow lamellar bone (green arrowhead)

within the distal region of the regenerate, indicating the BMP2-induced bone formation distal to the amputation plane remodels into a strong lamellar structure (Fig.2.13, H).

BMP2 Treatment of re-amputated 21WPA P2 Digits induces a Regeneration Response

We continued to investigate the potential for BMP2 to induce regeneration of older amputation injuries of the P2 digit. In order to accomplish this, we amputated P2, allowed the digit to heal for 21 weeks (5 months), followed by re-amputation of the digit at 21 weeks post amputation (WPA), and 0.500 µg/µl BMP2 or 0.1 % BSA sol-gel treatment 9 days post re-amputation. Based on our observations in the 24 DPA re-amputation plus BMP2 data set, we hypothesized that BMP2 treatment alone without re-amputation of the 21 WPA digit would not induce a regeneration response; therefore we chose to directly study the effect of BMP2 treatment after re-amputation of the digit. In order to track changes in bone regeneration, we scanned BMP2-treated (n = 4) and BSA-control (n = 3) digits from 1 DPI and scanning weekly for 4 total weeks.

3-D reconstructed images indicate both the BMP2-treated and the BSA-control 21 WPA re-amputated digits are composed primarily of smooth lamellar bone at 1 DPI, evident from the even appearance of the bone and the lack of pitting on the bone surface (Fig. 2.14, A and F). By 8 DPI, both samples show signs of periosteal remodeling (yellow arrowheads), yet the BMP2-treated digit displays non-uniform bone formation distal to the amputation level (orange dashed line) and across the entirety of the bone stump, whereas the BSA-control digit exhibits a small localized area of uniform bone growth distally (green arrowhead) (Fig. 2.14, B and G). The graphical data indicates that
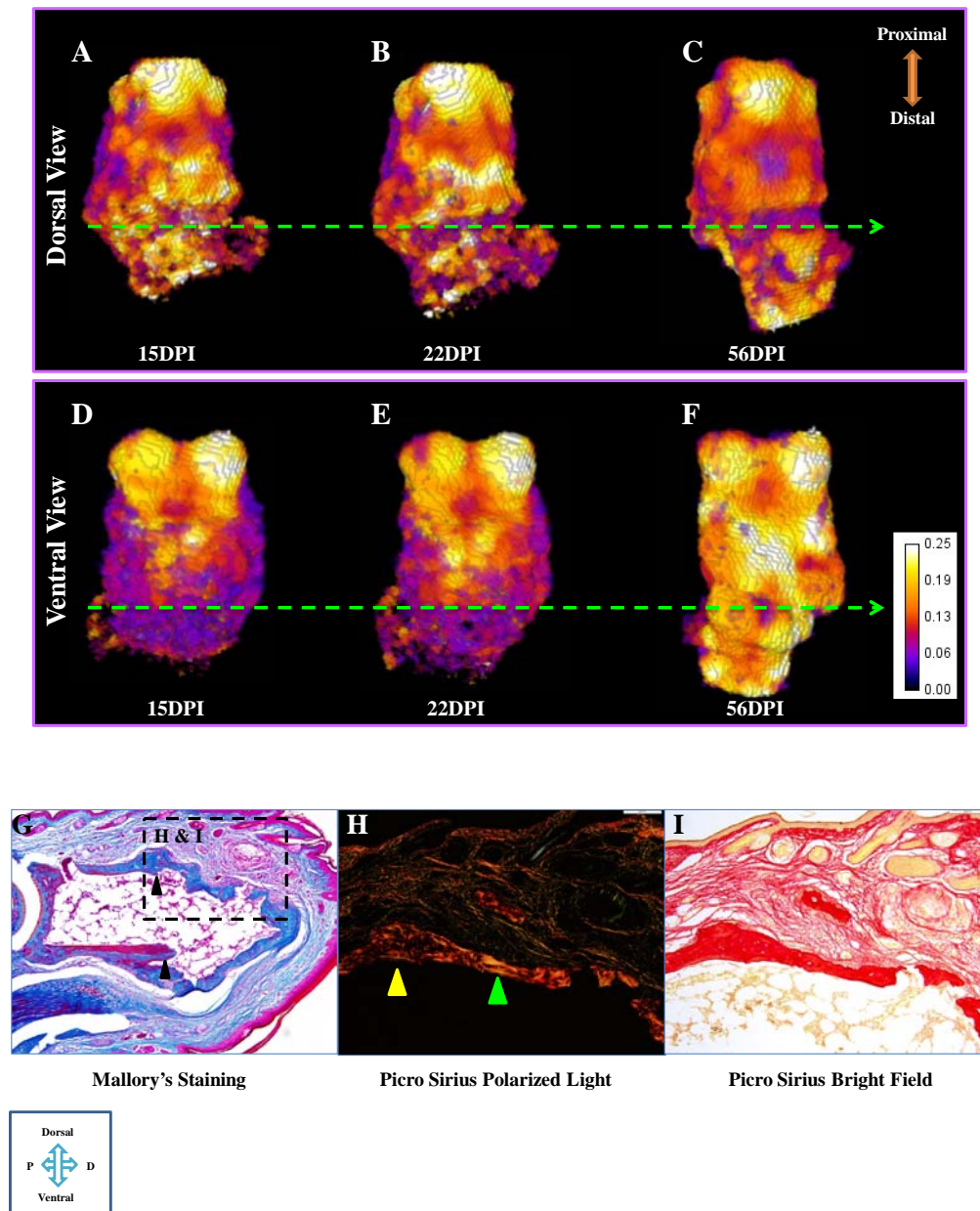
Figure 2.13 –Dawson et al.

Fig. 2.13 Histological and MicroCT Analysis of bone remodeling in the BMP2-treated 24DPA re-amputated digit. (A-F) MicroCT 3-D bone thickness images of the BMP2-treated 24DPA re-amputated bone, shown in the dorsal view (A-C), and the ventral view (D-F). (A-C) The bone distal to the amputation plane is increasing in length and thickness over time, with the most distal portion of the regenerate comprised of dark purple bone (suggestive of new bone formation) at 15 and 22 DPI, and comprised of white thicker bone by 56 DPI. (D-F) The ventral view of the bone shows the regeneration response is characterized by relatively thin bone formation at 15 and 22 DPI, with thick bone comprised of white and yellow colors by 56 DPI. (G) Mallory's staining of the 56 DPI digit shows the original re-amputation plane (arrowheads). (H) Inset image of Picro Sirius staining using polarized light microscopy shows woven bone (yellow arrowhead) and lamellar bone (green arrowhead). (I) Bright field of Picro Sirius staining. All digits sectioned at 5 μm.

both treatment groups are increasing in bone volume, yet they do not differ from each other significantly at 8 DPI (Fig. 2.14, K, $p < 0.05$). Conversely, the graphical data shows a significant change in bone length between the two groups at 8 DPI, with BMP2-treated digits showing an average percent increase in bone length of approximately 10%, while the BSA-control digits are relatively unchanged from the previous time point (Fig. 2.14, L, $p < 0.05$). At 15 DPI, the BMP2-treated digits continue to show signs of distal bone growth compared to BSA-control digits, with new boney islands forming adjacent to radiolucent areas, indicative of an endochondral event (Fig. 2.14, C and H). Likewise, graphical data shows BMP2-treated digits have increased by an overall average 25% from 1 DPI, compared to the relatively unchanged length of BSA-control samples (Fig. 2.14, L, $p < 0.05$). Both treatment groups, however, show a similar increase in bone volume at 15 DPI (Fig. 2.14, K. No significance, $p < 0.05$). The 3-D reconstructed image of the BMP2-treated digit at 21 DPI shows bone is forming within and filling the radiolucent spaces evident at 15 DPI, while the BSA-control digit is showing no increase in bone length (Fig. 2.14, D and I). By 28 DPI, the BMP2-treated digit has undergone continued remodeling, essentially filling in all spaces within the regenerated bone, yet still exhibiting some pitting on the surface (Fig. 2.15, E). The graphical data indicates both treatment groups show a similar trend in bone volume increases at 21 and 28 DPI (Fig. 2.14, K. No significance, $p < 0.05$), yet BMP2-treated samples continue to show a significant average increase in bone length compared to BSA-control digits, culminating with an approximate 30% increase from 1 DPI (Fig. 2.14, L, $p < 0.05$).
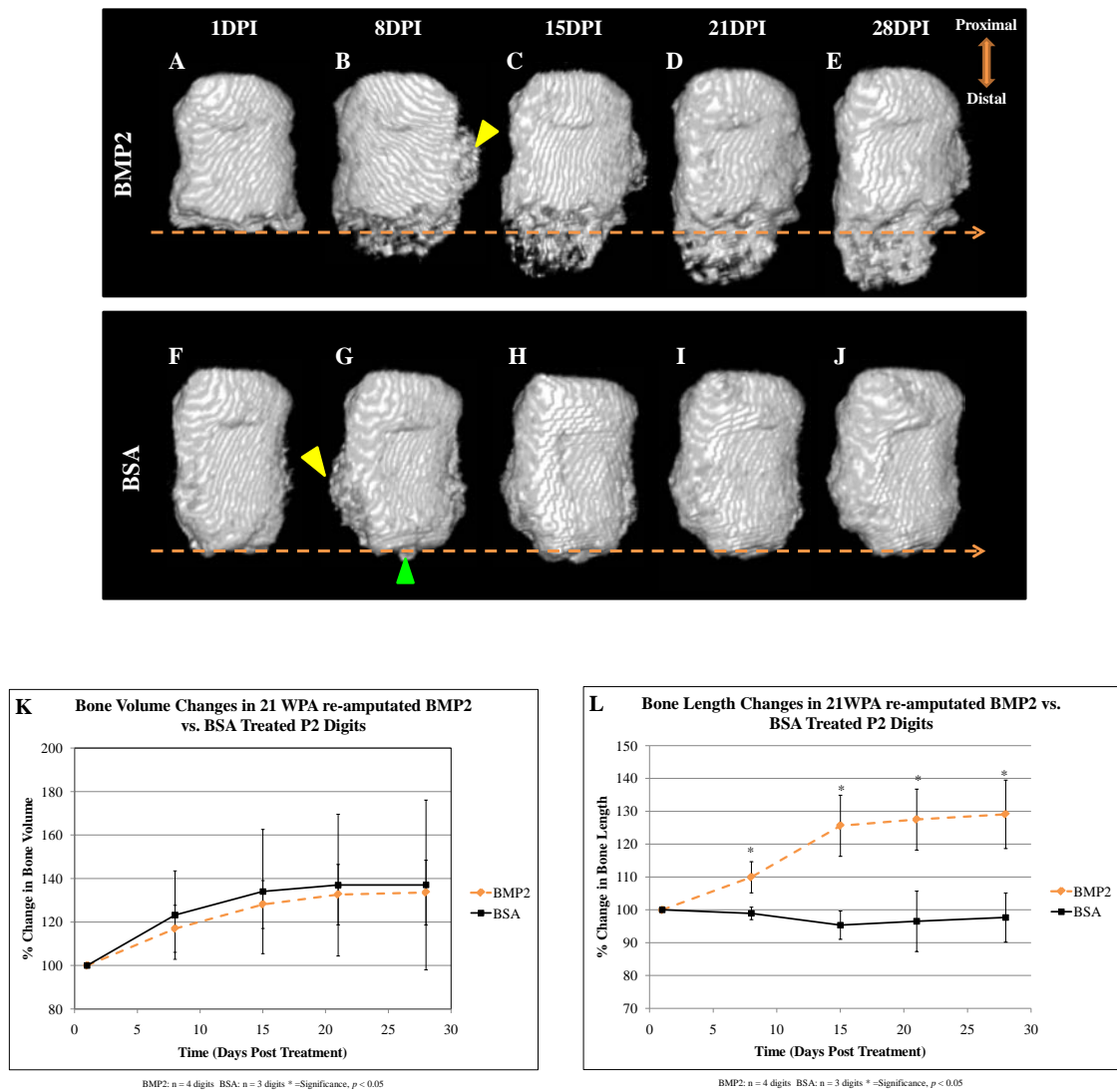
Figure 2.14 – Dawson et al.

Fig. 2.14 Induced regeneration and increase in bone length in re-amputated 21 WPA BMP2-treated vs. BSA control digits. (A-E) MicroCT 3-D reconstructed images of the re-amputated 21 WPA digit treated with BMP2 shows a regeneration response characterized by an increase in bone length beginning at 8 DPI. (F-J) 21 WPA BSA-control digits do not show an increase in bone length. (K) Percent changes in bone volume are not significantly different between the two groups at any time point ($p < 0.05$). (L) The percent increase in bone length of BMP2-treated digits is statistically significant from BSA-control digits at all time points after week one ($p < 0.05$). Student's t-test was used to calculate P value, bars specify standard error. Amputation plane indicated by orange line.

III. Discussion

We and others have shown that following amputation of the mouse P2 digit, the bone does not regenerate, alternatively, the amputation injury leads to scar formation without distal elongation of the bone stump (Neufeld and Zhao, 1993; Yu et al., 2012; Chapter One). We have also shown that the adult mouse P2 bone undergoes a healing response similar to that of fracture healing, whereby the amputated P2 bone represents the proximal half of the fracture. Indeed, much like fracture repair, following amputation of the adult mouse P2 bone, the injury milieu is characterized by an initial inflammatory response, followed by chondrocyte proliferation along the periosteal surface and subsequent woven bone formation over the cartilaginous template, and ultimately remodeling of the bone into a lamellar structure. Importantly, the transient periosteal-derived cartilaginous growth of the amputated digit occurs in such a way that the template expands perpendicular to the bone, with chondrogenesis very rarely occurring distal to the bone stump. Consequently, the woven bone formation occurs perpendicular to the bone over the cartilaginous template, culminating in an unpatterned bone stump lacking distal elongation. Thus, it is intuitive to: 1) look to methods to increase chondrocyte proliferation post P2 amputation injury in an effort to expand the template for subsequent bone formation, and 2) to induce chondrocyte proliferation distal to the bone stump, ultimately leading to regeneration of the amputated portion of the bone. Previous studies have demonstrated the effectiveness of BMPs in inducing a regeneration response post digit amputation (Yu et al., 2010; Yu et al., 2012). Regeneration incompetent proximal amputation injuries of the neonate P3 bone have been shown to undergo an induced regeneration response following the application of BMP2 and 7 (Yu

et al., 2010). The induced digit regeneration occurs via endochondral ossification, thus a cartilaginous template forms the outline for the subsequent bone development (Yu et al., 2010). Importantly, recent work has demonstrated the neonate P2 digit and the adult mouse hindlimb are also capable of BMP2-induced regeneration post amputation, and again, via a cartilaginous template (Yu et al., 2012). Here, we used the amputated adult mouse P2 digit as a model system to gain further understanding of BMP2-induced regeneration, focusing specifically on: 1) the temporal bone healing response of BMP2 treatment, 2) the periosteal contribution to P2 induced regeneration, and 3) the bone healing mechanism of induced regeneration (i.e., endochondral vs. intramembranous ossification). We show for the first time that optimizing the timing of BMP2 application is pivotal for inducing an effective P2 bone regeneration response, in that BMP2 treatment can either facilitate or hinder the bone regeneration capabilities of the P2 digit. Furthermore, our data suggests BMP2 implanted at the optimal time targets active periosteal tissue to induce a distal cartilaginous template for bone regeneration post amputation injury. Importantly, we provide evidence that new and old amputation injuries alike can respond to BMP2 treatment and undergo a regeneration response, thus our novel studies show immense therapeutic potential.

Temporal Dynamic of BMP2-induced Regeneration of the Adult Mouse P2 Digit

Previous work utilizing the amputated neonate P2 digit indicate that BMP2 induces regeneration of the digit via the accumulation of BMP-responsive cells distal to the bone stump, followed by the formation of an endochondral ossification center

comprised of proliferating and hypertrophic chondrocytes (Yu et al., 2012). Notably, the BMP2-induced distal cartilaginous growth creates a template for subsequent bone formation, and thus is integral to the induced regeneration response. Post adult P2 amputation, the bone naturally undergoes an endochondral healing response, with chondrocytes localized to the periosteal compartment; very rarely within the endosteal/marrow region or distal to the bone stump (Chapter One). Here, in an effort to optimize the neonate response in an adult model, we implanted BMP2 into the distal digit tip at 8 DPA (i.e., approximate time of P2 wound closure) to induce the formation of a cartilaginous cap distal to the amputation plane, and thus regenerate the amputated bone. Surprisingly, BMP2 treatment at 8 DPA led to an overall decrease in bone length, whereby BMP2-treated digits were significantly truncated compared to their BSA-control counterparts. In line with this, an earlier report showed BMP2 decreased the bone forming potential of a standardized bone growth technique in rabbits (Jeppsson and Aspenberg, 1996). Our histological and immunohistochemistry data indicate BMP2 treatment at 8 DPA did not induce chondrogenesis distal to the bone stump. BMP2 treatment, however, did not have a noticeably negative effect on the endogenous periosteal chondrogenesis of P2. Instead, the distal portions of the bone stump appeared to have undergone degradation, suggestive of osteoclast action. Indeed, studies have reported that BMP2 application post bone fracture have led to noticeable increases in osteoclast numbers as well as an increased production of the osteoclast stimulator RANKL combined with the decreased production of the osteoclast antagonist OPG (Yu et al., 2010a; Minear et al., 2010). Our collective data suggests an increase in osteoclast action, i.e., the decrease in bone length, the highly remodeled bone evident in the 3-D

reconstructed thickness map, and the histological samples, yet quantification of Cathepsin K immunostaining showed no significant difference in BMP2-treated samples vs. BSA control digits. Further studies must be performed to gain a greater understanding of the decrease in bone length and lack of induced-regeneration response in digits treated with BMP2 at 8 DPA.

We next explored the regenerative potential of the adult mouse P2 digit at 9 DPA. BMP2 treated digits showed marked increases in bone length compared to BSA controls, exhibiting an average length increase of 175% by the end of the study, thus showing the adult P2 digit is capable of undergoing a regeneration response. We found the length increase was mediated via a cartilaginous template, with the template testing positive for both Collage 2 and Aggrecan, indicating active chondrocyte proliferation and function. In line with previous neonate induced regeneration studies, the cartilaginous template was located distal and contiguous with the bone stump and proximal to the BMP2-source. Importantly, the distal cartilaginous growth appeared merged and contiguous with the endogenous periosteal chondrogenic response. Our histological samples indicate that the cartilaginous cap was replaced by woven bone and remodeled into a lamellar structure, ultimately resulting in a regenerated bone contiguous with the amputation stump.

These data provide evidence that the BMP2-induced regenerative potential of the P2 digit is time-dependent, in that BMP2 treatment at 8 DPA hinders the bone healing response, while BMP2 treatment at 9 DPA results in significantly longer bones than BSA controls. This novel finding is puzzling; here we show the same quantity of the same growth factor contributes to a truncated bone in earlier treated samples, yet leads to an impressive regeneration response in samples treated 24 hours later. Literature has

documented numerous studies in which animal models of BMP-treated-bone injury yielding positive results are not necessarily translational into human studies (Gautschi et al; 2007). Our data suggests that studies in which BMPs have shown to be ineffective may not be carried out at the correct time, and that perhaps in the dynamic wound environment, adjusting the treatment time may create a more conducive environment for a regeneration response.

Periosteal Contribution to the Distal Cartilaginous Template

Proliferating chondrocytes are essential for the induction of P2 regeneration, therefore it is crucial to determine their source in order to successfully recruit them to the P2 stump. In our investigation of the cellular contribution to the distal cartilaginous template formed after 9 DPA BMP2-treatment, we noted the distal chondrocytes merged with the chondrocytes located along the periosteal surface, indicating a periosteal contribution to the induced regeneration response. Our earlier studies demonstrated that the endogenous cartilaginous callus formed along the periosteal surface of the amputated P2 bone was derived from the locally injured periosteal compartment (Chapter One). In the absence of the periosteal tissue, the P2 bone did not form the cartilaginous callus, nor did it form the woven boney external callus. Importantly, the endosteal/marrow compartment did not compensate for the loss of periosteal tissue; instead, the endosteal/marrow compartment formed bone via intramembranous ossification only within the endosteal/marrow compartment. Furthermore, utilizing transgenic mouse studies in which we traced the fate of GFP-labeled injured P2 bones, we found that the

periosteal tissue did indeed give rise to chondrocytes, while the endosteal/marrow region only gave rise to bone. Fracture healing studies also found the same lineage tracing results (Colnot, 2009). Moreover, fracture healing studies utilizing BMP2 showed the growth factor specifically targeted periosteal-derived cells to form cartilage, while inducing intramembranous bone formation (Yu et al., 2012a) or no bone formation (Minear, et al., 2010) within the endosteal/marrow compartment. Studies also indicate that endogenous expression of BMP2 via periosteal cells initiates the healing response of fractured long bones, and is essential for the differentiation of mesenchymal cells into chondrocytes in the fracture environment (Tsuji et al., 2006; Wang et al., 2011). Here, we show that in the absence of the periosteal tissue, BMP2 treatment at 9 DPA does not induce a regeneration response, neither along the periosteal surface of the injured bone nor distal to the bone stump. Our results suggest the large BMP2-induced cartilaginous template is derived from periosteal tissue, either via increased proliferation of the existing chondrocytes at the time of BMP2 treatment, and/or the recruitment of local periosteal cells to the distal bone stump, and the subsequent formation of the cartilaginous cap. Importantly, the endosteal/marrow compartment of the amputated BMP2-treated P2 bone does not compensate in the absence of the periosteal tissue, evident from the lack of bone growth in digits lacking the periosteum. Taken together, we provide evidence that BMP2 targets the endogenous chondrogenic periosteal tissue of the 9 DPA P2 bone to form a distal cartilaginous template, thus inducing the regeneration of the amputated bone. The significance of this finding is remarkable in that understanding the cellular source, i.e., the periosteal contribution, to the regenerate will allow us to fine-tune our efforts to create a more successful induce-regeneration response.

Modification of Older Amputation Injuries facilitates a BMP2-induced Regeneration Response

Our results indicate BMP2-treatment can either hinder or facilitate the regeneration response during the early, i.e., chondrogenic, stages of P2 wound healing. In our efforts to explore the temporal response to BMP2-treatment, we found that addition of the growth factor at 24 DPA had no significant affect on bone healing. Importantly, 24 DPA digits lack active chondrogenesis; the cartilaginous template has been remodeled into a woven bone structure via the actions of osteoblasts and osteoclasts. Our results suggest BMP2 does not target the osteoblasts or surrounding tissues of 24 DPA P2 digits to induce regeneration or chondrogenesis. However, re-amputation, and thus re-activation of the periosteal compartment, of 24 DPA digits induces endogenous chondrogenesis along the periosteal surface, reminiscent of the original amputation healing response. Here, we show that BMP2 is able to induce regeneration of the re-amputated digit if implanted at 9 DPA, and importantly, the regeneration response is mediated via a distal cartilaginous template, followed by woven bone formation, and the ultimate remodeling of the regenerated bone into a lamellar structure, i.e., fully functional bone. Moreover, we show the BMP2-induced regeneration of re-amputated 21 WPA digits, thus indicating that fully healed amputation injuries have the potential to undergo induced-regeneration. Taken together, our re-amputation studies demonstrate that the regenerative potential of bones is not limited to a specific window of time, but rather the factors used to induce regeneration (BMPs, etc), may only facilitate the regeneration

process within a specific window of time, and that optimization of the temporal affects of growth factor application is pivotal to an efficient regeneration response. The discovery that modified older, and thus fully healed, amputation injuries in the adult mouse show the same or similar potential to respond to BMP2 treatment as do newer amputation injuries is immensely promising from a translational therapeutic perspective.

Chapter Three: Terminal Phalanx Fracture Repair occurs via Direct Periosteal Bone Repair and Novel Endosteal/Marrow Chondrogenesis

I. Introduction

Urodele amphibians, such as the axolotl and the newt, have the exceptional ability to regenerate various body parts post amputation, most notably the limb. Comparatively, mammals, such as mice and humans, have far less ability to regenerate missing appendages, capable only of regenerating the distal digit tip, the terminal phalanx (P3), post amputation (Han, et al., 2008; Zhao, et al., 1995; Mohammad, et al., 1999; Fernando, et al., 2011; Rinkevich, et al., 2011; Lehoczky, et al., 2011). However, there are limitations to the mammalian digit regeneration response; amputation approximately mid-way through P3 (termed the 'distal amputation') results in essentially complete regeneration of the missing tissues, include the bone and nail, yet amputation injuries including and proximal to the P3 nail matrix (termed the 'proximal amputation') result in scar formation (Neufeld, 1992; Borgens, 1982; Zhao, et al., 1995; Mohammad, et al., 1999; Han, et al., 2008; Fernando, et al., 2011; Takeo, et al., 2013; Turner et al, 2010; Agrawal et al., 2011; Agrawal et al., 2012; Mu et al., 2013). Following adult mouse distal amputation, P3 undergoes an inflammatory response followed by osteoclast-mediated degradation of the bone stump, ultimately exposing the marrow cavity

(Fernando, et al., 2011). Successive formation of the blastema, characterized as a population of proliferating undifferentiated mesenchymal cells and lineage-committed progenitor cells, occurs between the bone stump and the wound epidermis (Fernando, et al., 2011; Rinkevich, et al., 2011; Lehoczky, et al., 2011). The cells of the blastema do not undergo an initial chondrogenic response to rebuild the bone; instead bone formation occurs via intramembranous ossification, whereby osteoblasts within the blastema produce woven bone in a proximal to distal fashion, regenerating the digit tip (Han et al., 2008, Fernando, et al., 2011). Importantly, the solely intramembranous regeneration response differs from P3 development; P3 develops via a proximal epiphyseal growth plate, followed by appositional, i.e. intramembranous, bone growth distally (Han, et al., 2008). A previous study has shown that following amputation of neonate P3 digits at a regeneration-incompetent proximal level, digits were induced to undergo regeneration following exogenous application of BMP2 or 7, and strikingly, the induced-regeneration response occurred via endochondral ossification (Yu, et al., 2010). What determines the osteoblast phenotype instead of chondrogenesis of blastema cells during endogenous regeneration is unknown. Moreover, whether or not the P3 bone undergoes endochondral or intramembranous ossification following relatively less invasive bone injuries, such as during fracture repair, has not previously been ascertained. The adjacent digit, the middle phalanx (P2), responds to fracture and amputation injuries by way of an endochondral healing mechanism, with robust chondrogenesis, yet P2 does not have the intrinsic ability to regenerate (Chapters One and Two). A striking difference exists between the two amputation models, the regeneration competent P3 amputation milieu consists of the P3 bone encased by the nail organ and underlying skin components, while the regeneration

incompetent P2 amputation environment is not encased by the nail yet has hair follicles comprising its epidermis. Previous reports have shown the necessity of the nail organ for successful regeneration of the digit (Zhao, et al., 1995; Mohammad, et al., 1999; Takeo, et al., 2013.) However, whether the nail organ is responsible for the intramembranous bone formation of regeneration is unclear. Indeed, gaining a greater understanding of the P3 bone healing response, and in particular, the chondrogenic potential of P3, following fracture may prove useful in shedding light on the intramembranous regeneration response of P3 and the endochondral non-regenerative bone healing response of P2.

Following the fracture of long bones, the mechanism in which the bone heals is principally determined via stability of the local environment (Colnot, 2009; Gerstenfeld, etc). Unstabilized fractures heal by means of a periosteal endochondral callus with concomitant intramembranous ossification within the endosteal/marrow space, while stabilized fractures heal via intramembranous ossification with new bone formation occurring along the periosteal surface and within the endosteal/marrow space (Shapiro, 2008; Ferguson et al., 1999; Vortkamp, et al., 1998; Thompson et al., 2001; Colnot, 2008; Einhorn, 2005; Le, et al., 2000; Thompson, et al., 2001; Thompson, et al., 2001). Endochondral ossification is the chief mechanism of fracture repair, characterized by the formation of a periosteal-derived cartilaginous callus adjacent to the injury site whose dual function is to bridge the fracture gap and create a template for subsequent woven bone formation (Einhorn, 2005; Al-Aql et al., 2008; Shapiro, 2008). The woven bone, comprising the boney callus, is remodeled into a lamellar structure capable of supporting loads, ultimately rebuilding the injured bone to its pre-fracture morphology and strength (Einhorn, 2005; Al-Aql et al., 2008; Einhorn, 2005). Thus, successful unstabilized

fracture repair is dependent on the initial and sustained periosteal chondrogenic response (Einhorn, 2005; Tsuji, et al., 2006; Wang et al., 2011). Importantly, the periosteal-derived chondrocytes of the cartilaginous callus are located predominantly along the periosteal surface, not within the endosteal/marrow space of unstabilized fractures (Colnot, 2009; Gerstenfeld, et al., 2003). After stabilized long bone fracture, whereby fractured bones are stabilized by the use of intra-and-extra-medullary rods, studies indicate that osteo-chondroprogenitor cells along the periosteal surface differentiate directly to osteoblasts, depositing woven bone adjacent to the fracture gap (Le et al., 2000; Thompson, et al., 2001; Gerstenfeld, 2003; Einhorn, 2005; Histing et al., 2009; Colnot, 2009; Yu, et al, 2012a). However, reports suggest the periosteal contribution to stabilized fracture repair is minimal, with the majority of bone forming cells arising from the local endosteal/marrow space (Shapiro, 2008). In line with this, studies suggest the periosteal and endosteal/marrow spaces house distinct populations of cells with unique and limited bone forming potential; periosteal derived cells have the dual potential to differentiate into either chondrocytes or osteoblasts, while endosteal/marrow derived cells only differentiate into osteoblasts (Colnot, 2009). Importantly, the endosteal/marrow space does not inhibit chondrogenesis of periosteal derived cells, and conversely, the periosteal milieu does not induce chondrogenesis of endosteal/marrow-derived cells, indicating innate fate potentials within the cells regardless of their location (Colnot, 2009). Lastly, periosteal cells fated to undergo an osteogenic response in a stabilized fracture model can change their fate to a chondrogenic phenotype after exogenous BMP2 treatment, thus BMP2 acts to "over-ride" the intramembranous healing mechanism, instead inducing endochondral ossification (Yu et al., 2010a). Endosteal/marrow cells

within the fracture milieu, on the other hand, respond to exogenous BMP2-treatment either through intramembranous bone formation (Yu, et al., 2010a), or no bone formation at all (Minear et al., 2010). Taken together, establishing a fracture model for the P3 bone may be an effective method to investigate the chondrogenic potential of the digit.

To investigate the endogenous chondrogenic potential of the injured P3 bone, we created a P3 fracture model whereby the digit is fractured at approximately the P3 amputation level. We specifically integrated our P3 fracture studies with the P3 amputation model, in an effort to directly compare the bone healing response(s). We hypothesized the fracture healing response could occur in one of two ways: 1) the digit would heal via endochondral ossification along the periosteal surface, with concomitant intramembranous ossification within the endosteal/marrow space, thus following the predominant mechanism of fracture repair, or 2) the nail encasing the fractured bone would act as an natural "cast" thus stabilizing the fracture space and inducing intramembranous ossification within both the periosteal and endosteal/marrow spaces. Here, we report for the first time, the fractured P3 bone heals unlike any bone within the body, whereby a novel cartilaginous callus forms within the proximal endosteal/marrow space of the fractured bone. Furthermore, our studies indicate the P3 periosteal tissue undergoes solely intramembranous ossification in the fracture milieu, and surprising, exogenous BMP2-treatment cannot change the intramembranous fate of the periosteal cells. We also report that in the absence of the periosteal tissue, the P3 regeneration response is greatly attenuated. Moreover, using tissue grafting studies, we show the extrinsic and intrinsic chondrogenic/osteogenic potential of the injured P3 nail organ and bone.

II. Materials and Methods

Mice, P3 Amputation and Fracture

All mice used in this study were CD-1 females, ages 8-12 weeks, purchased from Jackson Labs. Mice were anesthetized using Isofluorane, with an initial dose of 3% Isofluorane, and maintained at 2% Isofluorane. P3 amputations were performed on 8 week old CD-1 female mice as described earlier (Fernando, et al., 2012). P3 digits were fractured at approximately the P3 amputation level, yet animal and technical variability created a spectrum of fracture levels; all fracture levels were used and assayed in this study. P3 fractures were performed via a scalpel, thus creating an open fracture, with the scalpel piercing through the dorsal nail region, the underlying skin and soft connective tissue, as well as the bone. Fractures were immediately closed using Dermabond. In some samples, the distal portion of the fracture fell off, thus becoming amputations; those samples were excluded from this study. Some digits were scanned using the MicroCT while others were harvested at various time points and processed for histology and immunostaining. All animal use and procedures were in compliance with Tulane University's Institutional Animal Care and Use Committee.

P3 Periosteal Removal

To remove the periosteal tissue from the P3 digit, we used micro-scissors to cut a thin line along the lateral portion of the nail, pulled the nail and underlying soft tissues

up, thus exposing the majority of the dorsal surface of the bone. Using a scalpel, we stripped the outer surface of the bone in an effort to remove the periosteal tissue. Importantly, only the dorsal portion of the bone was scraped with a scalpel; since exposing the ventral portion of the P3 bone would destabilize and injure the nail organ excessively. After scrapping the dorsal surface of the bone, the nail and underlying soft tissues were returned to place, and the wound was closed via Dermabond. Roughly 30 minutes to one hours after periosteum removal and wound closure, the P3 digit was amputated as normal and allowed to heal on its own. Control surgical procedures (nail lifting, Dermabond, and subsequent amputation) were performed on the other hind limb digits. Some digits were scanned using the MicroCT while others were harvested at various time points and processed for histology and immunostaining.

P3 BMP2 Bead Implantation

Preparation of 0.500 μg/μl BMP2 and 0.01% BSA beads was performed as described earlier (Yu, et al., 2012). Beads were placed on the tungsten needle and allowed to air dry. P3 fractures were performed as previously described. Approximately 2 beads were placed along the dorsal periosteal surface of the bone, underneath the nail, just proximal to the fracture gap. The fracture gap was then immediately closed with Dermabond. Digits were collected 8 days after fracture and BMP2 or BSA treatment and processed for histology and immunostaining.

P3 Bone and Nail Grafts into P2 Fracture Milieu

To assess the P3 healing environment, we grafted either the 7DPA amputated P3 bone or the 1 DPA amputated nail organ into the P2 fracture milieu. For grafting the 7 DPA amputated bone, we amputated digits 2 and 4 of one hind paw and allowed the amputation injuries to heal for seven days. At 7 DPA, we carefully amputated the whole P3 bone, including the nail organ, by severing the digit just proximal to the P2-P3 joint. The surrounding soft tissues and nail organ were separated from the P3 bone; care was taken to ensure the bone tissue was not injured in the process. At the time of P3 bone grafting, P2 fractures were carried out on digits 2 and 4 on the other hind paw of the same mouse as described in Chapter One. Grafts were placed in the same mouse to circumvent host rejection. Note the P3 amputation and the P2 fracture were carried out at separate time points, i.e., a 7 DPA P3 bone was placed into a 0 DPF fracture. Our P2 fractures are essentially 'open fractures', since we must open the surrounding tissues in order to break the bone. In the same opening, we placed the amputated 7 DPA P3 bone, closed the opening with Dermabond, and allowed the wound to heal for 11 days. At 11 DPF, the digits were collected and processed for histology and immunohistochemistry. For grafting the 1 DPA nail organ into the fracture milieu, we amputated the P3 bone on digits 2 and 4 on one hind paw, and allowed the injury to heal for 1 day. At 1 DPA, the nail organ was isolated from the bone via severing the P3 digit proximal to the P2-P3 joint, teasing away the bone, thus leaving the nail organ intact. One the other hind paw of the same mouse, we placed the 1 DPA nail graft into a newly fractured P2 bone environment. In addition to lengthwise, the width of the nail is a curved structure; we placed the nail (matrix side down) on the proximal bone fragment within the P2 fracture,

whereby the nail curved over the bone, thus lightly encasing it. After grafting, we closed the open wound using Dermabond, and allowed the digit to heal for 11 days. At 11 DPF, the digits were collected and processed for histology and immunohistochemistry.

Histological Staining

Histological staining was performed as outline in Chapters One and Two: All digits were collected at various time points and fixed between 24-96 hours in Z-fix (Anatech, LTD) at room temperature. Digits were then decalcified using Decalcifier I (Surgipath) for at least 8 hours, and no more than 24 hours. Digits were processed using a graded ethanol series, xylenes, and immersed in paraffin wax. Digits embedded in paraffin wax were sectioned at 4-5 μm thickness. In order to analyze the entire digit, digits were sectioned completely, and serial sections were created. Mallory's Trichrome staining was performed to determine the relative amounts of cartilage and bone formation. In order to visualize cartilage formation specifically, Toluidine blue staining was performed. All samples were imaged using the Olympus DP72 microscope using DP2-BSW software.

Antibodies and Immunohistochemistry

Immunostaining was performed as outline in Chapters One and Two: Digits were harvested and treated as described in Histological Staining. Slides were incubated at 60 degrees Celsius for 45 minutes, followed by a 15 minute-96 hour incubation at 37 degrees Celsius. Antigen retrieval was performed using Proteinase K solution (Dako) and incubated at either room temp for 12 minutes, or heat retrieval performed in 1X

citrate buffer solution (Dako). Slides were blocked using Protein Block for 30 minutes to 1 hour (Dako). Slides were incubated with primary antibody/antibodies over night at 4 degrees, washed in TBST solution and incubated in secondary antibody/antibodies for 45 minutes at room temperature. Slides were subsequently incubated in DAPI solution, dried, and mounted with Prolong Gold (Invitrogen). Primary antibodies used include Mouse-Anti Collagen Type II (Acris) at a 1:200 concentration and Proteinase K retrieval at room temp , Rabbit-Anti Osterix, SP7 (Abcam) at a 1:400 concentration and heat retrieval, and Rabbit-anti-Aggrecan (Millipore) at a 1:300 concentration using heat retrieval. Secondary antibodies used include Goat-Anti Rabbit 488 (Invitrogen) and Goat-Anti Mouse 647 (Invitrogen), all at 1:500 concentration in antibody diluent (Invitrogen). All samples were imaged using the Olympus BX61 microscope, with the Slidebook software.

Microtomography Scans & Fiji

P3 digits were scanned from one day post amputation, fracture, or periosteum removal and weekly thereafter for up to 5 weeks using the vivaCT 40 (SCANCO Medical, Wayne, PA) as described previously (Fernando, et al., 2011). Digits were scanned at 10.5μm voxel size and Energy 45 kVp and saved as dicom files. Using the boneJ Fiji plugin, 3-D reconstructed images were created in which bone volume, length, and relative bone thickness were measured.

III. Results

MicroCT Analysis of the Fractured P3 Bone indicates Bone Formation within the Fracture Gap with very little Periosteal Callus Formation and differences in the Bone Degradation Response vs. the Amputation Injury

To gain a greater understanding of the bone healing response post P3 fracture, we fractured digits and tracked their bone healing response, changes in bone volume, and relative thickness via the MicroCT; tracking digits beginning at 1 day post fracture (DPF), through various time points, and ending our study at 28 DPF (n = 4). To directly compare the P3 fracture response to the amputation response, we scanned amputated P3 digits in conjunction with the fractured digits, tracking their bone healing response and changes in bone volume (n = 4). We fractured the bone at approximately the distal amputation level via a scalpel, effectively creating an open fracture, and closed the open wound using Dermabond. Our aim was to create a standardized fracture plane; however there was considerable variation between fracture levels, either due to animal variability or technical error. Some fractured digits did not retain their distal half, with the bone, nail, and surrounding soft tissues distal to the fracture gap falling off; those digits were excluded from this study.

MicroCT 3-D reconstructed images of the fractured digit indicate the fracture plane is at an equivalent level as the amputation plane at 1DPF and 1 DPA, respectively (Fig. 3.1, A and H). The 3-D images at 3 DPF/DPA indicate both injured bones appear unchanged from the previous time point, however fractured digits show a slight decrease in average bone volume compared to amputated digits, yet this change is insignificant (Fig. 3.1, B, I, O, $p < 0.05$). By 7 DPF, the fracture gap appears to be increasing in size, presumably due to the forward growth of the nail organ and overlying soft connective

tissue inadvertently 'pulling' the distal bone fragment forward (discussed further in Fig. 3.2), however the bone does not appear to be undergoing an extensive degradation response as shown in the 7 DPA bone (Fig. 3.1, C and J). Continued bone degradation is apparent in the amputated P3 digits by 10 DPA, with the bone decreasing to 70% its initial volume on average, exhibiting significant differences in volume compared to fractured digits of the same time point (Fig. 3.1, D and K, $p < 0.05$). Of our scanned and/or collected for histology fractured P3 digits, only one exhibited a large degradation response, not shown. At 10 DPF, the fracture gap continues to increase in size, and no new bone formation is apparent in the 3-D image (Fig. 3.1, D). By 14 DPF/DPA, 3-D images show both injured digits are beginning the process of new bone formation, with new bone forming within the fracture gap and new bone islands forming distal to the amputated P3 stump, corresponding to a rise in average bone volume (Fig. 3.1, E and L). At 21 DPF, the fracture space is nearly filled with new bone formation, completely bridging the fracture, and the rough appearance of the new bone as well as the marrow spaces indicate the presence of woven bone within the fracture gap (Fig. 3.1, F). The 21 DPA 3-D image of the amputated digit also indicates a large amount of new bone formation from the previous time point, corresponding to a sharp increase in bone volume (Fig. 3.1, M). By the end of our study at 28 DPF/DPA, the fracture space has been completely filled with bone and the amputated P3 digit has undergone full regeneration (Fig. 3.1, G and N). Note, over the course of the fracture healing response, the formation and remodeling of a periosteal callus was not apparent, with new bone formation primarily localized to the immediate fracture gap, i.e., the endosteal/marrow cavity, thus the healed fracture occurred without lateral expansion of the bone. The 3-D images of

the amputation healing response, conversely, exhibited lateral expansion of the bone, yet whether this was due to a greater periosteal contribution to the regenerating digit and a lower periosteal cellular contribution to the fractured digit was not ascertained.

To further investigate the seeming lack of periosteal callus formation in the fractured digits, we created bone thickness maps using the MicroCT. All images are relative to each other, with thicker bone exhibiting white and yellow colors, indicating lamellar or more mature bone, and thinner bone comprised of blue and purple colors, thus indicative of newly formed bone or bone undergoing remodeling. Using another fractured digit than depicted in the prior 3-D reconstructed images, and therefore providing more evidence to show the lack of large periosteal callus, we show at 10 DPF no new bone formation is evident along the periosteal surface of the fractured digit, however thin bone is present within the fracture gap, as seen by the purple areas, but whether this is newly formed bone or older bone undergoing remodeling is unclear (Fig. 3.1, P, arrows). The same digit, at 14 DPF shows new bone formation on the periosteal surface adjacent to the fracture space (yellow arrowhead), as well as new bone formation within the gap (Fig. 3.1, Q, arrow). Seven days later, at 21 DPF, the fracture space has been filled and is largely comprised of purple bone areas (arrow), indicating localized new bone formation, with only a small area of new bone formation on the dorsal portion of the periosteal surface (Fig. 3.1, R, yellow arrowhead). Thus, the MicroCT 3-D images reveal the fractured P3 digit heals primarily via a medullary callus, with only minimal bone formation along the injured periosteal surface.

P ⟷ D

	Fracture		Amputation
1DPF	A	1DPA	H
3DPF	B	3DPA	I
7DPF	C	7DPA	J
10DPF	D	10DPA	K
14DPF	E	14DPA	L
21 DPF	F	21 DPFA	M
28DPF	G	28DPA	N

Bone Volume Changes Post P3 Fracture and Amputation

Fracture: n = 4digits   Amputation: n = 4digits   * =Significance, $p < 0.05$

P   10DPF   Q   14DPF   R   21DPF
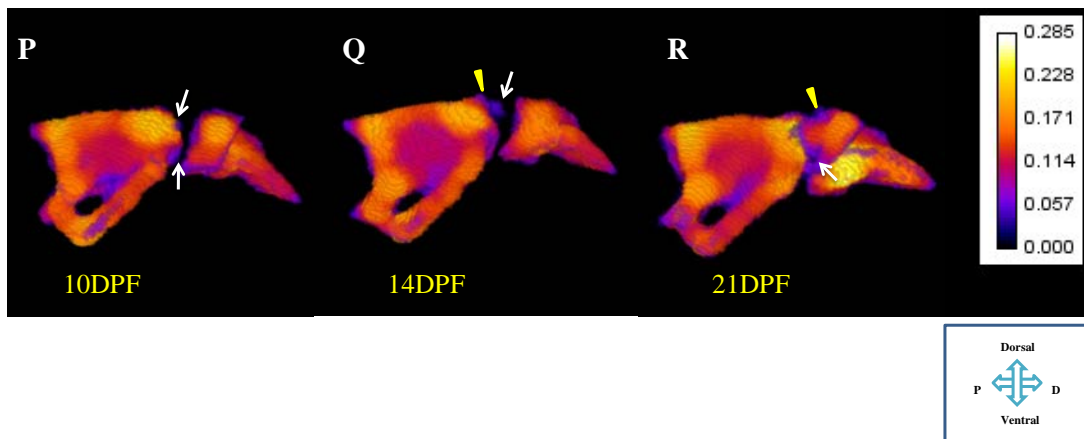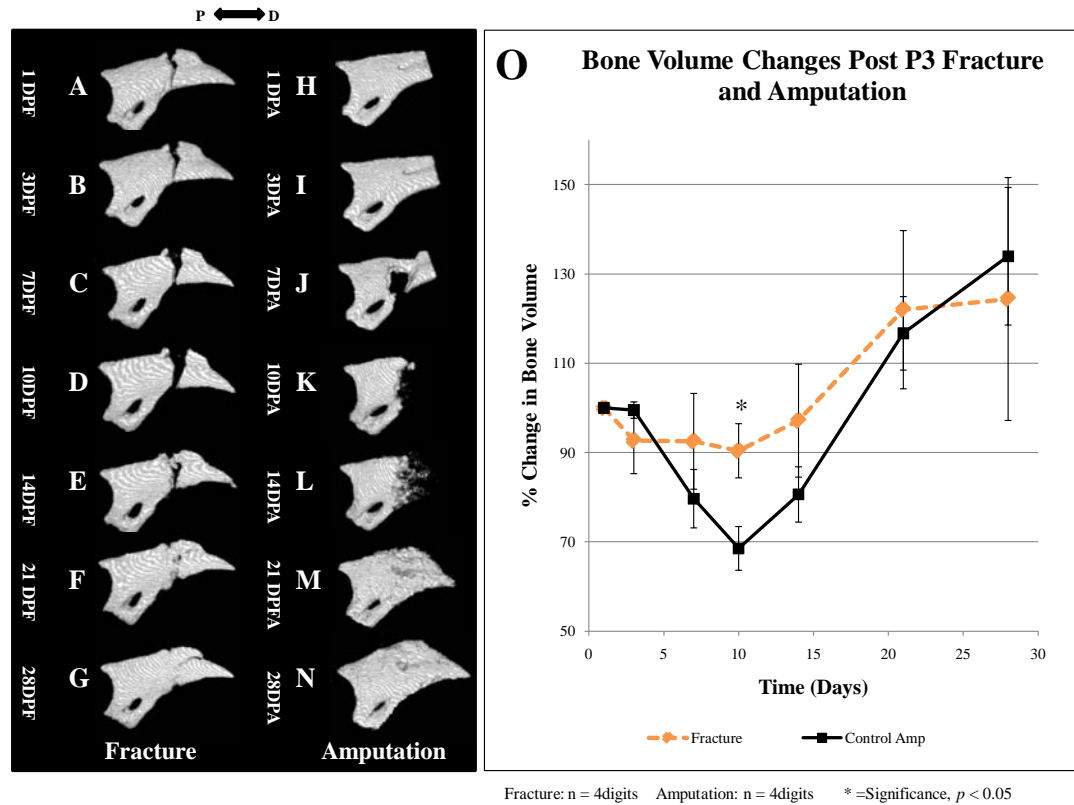
Figure 3.1 – Dawson et al.

Fig 3.1 MicroCT analysis of the P3 fracture and amputation healing responses. (A-G) MicroCT 3-D reconstructed images of the fractured P3 digit show the lack of large degradation response post fracture, followed by bridging of the fracture gap by 21 DPF. Note the lack of periosteal growth adjacent to the fracture gap. (H-N) MicroCT 3-D reconstructed images of the amputated P3 digit show the large degradation response evident by 7 DPA, followed by new bone formation evident at 14 DPA, and complete regeneration of the digit by 28 DPA. (O) The percent change in bone volume was insignificant at all time points except 10 days post fracture or amputation, coinciding with the lack of degradation response in the fractured digits ($p < 0.05$). (P-R) MicroCT 3-D thickness models show remodeling or newly formed thinner bone as purple, blue, and red shades, with thicker lamellar bone as white and yellows. (P) MicroCT 3-D thickness model of the 10 DPF digits shows thin (purple) bone within the fracture gap (arrows) and no new bone at the periosteal surface adjacent to the fracture gap. (Q) The thickness model of the 14 DPF digit shows new bone formation within the fracture gap (purple bone, arrow) and some new bone formation (purple) adjacent to the periosteal surface (arrowhead). (R) The 21 DPF thickness model shows the fracture gap has been bridged and largely consists of purple (arrow), blue, and red colored bone, while the periosteum shows slight new bone formation/remodeling (arrowhead). Student's *t*-test was used to calculate *P* value, bars specify standard error.

Histology of the P3 Fracture Healing Response Indicates Chondrogenesis within the Injured Endosteal/Marrow Region

To further investigate the P3 bone healing response post fracture, digits were collected and processed for histological staining at specific time points in an attempt to visualize the initial inflammatory response, the formation of both the external callus and the medullary callus, as well as various stages of bone remodeling, thus corresponding to published reports of long bone fracture healing as well as the fracture response of the adjacent digit, P2 (Shapiro, 2008; Schindeler et al., 2008; Chapter One) (Fig. 3.2).

Our histological samples show the initial inflammatory response of the newly fractured P3 bone is characterized by an influx of red blood cells at the fracture site, primarily localized to the soft connective tissue on the dorsal bone surface at 0 DPF (Fig. 3.2, A). Note the fracture plane does not transect the marrow space, however the nail does undergo considerable damage at the fracture cite (Fig. 3.2, A). At 7 DPF, the P3 nail and underlying soft connective tissue of the original fracture level are now located distal to the fracture site, indicating the continued growth of the nail organ and underlying soft connective tissue during P3 fracture healing (Fig. 3.2, B). The fracture level shown at 7 DPF transects the distal marrow region on both the dorsal and ventral portions of the bone, thus depicting the variation in fracture level previously mentioned (Fig. 3.2, B). Cellular condensation is present within the dorsal fracture area (boxed), associated with new bone formation chiefly localized to the marrow region and fracture gap, with very little periosteal response (Fig. 3.2, B). The histological staining at 11 DPF reveals the nail, epithelial wound, and underlying soft connective tissue have continued

their forward growth, thus the bone wound is no longer in direct contact with the overlying originally wounded tissue (Fig. 3.2, C). The 11 DPF injury shown here exhibits a large fracture gap on the dorsal bone surface, with a relatively smaller bone gap on the ventral surface, with only the dorsal injury showing active bone formation (Fig. 3.2, C). The 11DPF periosteal surface spanning the fracture space shows small areas of bone growth without the clear presence of cartilage formation, thereby forming a woven bone external fracture callus (Fig. 3.1, C). Notably, stabilized fractures heal via intramembranous ossification, with a relatively small non-cartilaginous periosteal contribution (Le, et al., 2000; Thompson, et al., 2001; Shapiro, 2008; Histing, et al., 2009; Colnot, 2010). The presence of a medullary callus is also apparent at 11 DPF, with a large area of bone formation spanning the central region of the digit endosteal/marrow space (Fig. 3.2, C). Importantly, immunostaining of a serial section of the endosteal/marrow bone formation at 11 DPF indicated the presence of osterix (a transcription factor involved in osteoblast differentiation) positive cells within the cellular mass, and the lack of Col2 (a marker for chondrocytes) positive cells, thus confirming bone formation without an intermediate cartilaginous step (not shown). Histological staining at 13 DPF indicates the nail organ and surrounding soft tissues of the digit have been replaced and/or healed, while the bone is undergoing active new cellular growth (Fig. 3.2, D). The relatively small dorsal periosteal callus (arrowheads) appears comprised of woven bone at 13 DPF (Fig. 3.2, D). Strikingly, the dorsal and ventral endosteal/marrow callus is comprised of a mass of round cells seemingly undergoing hypertrophy, indicative of cartilaginous growth (Fig. 3.2, D. Boxed). Note, the dorsally located soft connective tissue juxtaposed between the nail and the bone is densely

populated with cells between 7 and 13 DPF (Fig. 3.2, B, C, and D) and loosely populated with cells and fibrous tissue at later time points (Fig. 3.2, E and F). Earlier studies have reported the adult P3 bone undergoes a secondary degradation response mediated via osteoclasts post amputation injury, beginning at approximately 7 DPA, yet no apparent bone degradation is observed at 7, 11, or 13 days following the fracture injury (Fernando, et al., 2012). By 21 DPF, the fracture gap has been completely bridged and the fracture callus is composed of woven bone, evident from the irregularly shaped bone and plentiful marrow spaces (Fig. 3.2, E). The 28 DPF fracture callus shows signs of continued bone remodeling, possibly indicating the bone is undergoing remodeling into a lamellar structure, much like that of uninjured P3 bone (Fig. 3.2, F). Note, the fracture plane in both the 21 and 28 DPF samples appears to be distal to the marrow space, once again showing the fracture level variability between the samples (Fig. 3.2, E and F). Taken as a whole, histological sections indicate the periosteal response of the fractured P3 bone undergoes an intramembranous bone formation pathway without a cartilaginous intermediate, thus similar to previous reports of stabilized bone fracture healing (Le, et al., 2000; Thompson, et al., 2001; Gerstenfeld, 2003; Einhorn, 2005; Histing, et al., 2009; Colnot, 2010; Yu, et al, 2012a). However, the cartilaginous formation within the marrow cavity is, to our knowledge, a novel finding, yet it contradicts the assumption the P3 fracture healing milieu is an inherently stable model due to stability imposed by the nail organ.
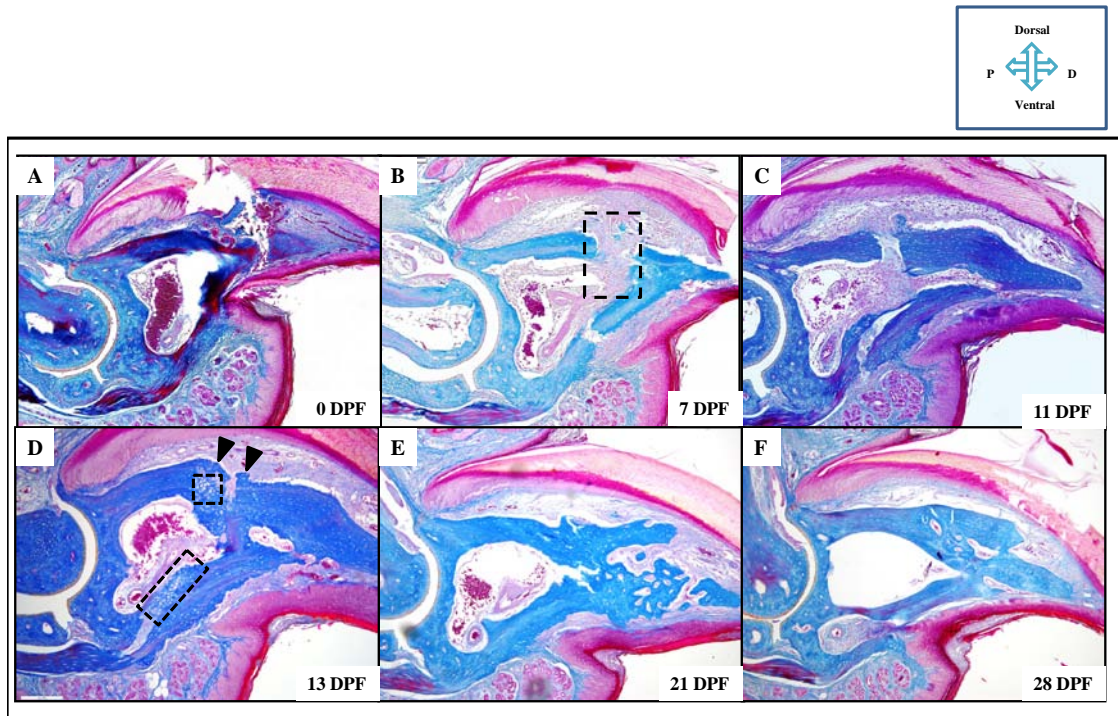
Figure 3.2 – Dawson et al.

Fig. 3.2 Histological analysis of the P3 fracture healing response indicates an endochondral healing event within the endosteal/marrow space. (A) Mallory's staining of the 0 DPF digit shows the digit immediately after fracture, with the fracture transecting multiple tissue types, including the nail, underlying skin and connective tissue, and the bone. (B) The 7 DPF digit shows cellular condensation within the fracture gap (boxed). (C) The 11 DPF digit shows a small amount of new formation along the periosteal surface, with the majority of cell condensation/new bone formation within the endosteal/marrow space. (D) Arrowheads indicate periosteal intramembranous bone growth at 13 DPF. (D) Note the areas of chondrogenesis within the endosteal/marrow space (boxed). (E) The fracture gap has been bridged by 21 DPF, consisting of woven bone. (F) The 28 DPF digit is undergoing remodeling into a lamellar structure, evident from the smooth surface of the bone. All samples 100X, sectioned at 5μm.

Immunohistochemistry Probing for Osteoblasts and Chondrocytes over the course of P3 Fracture Healing Indicates Transient Endosteal/Marrow localized Chondrogenesis at 13 DPF

The localization of cartilage to the periosteal callus and the absence of cartilage within the endosteal/marrow space has long been established in unstabilized long bone fracture (Le, et al., 2000; Gerstenfeld, 2003; Einhorn, 2005; Histing, et al., 2009; Colnot, 2010; Yu, et al, 2012a). Moreover, an equivalent periosteal localization of cartilage and direct bone formation within the endosteal/marrow space was found post fracture of the adjacent digit, P2 (Chapter One). Furthermore, in stabilized fractures which do not heal via an external cartilaginous intermediate, and instead heal through intramembranous ossification, the presence of endosteal/marrow chondrogenesis has not been reported (Le, et al., 2000; Shapiro, 2008; Histing, et al., 2009). To confirm our histological findings of a chondrocytes localized to the endosteal/marrow region post P3 fracture, we probed serial sections of fractured digits harvested at various time points (7, 11, 13, and 21 DPF) for osteoblasts and chondrocytes, using Osx and Col2, respectively. At 7 DPF, the endosteal/marrow region shows cells staining immunopositive for Osx, principally localized to the distal endosteal surface (Fig. 3.3, A). An adjacent section stained for chondrocytes indicates the lack of Col2 immunostaining within the endosteal/marrow space of the fractured digit at 7 DPF (Fig. 3.3, E). Immunostaining for Osx shows many positive cells within the distal endosteal/marrow space of the digit at 11 DPF, as well as several positive cells along the periosteal surface, and a large area of staining within the fracture gap (boxed) (Fig. 3.3, B). Conversely, an adjacent serial section indicates no

Col2 positive cells, thus the lack of chondrocytes at 11 DPF, both along the periosteal surface, the fracture gap (boxed) and within the endosteal/marrow space (Fig. 3.3, F). At 13 DPF, the endosteal/marrow space of the fractured digit tests immunopositive for Osx, yet the cells are no longer associated with the endosteal surface, instead, Osx immunopositive cells are scattered within the marrow cavity (Fig. 3.3, C). Unlike the earlier time points, the 13 DPF digit tests immunopositive for Col2, showing a large mass of chondrocytes within the marrow cavity (boxed), and no chondrogenesis along the periosteal surface (not shown) (Fig. 3.3, G). Importantly, not all of the 13 DPF fractured digits assayed were positive for chondrocytes within the marrow cavity (2 of the 4 samples processed for histology). By 21 DPF, Osx positive cells are primarily localized to the distal periosteal surface, and the fracture area does not test immunopositive for Col2, however whether the fracture space of this particular sample ever contained chondrocytes is unknown (Fig. 3.3, G and H).

To gain a greater understanding of the chondrocytes localized to the endosteal/marrow cavity of the fractured P3 digit, we performed various histological stains and immunostaining on a 13 DPF serial sectioned sample (Fig. 3.4). Corresponding to the Mallory stained section (A), toluidine blue staining, a stain used to highlight cartilaginous tissue, shows a cartilaginous mass between the ventral endosteal bone surface and the large vessel within the marrow compartment (Fig. 3.4, B, dashed box). Faint toluidine blue staining of the dorsal callus, located within the fracture gap (solid box), indicates the presence of cartilage (Fig. 3.4, B). Immunostaining for Col2 confirms the toluidine blue findings, showing the large mass within the marrow cavity is

7 DPF   **11 DPF**   **13 DPF**   **21 DPF**
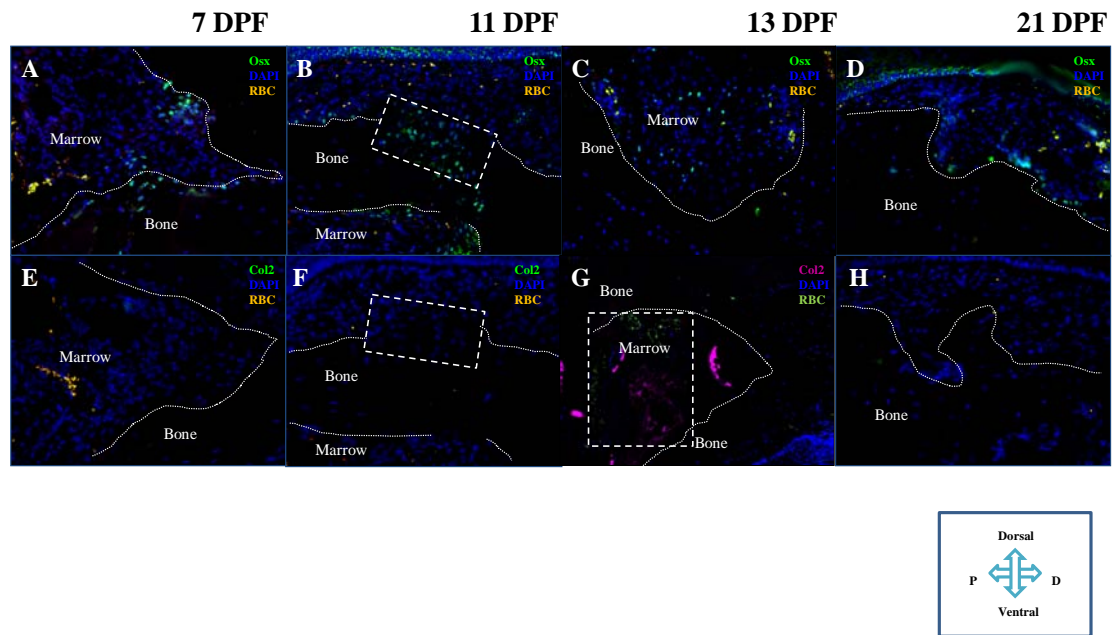
Figure 3.3 – Dawson et al.

Fig. 3.3 Immunohistochemistry probing for osteoblasts and chondrocytes during P3 fracture healing. (A) Osx immunostaining for osteoblasts reveals positive cells within the distal portion of the endosteal/marrow region at 7 DPF. (B) By 11 DPF, Osx-positive cells are present within the fracture gap (boxed), the endosteum, and well as several cells along the periosteal surface. (C) At 13 DPF, Osx-positive cells are localized to the central marrow cavity. (D) At 21 DPF, Osx positive cells are found lining the periosteum of the healed bone. (E) Chondrocyte immunostaining for Col2 shows no positive cells in the 7 DPF digit. (F) The 11 DPF fracture gap (boxed) is not comprised of Col2 positive cells. (G) The 13 DPF digit shows a large area of Col2 positive cells localized to the endosteal/marrow region (boxed). (H) By 21 DPF no Col2 positive cells are found within the fracture space. All samples 100X, sectioned at 5µm.

comprised of chondrocytes embedded in a Collagen 2 matrix, with large round chondrocytes, indicative of terminal differentiation to hypertrophy (Fig. 3.4, C). We also probed the sample using another cartilage matrix marker, Aggrecan (Agc1), and observed immunopositive cells within the dorsal fracture space (Fig. 3.4, D). To determine the extent of bone formation within the endosteal/marrow region of the 13 DPF digit, we probed for Osx positive cells and observed several positive cells (arrowheads) located ventral to the marrow callus (outlined oval), and several positive cells located dorsal to the callus (not shown) (Fig. 3.4, E). Importantly, the periosteal cartilaginous callus formed after long bone and P2 digit fracture has been shown to be encircled by a thin layer of osteoblasts (Gerstenfeld, et al., 2003; Chapter One), thus our P3 fracture model shows a novel inverted healing response, with the osteoblasts surrounding the cartilaginous callus within the endosteal/marrow space.

Cartilage specific histological staining reveals Chondrogenesis in the Marrow Space of the Proximal P3 Fracture, but not the Distal Fracture

As previously mentioned, we were unable to standardize the P3 fracture level, either due to animal variability or technical error. We observed that fractures were either well within the endosteal/marrow region, thus within the proximal portions of the bone (Fig. 3.5, A and B), or, the fractures were located at a more distal level, with very little injury to the endosteal/ marrow cavity (Fig. 3.5, C). We observed that two of the four 13 DPF fractures were distally located, and showed no cartilage formation; the other two
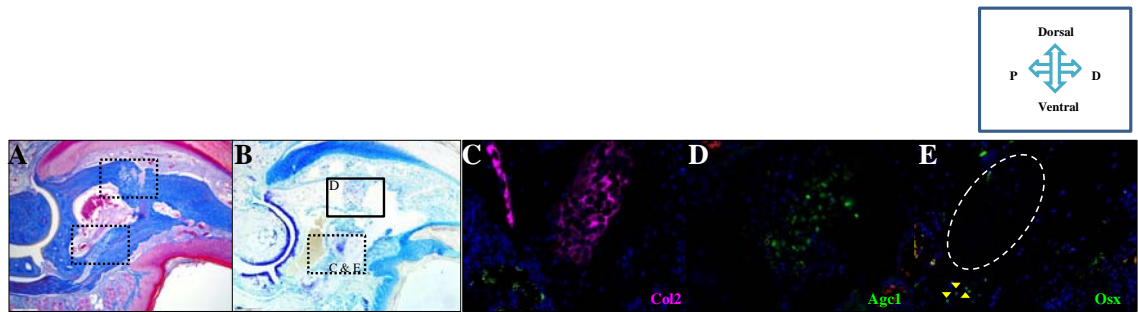
Figure 3.4 – Dawson et al.

Fig. 3.4 Chondrogenesis Localized to the Marrow/Endosteal Region of the Proximal P3 Fracture at 13DPF. (A) Mallory's staining of the proximal fracture at 13 DPF shows chondrocytes localized to the dorsal and ventral fracture gaps (boxed). (B) Toluidine blue staining shows the ventral callus is positive for chondrocytes, as well as light staining localized to the dorsal callus. Note, the articular cartilage is an internal positive control for toluidine blue staining. (C) Col2 immunostaining of the ventral fracture callus shows immunopositive cells localized to the endosteal/marrow region. (D) Agc1 immunostaining of the dorsal fracture callus shows immunopositive cells. (E) Osx immunostaining for osteoblasts indicates immunopositive cells are located below the endosteal/marrow cartilaginous fracture callus (outlined). All samples 100X, sectioned at 5μm.

fractures collected were fractured within the proximal marrow region, and did show medullary chondrogenesis. To explore this further, we stained serial sectioned slides with both Mallory's Trichrome Stain and toluidine blue stain, a stain useful in cartilage visualization. Mallory's staining of a proximally located fracture shows the fracture level is adjacent to the P3 joint, yet does not invade the epiphysis, with a large area of chondrogenesis within the endosteal/marrow region (Fig. 3.5, D, boxed). Corresponding to the Mallory's image, toluidine blue staining reveals a large stained mass of chondrocytes within the endosteal/marrow cavity, with the cartilaginous mass comprised of both proliferating and large round hypertrophic chondrocytes (note: the articular cartilage of the P2-P3 joint stains with toluidine blue as well, acting as an internal staining control) (Fig. 3.5, G, boxed). Importantly, we observed no cartilage formation along the periosteal surface of the proximally fractured P3 digit. Mallory's staining of the distally fractured bone shows woven bone formation within the fracture gap (outlined), with no evidence of chondrogenesis, either within the endosteal/marrow space, the fracture gap, or the periosteal surface (Fig. 3.5, E). Toluidine blue staining confirms these findings, showing only blue staining of the articular cartilage, not the fracture space (outlined), the endosteal/marrow space, or the periosteum (Fig. 3.5, H). The endogenous P3 regeneration response occurs via intramembranous ossification, thus bone formation without a cartilaginous intermediate (Han, et al., 2008; Fernando, et al., 2012). To compare our P3 fracture findings to the regeneration response, we performed Mallory staining and Toluidine blue staining on 13 DPA P3 digits. Mallory staining of the 13 DPA digit revealed no chondrogenesis distal to the original bone stump (dashed

line) (Fig. 3.5, F). Likewise, in the toluidine blue stained serial section we observed no cartilage specific staining except for the articular region (Fig. 3.5, I).

BMP2-Treatment of the Periosteal Region of the P3 Fracture Milieu does not Induce Chondrogenesis within the External Callus

Stabilized long bone fracture repair occurs via intramembranous ossification, both within the periosteal and the endosteal/marrow compartment, with predominant cellular contribution to the fracture callus from the endosteal/marrow compartment (Colnot, 2009; etc). Due to the lack of chondrogenesis along the periosteal surface and the relative lack of periosteal callus in the P3 fracture, we indirectly investigated whether or not the injured P3 periosteum was experiencing a localized endogenous stabilized environment, namely via stabilization from the nail encasing the bone. Importantly, it has been shown that the periosteal tissue of a stabilized fracture environment can be induced to form chondrogenesis via BMP2 application, whereby BMP2, a member of the transforming growth factor β (TGF-β) super family of signaling molecules, in effect 'over-rides' the intramembranous healing pathway, and induces endochondral ossification, specifically within periosteal tissue (Yu, et al., 2012a). Therefore, we investigated the chondrogenic potential of the P3 fracture periosteal tissue via the application of 0.500 μg/μl BMP2 or 0.1% BSA coated beads, implanted at the time of fracture, and harvested at 8 DPF. Histological staining indicates a large area of woven bone formation between the nail matrix and the periosteal surface, located proximal to the BMP2 bead at 8 DPF (Fig. 3.6, A). Conversely, we observed no apparent bone formation

Dorsal
P   D
Ventral

A   B   Vs.   C

&

Proximal P3 Fracture, 13DPF   Distal P3 Fracture, 13DPF   Distal P3 Amputation, 13DPA

D   E   F

G   H   I
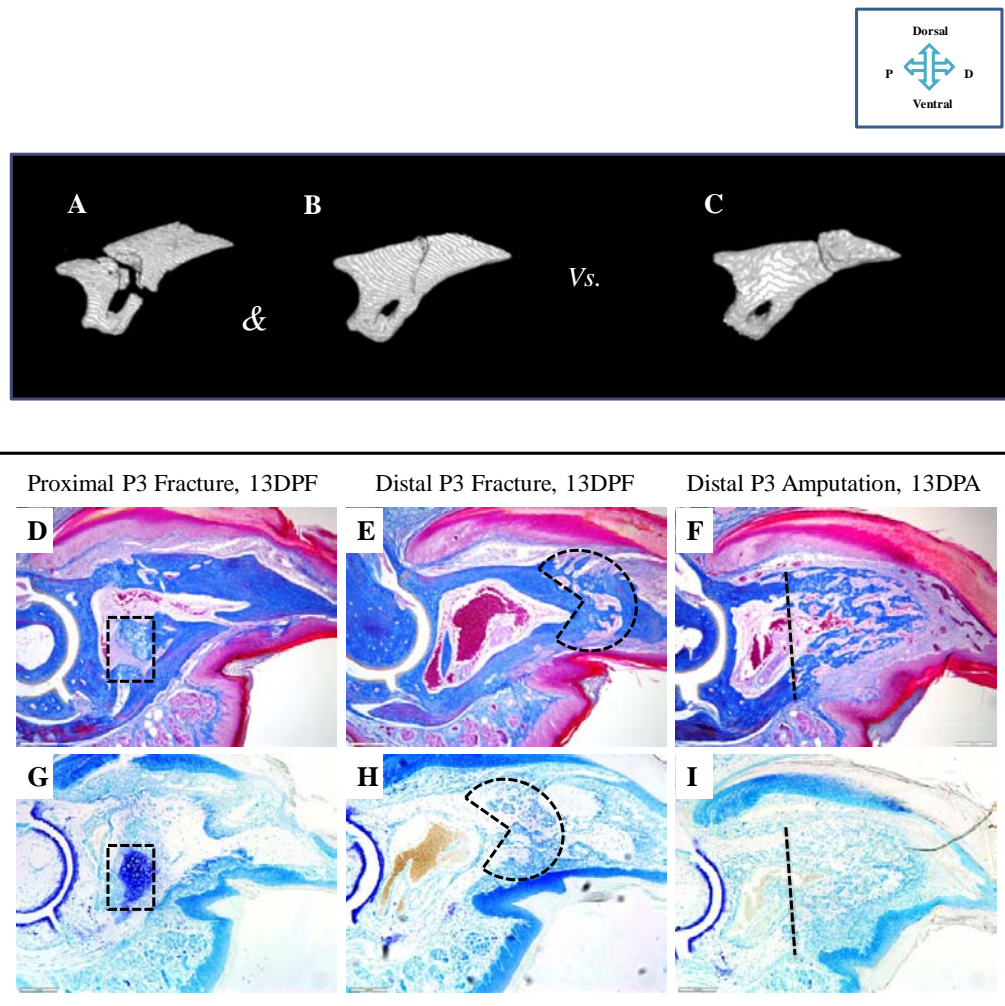
Figure 3.5 – Dawson et al.

Fig 3.5 Toluidine Blue histological staining reveals chondrogenesis in the endosteal/marrow space of the proximal P3 fracture, but not the distal fracture. (A-C) MicroCT 3-D reconstructed images depicting examples of the proximal fracture levels (A and B) and the distal fracture level (C). (D and G) Mallory's and Toluidine blue staining indicates cartilaginous callus formation in the endosteal/marrow space of the 13 DPF P3 proximal P3 fracture. Note the fracture plane is adjacent to the P3 physis. (E and H) Mallory's and Toluidine blue staining of a comparatively distal fracture level shows no cartilaginous growth within the fracture gap at 13 DPF. (F and I) Mallory's and Toluidine blue staining of the amputated P3 bone at 13 DPA shows no cartilaginous growth is associated with the regeneration response. (G-I) The articular cartilage acts as an internal control for positive staining. All samples 100X, sectioned at 5μm.

along the periosteal surface of the BSA-control digit at 8 DPF (Fig. 3.6, D). Osx immunostaining reveals osteoblasts surrounding and within the newly formed woven bone islands along the periosteal surface of the BMP2-treated digit, as well as surrounding the bead (Fig. 3.6, B). Osx immunostaining of the BSA-control sample shows one positive cell along the periosteal surface, thus corresponding to the histological sample (Fig. 3.6, E). Immunostaining for proliferating chondrocytes revealed no Col2 positive cells within the large periosteal response of the BMP2-treated digit, and likewise, no Col2 positive cells in the BSA-control digit (Fig. 3.6, C and F). Our results indicate the response of the periosteal tissue post BMP2 treatment does not match that of published reports of stabilized fracture healing (Yu, et al., 2012a), however, the intramembranous bone formation shown here along the periosteal surface is similar to published reports of the P3 regeneration response post amputation injury (Han, et al., 2008; Fernando, et al., 2011).

MicroCT Reveals Lack of a Robust Regeneration Response in the Absence of the P3 Periosteal Tissue Post Amputation Injury

Our studies show a relative lack of periosteal callus formation post P3 fracture, which indicates a small periosteal cellular contribution to the P3 fracture healing event. Furthermore, it suggests the periosteum may not play a significant role in the healing response of the P3 bone, regardless of the injury. Whether or not the P3 periosteal tissue plays an integral role following amputation injury is unclear, therefore, determining the contribution of the P3 periosteum to the amputation response will give
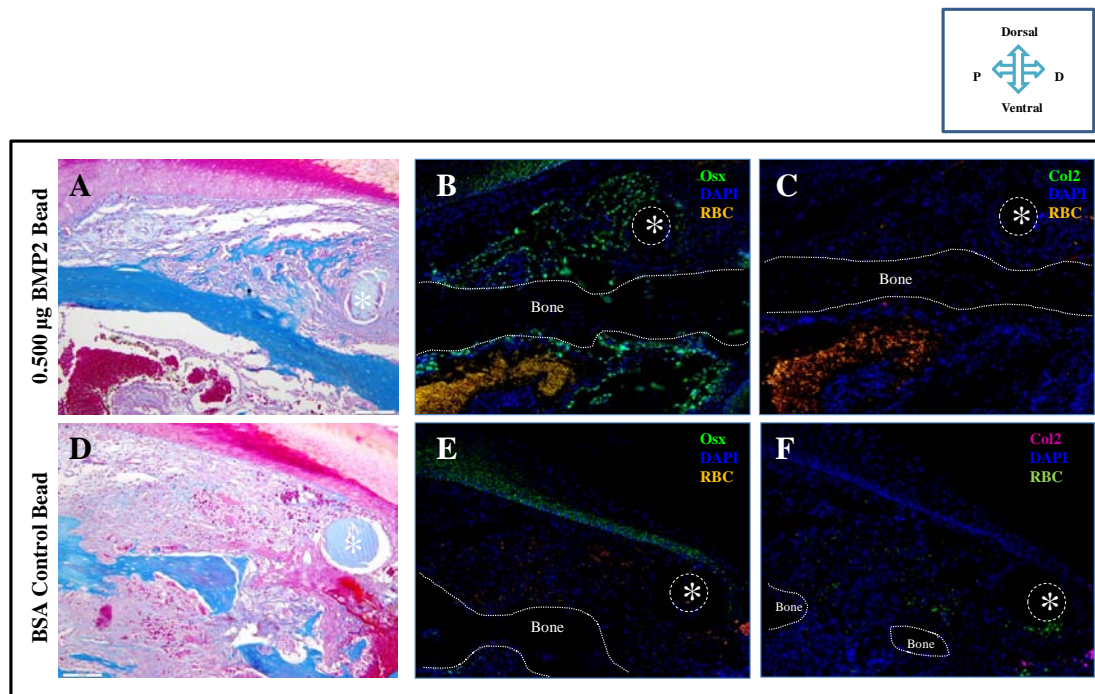
Figure 3.6 – Dawson et al.

Fig. 3.6 BMP2-treatment induces intramembranous ossification along the periosteal surface post P3 fracture. (A-F) P3 digits were fractured and immediately treated with 0.500 µg BMP2 or .01% BSA coated beads adjacent to the periosteal surface and fracture gap, and harvest at 8 DPF. (A) Mallory's staining of the BMP2 treated digit shows boney growth along the periosteal surface adjacent to the bead at 8 DPF. (B) Immunohistochemistry probing for osteoblasts reveals Osx positive cells in the new boney growth along the periosteal surface and adjacent to the BMP2 bead. (C) Note the lack of Col2 positive cells. (D) Mallory's staining of the BSA control digit does not show a large amount of periosteal growth adjacent to the bead at 8 DPF. (E) Immunostaining for Osx positive cells reveals only several immunopositive cells, mainly localized to the marrow region. (F) Col2 immunostaining indicates no chondrocytes are present within the BSA treated sample. Sectioned at 5µm.

us additional insight into the behavior of the tissue post fracture. To test the periosteal contribution to the P3 blastema and regenerate post amputation injury, we stripped the outer layer of the dorsal and medial surfaces of the P3 bone in an attempt to remove the periosteal tissue. The ventral portion of the bone still contained intact periosteal tissue, since removal of all of the periosteum would require excessive injury to the nail organ. Following removal of the tissue, P3 amputations were performed as outlined earlier. In the absence of the periosteum, we aimed to assess the potential periosteal contribution to the P3 regenerate, and thus indirectly determine the contribution of the P3 endosteal/marrow compartment to the regeneration response. Bone healing morphology, volume, and length of P3 digits with periosteum intact and periosteum removed were tracked using the MicroCT beginning at 1 DPA, with continued weekly scans for a total of 5 weeks.

MicroCT 3-D images at 1 DPA reveal that periosteum-intact digits (n = 6) do not show any apparent morphological differences from the periosteum-removed digits (n = 6) (Fig. 3.7, A and G). Likewise, 3-D images of the 7 DPA digits indicate the periosteum-removed digits are undergoing a similar degradation response as the periosteum-intact digits, with no significant differences in bone volume and length between the two groups (Fig. 3.7, B, H, M, and N, $p < 0.05$). At 14 DPA, the periosteum-intact digits are showing signs of new bone formation distal to the bone stump, while the digits lacking the periosteum do not show the formation of new bone islands distal to the bone stump (Fig. 3.7, C and I). The graphical trends also indicate a greater volume and length in the periosteum-intact digits, yet the differences between the periosteum-removed digits are insignificant (Fig. 3.7, M and N, $p < 0.05$). By 21 DPA, the periosteum-intact digits

show a robust regeneration response, with an average increase in volume and length of approximately 40% from the previous time point (Fig. 3.7, D, M and N). 21 DPA digits lacking the periosteum do not show a comparatively robust regeneration response, with only a small amount of new bone formation distal to the bone stump (Fig. 3.7, J). In line with this, statistical analysis reveals significant differences between the periosteum-intact digits and periosteum-removed digits at 21 DPA (Fig. 3.7, Graphs M and N, $p < 0.05$). By 28 DPA, the 3-D image of the periosteum-intact digit shows the digit has completely regenerated, however the digit lacking the periosteum shows a comparatively attenuated regeneration response (Fig. 3.7, E and K). Statistical analysis confirms these findings, with an average overall increase in volume of 170% in periosteum-intact digits, compared to an average increase in volume of 117% in periosteum-removed digits, and an average overall increase in length of 137% in periosteum-intact digits vs. 103% in periosteum-removed digits (Fig. 3.7, M and N, $p < 0.005$). At the end of our study, at 35 DPA, the digits lacking the periosteum lacked a comparable regeneration response to the digits with the periosteum-intact, with clear differences in both bone volume and length compared to the control periosteum-intact digits (Fig. 3.7, F, L, M, and N, $p < 0.005$, significant).

Histology and Immunohistochemistry reveal no Defined Blastema and Truncated Bones post P3 Periosteum Removal and Amputation vs. Control P3 Amputation Digits with Periosteum-Intact

To continue our investigation of the potential periosteal contribution to the regenerating P3 digit, we harvested periosteum-removed and periosteum-intact digits at

P ⟷ D

Figure 3.7 – Dawson et al.

Periosteum-intact: n = 6
Periosteum-removed: n = 6
* =Significance, $p < 0.05$, * * =Significance, $p < 0.005$
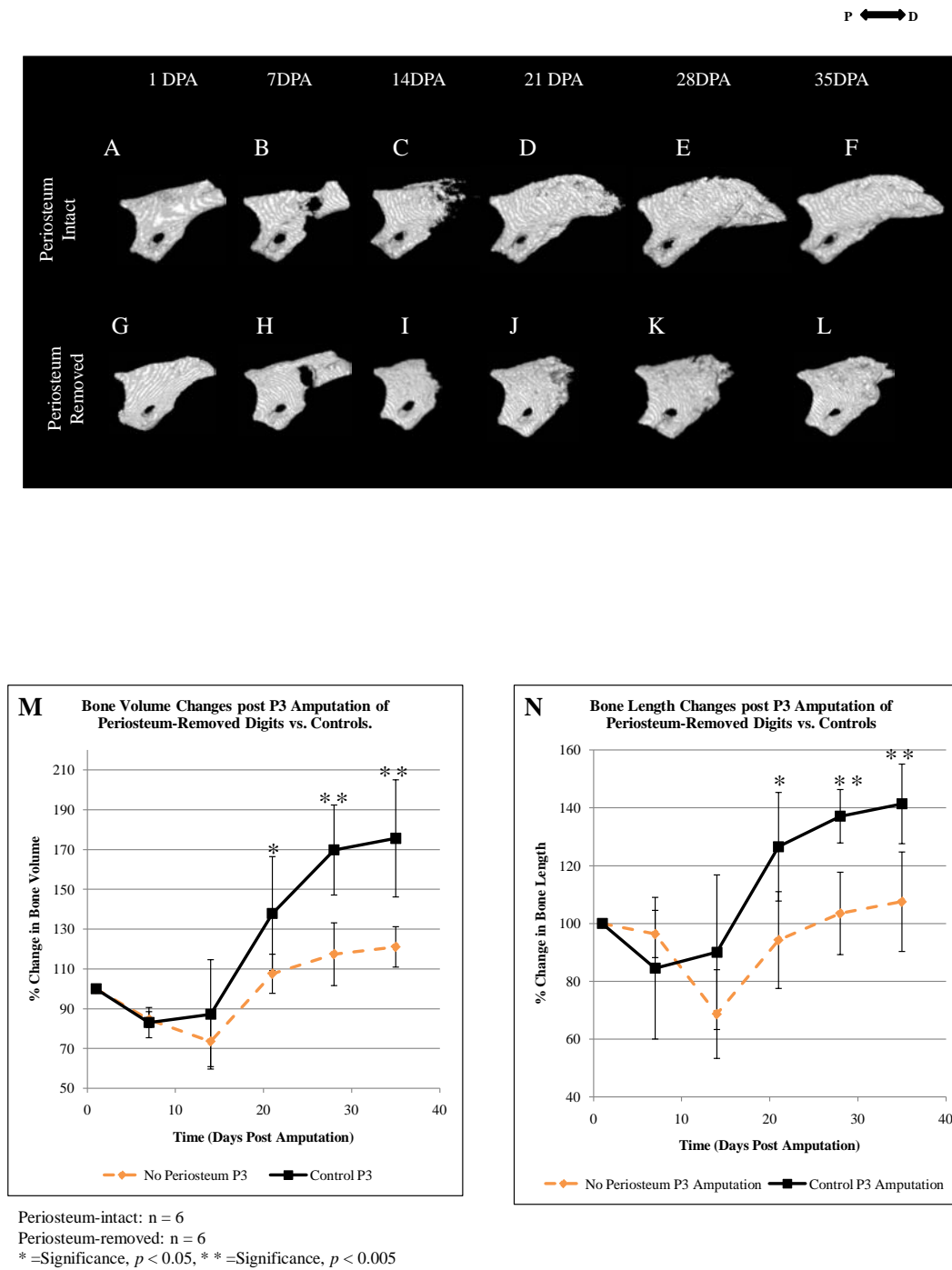
Fig. 3.7 P3 Bones lacking the Periosteum show a decreased volume and length growth response post amputation vs. control Digits. (A-F) MicroCT 3-D reconstructed images of the P3 regeneration response with intact periosteum show the degradation response at 7 DPA, new bone formation at 14 DPA, and complete regeneration by the end of the study, at 35 DPA. (G-L) MicroCT 3-D reconstructed images of the P3 regeneration response with periosteum removed prior to amputation show the degradation response at 7 DPA, similar to the control digit, yet no new bone formation by 14 DPA, culminating in a truncated bone lacking distal growth by the end of the study, at 35 DPA. (M and N) The percent change in bone volume and length was insignificant between the two groups during the degradation response (7 DPA) and the initial bone re-growth (14 DPA) ($p < 0.05$), yet 21 DPA showed significant differences between the two groups ($p < 0.05$), as well as 28 and 35 DPA ($p < 0.005$). Student's *t*-test was used to calculate *P* value, bars specify standard error.

specific time points: the degradation event at 7 DPA, blastema formation at 10 DPA, new bone formation at 14 DPA, and near complete regeneration of the amputated digit at 28 DPA. Mallory stained 7 DPA digits with the periosteum-intact show a large degradation response at 7 DPA, coinciding with published reports of the regenerating digit (Fernando, et al., 2012) (Fig. 3.8, A). Likewise, we observed a similar bone degradation response in the P3 digits lacking a periosteum at 7 DPA, indicating the periosteal tissue is not necessary for the degradation response (Fig. 3.8, E). By 10 DPA, the periosteum-intact digits exhibit a large blastema distal to the bone stump, as well as new woven bone formation within the proximal blastema region, including several boney formations contiguous with the bone stump (Fig. 3.8, B). Conversely, the 10 DPA periosteum-removed digit has not undergone wound closure, lacks a defined blastema, and shows no new bone formation along the periosteal surface (Fig. 3.8, F). Probing for osteoblasts, we performed immunohistochemistry using Osx and observed immunopositive cells distal to the bone stump of the 10 DPA periosteum-intact digit (outlined), coinciding with the histological section (B) (Fig. 3.8, I). The periosteum-removed digit, however, lacked robust immunostaining for Osx distal to the bone stump, showing several positive cells adjacent to the bone stump (boxed), as well as positive cells within the endosteal marrow region (oval), indicating that in the absence of the P3 periosteum, bone formation post amputation is attenuated (Fig. 3.8, J). At 14 DPA, the periosteum-intact digits show robust new bone formation within the proximal blastema and the formation of new boney islands in the distal portion of the blastema (arrowhead) (Fig. 3.8, C). We observed a small blastema in the 14 DPA periosteum-removed digit and the presence of new woven bone, yet the new bone formation remained confined to

the space surrounding the marrow, without the distal elongation seen in the periosteum-intact digit (Fig. 3.8, G). Additionally, the nail appears truncated at 14 DPA, lacking distal growth. Immunohistochemistry for Osx revealed positive cells throughout the 14 DPA blastema (outlined), with a greater proportion of immunopositive cells in the distal region of the blastema, coinciding with areas of new boney island formation (Fig. 3.8, K). Osx immunostaining of the 14 DPA periosteum-removed digits revealed many positive cells within the newly forming bone (outlined), yet the Osx-positive cells were largely localized to bone surrounding all portions of the marrow region, thus in a comparatively proximal region of the digit vs. periosteum-intact digits of the same time point (Fig. 3.8, L). By 28 DPA, the regenerated P3 digit exhibits bone formation extending distal and seemingly dorsal to the bone stump, enveloped by a large nail organ (Fig. 3.8, D). The 28 DPA periosteum-removed digit, however, does not exhibit bone growth along the dorsal periosteal surface, nor does it show robust distal elongation (Fig. 3.8, H). The 28 DPA periosteum-removed digit did feature a long nail, yet the nail was curved out of the plane of the section, indicating that in the presence of a long nail, the periosteum-removed digit lacks distal bone growth. Taken together, our studies show the periosteal tissue of the amputated P3 bone may contribute greatly to the blastema and to distal bone growth of the regenerate.

Tissue Grafting Studies indicate the P3 Nail Matrix may Inhibit Periosteal Chondrogenesis
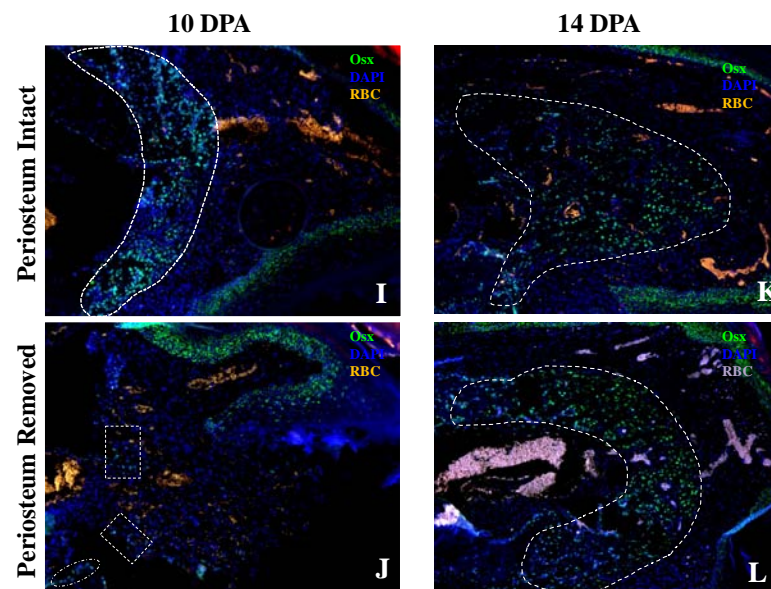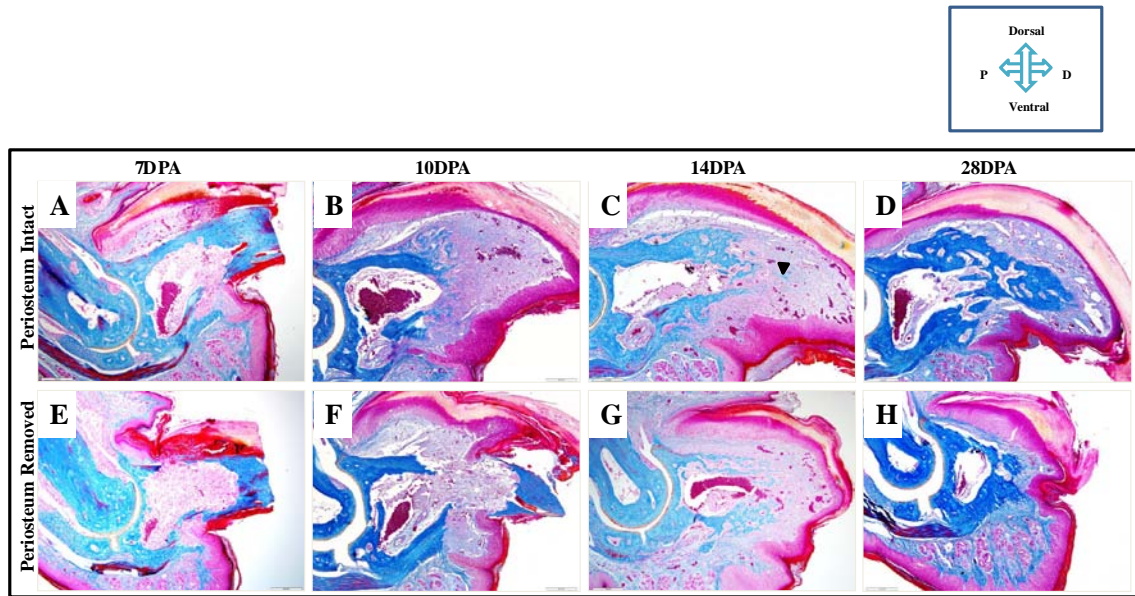
Figure 3.8 – Dawson et al.

Fig. 3.8 Histology and Immunohistochemistry reveal no defined blastema, less bone formation, and truncated bones post P3 Periosteum Removal and Amputation vs. Control P3 amputation digits. (A and E) Mallory's staining of the control periosteum-intact and the periosteum removed P3 digits show they undergo a similar 7 DPA bone degradation response. (B and F) AT 10 DPA, the digit without periosteum shows no new bone formation, no defined blastema, and a delay in wound closure compared to the control digit with intact periosteum. (I and J) Immunohistochemistry of the 10 DPA digit with intact periosteum shows Osx positive cells within the blastema (outlined), yet the digit lacking the periosteum shows comparatively less osteoblasts, with several Osx positive cells distal to the bone stump (boxed), and some within the endosteum/marrow space (oval). (C and G) Mallory's staining of the 14 DPA digit with intact periosteum shows new bone formation extending distal to the bone stump, as well as new boney island formation in the distal blastema (arrowhead), while the digit lacking the periosteum shows proximal bone remodeling and a shorter overall bone. (K and L) Accordingly, immunohistochemistry of the 14 DPA digit with intact periosteum reveals a large area of new bone formation (outlined) in the control digit, while the digit lacking the periosteum shows a more proximal level of bone growth. (D and H) Mallory's staining of the regenerated digit with intact periosteum shows large distal bone growth at 28 DPA, whereas the digit lacking the periosteum exhibits a truncated bone. All samples 100X, sectioned at 5μm.

Our studies indicate the fractured P3 bone undergoes healing without the formation of a periosteal chondrogenic callus, exhibits a novel fracture healing chondrogenic response within the endosteal/marrow space, and its presumed periosteal cells respond to BMP2 treatment unlike any other periosteal cells of the long bones. However, while the periosteum may potentially play a minimal/perplexing role in P3 fracture healing, we have shown the P3 periosteal tissue play a role in the robust intramembranous regenerative response post amputation. In an effort to further investigate the P3 periosteal intramembranous healing pathway, we tested if the unique extrinsic environment of P3, namely, the nail organ and associated epidermal components, played a role in the healing mechanism. In order to do so, P3 digits were amputated and allowed to heal for one day, and at 1 DPA, the nail organ with matrix intact was grafted into a newly fractured P2 digit of the same mouse. The fractured P2 digit is a highly chondrogenic environment, therefore an ideal environment to test the potential anti-chondrogenic properties of the P3 nail/nail matrix (Chapter One). Digits were harvested 11 days post grafting and analyzed for chondrogenesis/bone formation along the periosteal surface of the fractured P2 bone adjacent to the nail organ transplant. As a control, P3 nails without intact matrix were grafted into the P2 fracture environment. Histological staining shows the location of the grafted nail/nail matrix on the dorsal portion of the sample (outlined) and a lack of chondrogenesis along the dorsal portion of the proximal fracture fragment directly below the nail/nail matrix graft (Fig. 3.9, A). A small amount of chondrogenesis is present on the ventral portion of the proximal fracture fragment and bone formation on the distal dorsal fracture fragment (boxed) (Fig. 3.9, A). On a serial sectioned sample in which we performed immunohistochemistry for Col2 we

observed no positive signal, indicating a lack of chondrogenesis within the periosteal compartment of the fractured P2 bone following grafting of the P3 nail/nail matrix (Fig. 3.9, B). Immunohistochemistry for Osx shows positive cells along the periosteal surface of the distal proximal fragment (Fig. 3.9, C, boxed). In the histological staining of the control sample containing only the nail graft, without intact matrix, we observed chondrogenesis along the periosteal surface of the proximal P2 bone fragment, located directly below the nail graft (Fig. 3.9, D, boxed). A small amount of new chondrogenesis was also observed on the distal bone fragment (D, circled). Immunohistochemistry for Aggrecan confirmed the presence of chondrocytes, with positive staining along the periosteal surface of the proximal bone fragment below the grafted nail (Fig. 3.9, E, boxed). Probing for osteoblasts revealed Osx-positive cells along the periosteal surface of both the proximal and distal bone fragments in the control sample (Fig.3.9, F, solid outline).

Tissue Grafting Studies indicate the Amputated P3 Bone Intramembranous Ossification healing Response is an Intrinsic Event

In order to determine if the P3 bone tissue acts autonomously, i.e. if the intramembranous bone formation of the P3 periosteum is an intrinsic property of the bone itself, we grafted 7 DPA P3 bones into the newly fractured P2 bone environment of the same mouse. The P3 bone was carefully teased away from the surrounding nail organ and soft tissues in an effort to preserve the periosteal tissue. If the P3 periosteum formed chondrocytes in the highly chondrogenic P2 fracture environment, it would suggest the
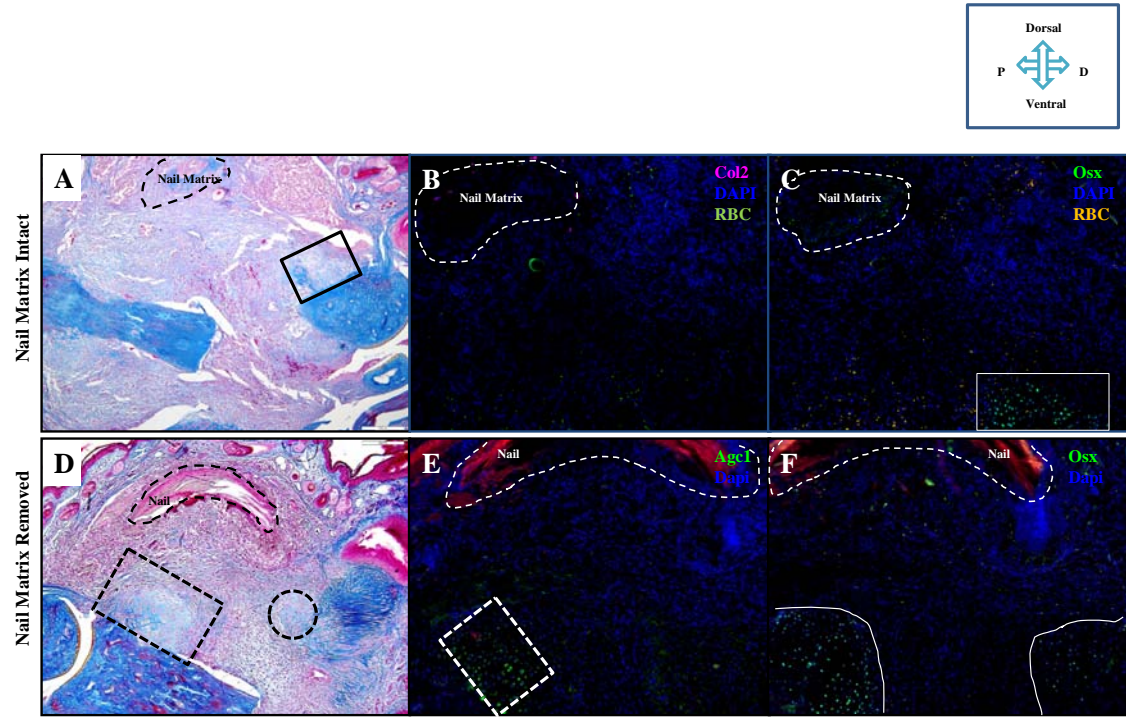
Figure 3.9 – Dawson et al.

Fig. 3.9 Testing the extrinsic properties of the amputated P3 nail organ. (A-C) 1 DPA nail organs (nail and nail matrix) were grafted into the 0 DPA P2 fracture milieu, allowed to heal for 11 days, followed by harvesting the digits and processing for histology and immunohistochemistry. (D-F) Control digits only received grafts of the nail without intact nail matrix. (A) Mallory's staining of the 11 DPF P2 fracture shows the nail matrix located dorsal to the bone (outlined), and no chondrogenesis along the periosteal surface of the bone, yet some new bone formation on the distal fracture fragment (boxed). (B) Col2 immunostaining for chondrocytes indicates no positive cells on the fractured P2 bone. (C) Immunostaining for Osx indicates osteoblasts are present only on the periosteal surface of the distal bone fragment (boxed), coinciding with the bone formation seen in the Mallory's stained sample (A, boxed). (D) Mallory's staining of the control sample lacking the nail matrix shows the grafted nail located dorsal to the bone fragment (outlined), chondrocyte formation on the proximal P2 bone fragment (boxed), and new bone formation on the distal bone fragment (circled). (E) Immunostaining for Agc1 shows chondrocytes are present on the P2 bone, adjacent to the nail graft without intact nail matrix. (F) Osx immunostaining shows osteoblasts are also present on the proximal and distal P2 fracture fragments. All samples 200X, sectioned at 5μm.

P3 intramembranous bone healing response may be dependent on its local environment, such as the surrounding nail/nail matrix. Previously, we had grafted 0 DPA P3 bones into the P2 fracture environment, yet MicroCT data showed no change in bone formation, degradation, and morphology over a several week time span (not shown). 7 DPA P3 bones were grafted instead due to the tissue undergoing an active bone degradation process, which has been shown to be followed by an active bone regeneration process (Fernando, et al., 2011). Samples were collected 11 days post fracture and grafting, and assayed for chondrogenesis along the grafted P3 periosteal surface. Histology shows the grafted P3 bone exhibits intramembranous ossification along the periosteal surface, indicating the intramembranous bone forming potential of P3 is intrinsic to the periosteal tissue (Fig. 4.10, A). Note the bone islands as well as the small areas of continuity between the newly formed bone and the bone stump (Fig. 4.10, A, arrowheads). Using a serial section, we probed for osteoblasts using immunohistochemistry for Osx, and observed positive cells adjacent to the periosteal surface, coinciding with the areas of new formation shown in the histological sample, as well Osx-positive cells within the endosteal/marrow region of the P3 bone (Fig. 4.10, B). Lastly, we assayed the tissue for chondrogenesis via immunostaining for Agc1, and observed no positive staining along the periosteal surface or within the endosteal/marrow region, indicating the P3 periosteal tissue and other bone components do not undergo chondrogenesis in the highly chondrogenic P2 fracture milieu (Fig. 4.10, C). Notably, the presence of the grafted P3 bone did not deter cartilage formation of the host P2 bone (not shown).
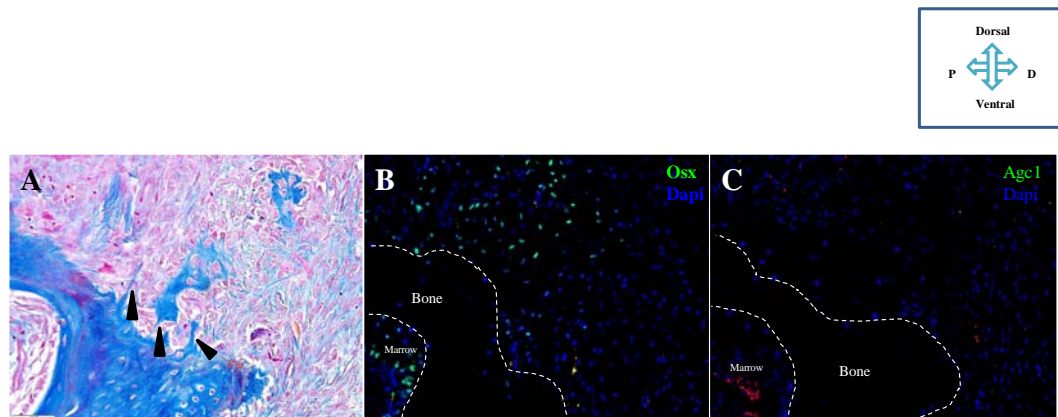
Figure 3.10 - Dawson et al

Fig. 3.10 Testing the intrinsic properties of the amputated P3 bone/periosteum. 7 DPA amputated P3 bones were grafted into the P2 fracture milieu at the time of fracture, and harvested 11 days later for histology and immunohistochemistry. (A) Mallory's staining shows new bone formation along the periosteal surface of the grafted P3 bone, including areas of continuity between the newly formed bone and the bone stump (arrowheads). (B) Immunohistochemistry confirms the presence of osteoblasts, with Osx positive cells along the periosteal surface as well as within the endosteal/marrow compartment. (C) Immunohistochemistry for Agc1 indicates a lack of chondrocytes present in the periosteal or endosteal/marrow regions of the grafted P3 bone. All samples 200X, sectioned at 5μm.

III. Discussion

Following amputation of the distal portion of the mouse P3 digit, the bone regeneration response is mediated via intramembranous ossification, whereby osteoblasts deposit woven bone directly, regenerating the amputated portion (Han, et al., 2008; Fernando, et al., 2011). The adjacent digit, P2, does not regenerate after amputation; the digit fails to increase in length and undergoes scar formation (Chapter One). The P2 bone, while incapable of endogenous regeneration, does exhibit bone formation following amputation, yet unlike P3, the bone formation occurs via endochondral ossification, thus mediated via a cartilaginous template (Chapters One and Two). Importantly, regeneration-incompetent proximal amputation injuries of the neonate P3 bone have been shown to undergo an induced regeneration response following BMP 2 or 7 treatment, with the bone regenerating by way of endochondral ossification (Yu, et al., 2010). Here, we investigated whether the intramembranous ossification of the regenerating P3 bone is specific to the amputation injury, and if P3 exhibits innate chondrogenic potential following relatively less invasive injuries, such as a bone fracture. The fracture healing response of long bones can occur via intramembranous ossification, however endochondral ossification is the chief mode of fracture repair, characterized by robust chondrogenesis along the injured periosteal surface, and thus is a great model to study chondrogenesis of the injured P3 bone (Le, et al., 2000; Gerstenfeld, 2003; Einhorn, 2005; Histing, et al., 2009; Colnot, 2010; Yu, et al, 2012a). We used the adult mouse P3 fracture model and amputation model to investigate: 1) the endogenous cartilaginous healing potential of the fractured bone, 2) the healing mechanism of BMP2-treated periosteal tissue in the fracture milieu, 3) the periosteal contribution to the regenerating

P3 digit, and 4) using tissue grafting techniques, we investigated the ability of the nail organ to promote intramembranous ossification, i.e. testing the extrinsic environment of P3, and inversely, testing if the P3 bone tissue acts autonomously, i.e. if the intramembranous bone formation of the P3 region is an intrinsic property of the tissue itself.

The Novel P3 Fracture Healing Response occurs via Endosteal/Marrow Chondrogenesis and Periosteal Intramembranous Bone Formation

Previous fracture healing studies showed intramembranous bone formation of the periosteal and endosteal/marrow spaces solely associated with stabilized fractures, and endochondral ossification of the periosteum solely associated with unstabilized fractures (Le, et al., 2000; Thompson, et al., 2001; Gerstenfeld, 2003; Einhorn, 2005; Histing, et al., 2009; Colnot, 2010; Yu, et al, 2012a). Notably, regardless of the fracture stability, studies indicate the injured endosteal/marrow space always forms bone via intramembranous ossification (Colnot, 2009; Yu, et al, 2012a). Here, using the fractured P3 bone as a model, we show a lack of chondrogenesis within the periosteal compartment of the injured bone. Our histological and immunological studies show some level, albeit low, of active bone formation along the P3 periosteal surface adjacent to the fracture gap, indicating not only that the periosteum does play a role in the fracture healing event, but also that the fracture healing milieu may be an example of endogenous stabilization, perhaps via the nail stabilizing the environment. As previously stated, unstabilized fracture repair is the predominant form of healing, underscored by the fact that stabilized fracture healing studies are tightly controlled systems mediated via cumbersome intra-and-extra-medullary rods (Le, et al., 2000; Thompson, et al., 2001; Histing, et al., 2009;).

However, contrary to previous fracture healing studies, we show chondrogenesis within the endosteal/marrow region of the fractured P3 digit, thus indicating the P3 fracture milieu is unlikely to be an example of endogenous stabilization. Chondrogenesis localized to the endosteal/marrow space is intriguing; while studies suggest the endosteal/marrow space does not produce anti-chondrogenic factors, studies indicate the cells that comprise the endosteal/marrow fracture space do not possess chondrogenic potential in-vivo, even when transplanted to the periosteal space of unstabilized fractures (Colnot, 2009). Our studies show chondrogenesis is localized to the proximal endosteal/marrow region only, corresponding to relatively proximal fracture levels, with distal fracture levels not showing active chondrogenesis within the endosteal/marrow region. One explanation for the proximal localization of the cartilaginous fracture callus and the distal localization of the intramembranous fracture callus may be that the fractured P3 bone heals via recapitulation of its developmental mechanisms; P3 develops by a proximal epiphyseal growth plate, followed by intramembranous appositional bone growth distally (Han, et al., 2008). Thus, the fracture repair and developmental mechanisms within the proximal portion of the endosteal/marrow space occur by way of endochondral ossification, and the fracture repair and developmental mechanisms of the distal portion of the P3 bone occur by way of intramembranous ossification. However, that does not explain the endosteal/marrow localization of chondrogenesis. Further investigation is needed to gain greater insight into the proximal endosteal cartilaginous callus formation post P3 fracture.

BMP2-treatment of the Fractured P3 Bone does not induce Chondrogenesis within the injured Periosteum

Previous studies have shown that endogenous periosteal-cell-derived BMP2 is essential for the initiation and maintenance of the periosteal cartilaginous callus following long bone fracture (Tsuji, et al., 2006; Wang, et al., 2011). Studies have also shown that exogenous application of BMP2 primarily targets periosteal-derived cells of the fracture milieu to form cartilage (Yu, et al., 2010a; Minear, et al., 2010; Chapter Two). Moreover, it has been reported that exogenous BMP2 can change the fate of periosteal cells in a stabilized fracture environment, thus inducing the formation of chondrocytes in an otherwise osteogenic milieu (Yu, et al., 2010a). To explore the lack of chondrogenesis within the periosteal space further, we treated the periosteal tissue with affi-gel micro-carrier beads coated with 0.500μg/μl BMP2 at the time of fracture with the specific intent to induce endochondral ossification within the periosteum. Studies suggest cells within the fractured periosteum commit to either a chondrogenic or osteogenic cell fate approximately 96 hours post fracture, thus we implanted BMP2 at the time of fracture to ensure a chondrogenic fate (Thompson et al., 2001). Following P3 fracture, we observed active bone formation along the periosteal surface of BMP2-treated digits compared to BSA-control samples, and surprisingly, the lack of chondrogenesis in the periosteal space. Our method to determine the stability of the P3 fracture environment was an indirect one, in that if the P3 periosteal compartment formed chondrocytes post BMP2-treatment, it would suggest, based on previous reports, the periosteal compartment of the fracture milieu may indeed be stabilized, presumably by

way of the nail organ (Yu, et al., 2010a). However, with the lack of chondrocyte formation in the periosteum and the localization of chondrocytes to the endosteal/marrow cavity, we provide evidence the P3 fracture healing mechanism is not redundant; it is unlike both stabilized and unstabilized fracture repair. Moreover, recent studies indicate the nail organ and associated epidermal components may not necessarily act to stabilize the P3 bone, but instead function as a signaling center (Takeo, et al., 2013). The study highlighted the necessity of Wnt expression in epidermal cells located within the distal nail matrix following amputation of the P3 digit, finding that Wnt-signaling is essential for regeneration of the nail organ as well as the bone regeneration response (Takeo, et al., 2013). Interestingly, it has been shown that the downstream conical mediator of Wnt signaling, Beta-catenin, destabilizes Sox9, a transcription factor upstream of Collagen 2 production, i.e. of chondrocyte proliferation (Minear, et al., 2010). Further studies must be performed to determine how the nail-organ-derived factors may potentially suppress chondrocyte formation in the P3 periosteum after bone fracture and BMP2-treatment.

The P3 the Periosteum is an Integral Component of the Regeneration Response

Our MicroCT 3-D reconstructed images, histology, and immunohistochemistry data all suggest the periosteal callus formation post P3 fracture, while clearly present, was minimal in comparison to the endosteal/marrow callus in the healing event. In an effort to determine if the lack of periosteal chondrogenesis was due to an overall lack of periosteal contribution to the injured P3 bone, regardless of injury type, we investigated the periosteal contribution to the regenerating P3 digit. Here, we report that after

periosteum removal and P3 amputation, MicroCT scans indicate the digits lacking the periosteal tissue underwent a similar degradation response compared to control periosteum-intact digits, however the subsequent bone regeneration response was greatly attenuated in the absence of the periosteum, with digits lacking distal bone elongation and exhibiting marked decreases in bone volume and length at the end of our study, suggesting the periosteal-derived cells play a role in bone formation post amputation. Furthermore, our studies revealed the lack of robust distal blastema formation and minimal osteoblast formation in the digits without intact periosteum. Our work suggests P3 periosteal-derived cells play a key role in blastema formation and subsequent distal bone growth post amputation, and that in the absence of the local periosteum, non-local periosteal and non-periosteal tissues do not compensate for the loss of the P3 periosteum. Indeed, our experimental design does not control for the local periosteal tissue playing a role in cellular recruitment to the blastema, therefore it does not definitely determine periosteal cellular contribution to the blastema, however our work does indicate the periosteal tissue is an integral component of the regeneration response. Taken together, we provide evidence that the periosteum of the injured P3 bone has the potential to contribute to the regeneration response, indicating the minimal formation of the fracture periosteal callus is not due to a lack of healing potential of the P3 periosteum.

Tissue Grafting Studies indicate Extrinsic and Intrinsic Properties Influencing the Periosteal Intramembranous P3 Bone Healing Response

Our previous efforts to study the periosteal intramembranous bone healing response of P3, regardless of fracture or amputation injury, were all performed with an

intact nail organ. To gain further insight into the complex P3 bone repair response, we isolated the P3 bone and nail organ to ascertain whether the bone and nail organ act independently of each other to induce intramembranous ossification and/or inhibit endochondral ossification. In grafting studies whereby we placed the 1 DPA nail/nail matrix in the newly fractured P2 injury milieu, we observed a lack of P2 periosteal chondrocytes and less osteoblasts in areas of the bone sample associated with the nail/nail matrix graft. Conversely, in nail grafts without an intact nail matrix, we observed robust chondrogenesis and the presence of osteoblasts on the P2 periosteal surface in close proximity to the nail graft. Our studies indicate the 1 DPA nail matrix acts as an extrinsic influence in the process of P3 bone repair, in that in its presence, there is a lack of chondrogenesis and less osteoblastogenesis on nearby injured bone. This is surprising, in that earlier studies suggest grafted nail organs transplanted into the amputated P2 digit result in new bone formation associated with the nail organ, yet this report does not distinguish between intramembranous or endochondral bone formation (Mohammad, et al., 1999). Our studies indicate the nail matrix may produce factors that inhibit chondrogenesis, coinciding with previous reports of the nail matrix functioning as a signaling center (Takeo, et al., 2013), however more studies must be performed in order to determine what factor(s) are possibly contributing to the chondrocyte suppression.

To test if the P3 bone tissue acts autonomously, i.e. if the intramembranous bone formation of P3 is an intrinsic property of the tissue itself, we grafted the 7 DPA P3 bone into the newly fractured P2 injury milieu. We observed no chondrogenesis in the periosteum of the grafted P3 bone; instead the bone exhibited boney islands complete with osteoblasts adjacent to the periosteum. Our work suggests the intramembranous

bone healing response of the P3 periosteum is an intrinsic property of the bone, in that P3 chondrocyte formation could not be induced in the highly chondrogenic P2 bone healing environment. Note, newly amputated and grafted P3 bones (0 DPA) did not undergo a degradation response or subsequent bone regeneration response when grafted into the P2 fracture environment, therefore we chose the 7 DPA P3 digit to investigate the intrinsic properties of the bone. As previously stated, cells within the injured periosteum of long bones commit to either a chondrogenic or osteogenic cell fate approximately 96 hours post injury (Thompson, et al., 2001). Keeping that in mind, there may be two possibilities for the intramembranous bone formation of the grafted P3 bone: 1) the periosteal cells may have already committed to the osteoblast cell fate, or 2) the nail organ may have played a critical role in suppressing chondrogenesis prior to grafting.

Overall, our studies provide evidence that P3 is unique not only due to its extraordinary regeneration potential, but also the distinctive bone healing response post fracture. Our studies indicate the P3 periosteum forms very little callus post fracture, does not form cartilage, and furthermore, cannot be induced to form cartilage with BMP2 application at the time of fracture. Importantly, we show the P3 periosteum does play a role in the regeneration response, thus showing that while it may not perform as long-bone-periosteal-tissue post fracture, it does indeed aid greatly in the regeneration process, possibly through providing cells to the blastema. Moreover, we observe chondrogenesis in the endosteal/marrow cavity post fracture, a novel finding that further shows the unique injury milieu of P3. Ultimately, our goal is to elucidate the mechanisms behind the unique healing abilities of the P3 bone to enhance future regeneration and fracture repair studies.

Conclusions and Future Studies:

Taken as a whole, this dissertation has two defining themes: 1) the periosteal contribution to both the endogenous healing response and the induced-regeneration of the amputated P2 bone, and 2) blending the techniques and advances made in the fracture repair field to enhance the regeneration response of amputated bones. Indeed, we have concluded the local periosteal tissue of the amputated adult mouse P2 bone is essential for the endogenous cartilaginous callus. An earlier study concluded the amputated P2 bone formed cartilage along the periosteal surface only after the addition of a "cryptic peptide," thus, until now, careful characterization of the cartilaginous callus had not been performed (Agrawal et al., 2011). It was our careful characterization of the endogenous callus that led to the idea that the amputated adult P2 bone is analogous to the proximal bone fragment in a fracture milieu, thus leading to the findings that chondrocytes are derived from the local injured periosteum, and that exogenous BMP2 targets the periosteal tissue actively undergoing chondrogenesis to induce the regeneration of P2. Importantly, our findings that the same concentration of BMP2 can effectively impede, induce, or have no effect on the regeneration response of the P2 bone may have immense therapeutic potential for the advancement of fracture repair. Our discovery that re-injury of the previously amputated P2 bone creates an environment conducive for induce-regeneration is incredibly exciting; if mouse studies translate to human studies, then older amputation wounds of humans may have the potential to undergo a regeneration response.

Indeed, while not included in this dissertation, future studies have begun on elucidating the potential for other BMPs to target the periosteal tissue of the amputated

P2 bone. Our recent preliminary studies indicate that exogenous treatment of BMP9, placed into the BMP2-induced regeneration milieu of the P2 bone approximately 7 days after BMP2 treatment, may increase chondrocyte proliferation and/or decrease chondrocyte matrix remodeling, thus creating a larger template for bone growth. Strikingly, our preliminary studies show that 5 days after BMP9 application in the BMP2-treated samples, a joint-like cavitation forms in the general proximity of the BMP9 source, whereby two separate zones of proliferating and hypertrophic chondrocytes are opposing each other (much like growth plates on either side of a joint), with a space of fibroblasts separating the two zones (n = 3). Importantly, our preliminary MicroCT data shows the 21 DPI BMP2-induced regenerated bone shows a large area of incomplete cavitation at the distal end of BMP9-treated bones (n = 3), suggesting that ossification occurred, yet did not close the cavitation space at this time point. Further studies must be performed to test the chondrocytes surrounding the cavitation for articular cartilage markers. Next, we tested the ability of BMP9-treatment alone to induce a regeneration response in the amputated P2 bone, and found that indeed, BMP9 did induce a statistically significant increase in bone length compared to BSA-control samples (n = 4). While BMP9-treatment alone did not induce a cavitation, the contiguous regeneration response occurred via endochondral ossification, whereby chondrocyte proliferation occurred distal to the amputation plane. Furthermore, in the absence of the local periosteum, we observed no increase in bone length, indicating that BMP9 targets the periosteal cells to induce distal bone regeneration (n = 4). We did however find a significant increase in contiguous bone width in BMP9-treated digits without an intact periosteum, suggesting that the periosteum is not the only source of cells that plays a role

in the BMP9-induced regeneration response (n = 4). Surprisingly, in one BMP9-treated sample missing the periosteum, histology and immunohistochemistry revealed the presence of chondrocytes within the distal portion of the marrow cavity, indicating that BMP9 may have the potential to induce chondrocyte differentiation of non-periosteal cells, yet this exciting response did not lead to a regeneration response. Overall, future studies are underway to characterize and optimize the potential joint formation response post BMP9 treatment to the amputated adult mouse P2 bone.

Lastly, we investigated the P3 fracture response and the chondrogenic potential of the periosteal compartment of the fractured P3 bone. Our findings were puzzling; the fractured P3 bone lacked a large periosteal callus that tested immunonegative for chondrogenesis, the periosteal compartment could not be induced via exogenous BMP2-treatment to form chondrocytes, and the endosteal/marrow compartment formed chondrocytes in fractures located within the proximal portion of the bone. Furthermore, we showed that amputated P3 bones lacking the periosteum exhibited a substantially smaller blastema and an attenuated bone regeneration response, indicating that while the periosteum may not form a large callus post fracture, it is an integral component of the regeneration response. Future studies are needed to gain a greater understanding of the lack of chondrogenesis in the periosteum and the formation of chondrocytes in the endosteum post fracture. Furthermore, we will focus on investigating how the P3 bone responds to fractures of a critical dimension, i.e. fractures that do not heal on their own due to the large gap. In particular, we will test if the P3 bone forms a blastema between the large fracture gap, thus employing the regeneration mechanism to heal the fracture.

References

Agrawal, V., Kelly, J., Tottey, S., Daly, K.A., Johnson, S.A., Siu, B.F., Reing, J., Badylak, S.F. (2011). An isolated cryptic peptide influences osteogenesis and bone remodeling in an adult mammalian model of digit amputation. Tissue Eng Part A. 17(23-24):3033-44.

Agrawal, V, Siu, B.F., Chao, H., Hirschi, K.K., Raborn, E., Johnson, S.A., Tottey, S., Hurley, K.B., Medberry, C.J., Badylak, S.F. (2012). Partial characterization of the Sox2+ cell population in an adult murine model of digit amputation. Tissue Eng Part A. 18(13-14):1454-63.

Al-Aql, Z. S., Alagl, A.S., Graves, D.T., Gerstenfeld, L.C., Einhorn, T. A. (2008). Molecular Mechanisms Controlling Bone Formation during Fracture Healing and Distraction Osteogenesis. J DENT RES 87, 107.

Borgens, R.B. (1982). Mice regrow the tips of their foretoes. Science. 217(4561):747-50.

Chang, H., Knothe Tate, M.L. (2012). Concise review: the periosteum: tapping into a reservoir of clinically useful progenitor cells. Stem cells Transl Med. 1(6):480-91.

Cho, T.J., Gerstenfeld, L.C., Einhorn, T.A. (2002). Differential temporal expression of members of the transforming growth factor beta superfamily during murine fracture healing. J Bone Miner Res. 17(3):513-20.

Colnot, C., Lu, C. Hu, D., Helms, J.A. (2004). Distinguishing the contributions of the perichondrium, cartilage, and vascular endothelium to skeletal development. Dev Biol. 269 (1):55-69.

Colnot, C. (2008). Skeletal Cell Fate Decisions within Periosteum and Bone Marrow During Bone Regeneration. J Bone and Miner Res 24, 274-282.

Colnot, C., Zhang, X., Knothe Tate, M.L. (2012). Current insights on the regenerative potential of the periosteum: molecular, cellular, and endogenous engineering approaches. J Orthop Res. 30(12):1869-78.

Dwek, J. R. (2010). The periosteum: what it is, where it is, and what mimics it in its absence? Skeletal Radiol **39**, 319-323.

Einhorn, T. (2005). The Science of Fracture Healing. J Orthop Trauma 19, S4-S6.

Ferguson, C., Alpern, E., Miclau, T., Helms, J. A. (1999). Does adult fracture repair recapitulate embryonic skeletal formation? Mechanisms of Development 87, 57-66.

Fernando W.A., Leininger, E., Simkin, J., Li, N., Malcom, C.A., Sathyamoorthi, S., Han, M., Muneoka, K. (2011). Wound healing and blastema formation in regenerating digit tips of adult mice. Dev Biol. 350(2):301-10

Franz-Odendaal, T.A. (2011). Induction and patterning of intramembranous bone. Front Biosci. 16:2734-46.

Gautschi, O.P., Frey, S.P., Zellweger, R. (2007). Bone morphogenetic proteins in clinical applications. ANZ J Surg. 77(8):626-31.

Gerstenfeld, L. C., Cullinane, D. M., Barnes, G. L., Graves, D. T., Einhorn, T. A. (2003). Fracture Healing as a Post-Natal Developmental Process: Molecular, Spatial, and Temporal Aspects of its Regulation. J. Cell. Biochem. 88, 873-884.

Govender,S., Csimma, C., Genant, H.K., *et al*. (2002). Recombinant human bone morphogenetic protein-2 for treatment of open tibial fractures: a prospective, controlled, randomized study of four hundred and fifty patients. J Bone Joint Surg Am. 84-A(12):2123-34.

Han, M., Yang, X., Farrington, J.E., Muneoka, K. (2003). Digit regeneration is regulated by Msx1 and BMP4 in fetal mice. Development. 130(21):5123-32.

Han, M., Yang, X., Lee, J., Allan, C. H., Muneoka, K. (2008). Development and regeneration of the neonatal digit tip in mice. Dev Biol 315, 125-35.

Histing, T., Garcia, P., Matthys, R., Leidinger, M., Holstein, J.H., Kristen, A., Pohlemann, T., Menger, M.D. (2010). An internal locking plate to study intramembranous bone healing in a mouse femur fracture model. J Orthop Res. 28(3):397-402

Hutchison, C., Pilote, M., Roy, S. (2007). The axolotl limb: a model for bone development, regeneration and fracture healing. Bone. 40(1):45-56.

Ito, Y., Fitzsimmons, J. S., Sanyal, A., Mello, M. A., Mukherjee, N., O'Driscoll, S. W. (2001). Localization of chondrocyte precursors in periosteum. Osteoarthr Cartilage **9**, 215-223.

Jeppsson, C., Aspenberg, P. (1996) BMP-2 can inhibit bone healing. Bone-chamber study in rabbits. Acta Orthop Scand. 67(6):589-92.

Karsenty, G., Kronenberg, H. M., Settembre, C. (2003) Genetic Control of Bone Formation. Annu. Rev. Cell Dev. Biol. 25, 629-48.

Kitaori, T., Ito, H., Schwarz, E. M., Tsutsumi, R., Yoshitomi, H., Oishi, S., Nakano, M., Fujii, N., Nagasawa, T., Nakamura, T. (2009). Stromal Cell-Derived Factor 1/CXCR4 Signaling Is Critical for the Recruitment of Mesenchymal Stem Cells to the Fracture Site During Skeletal Repair in a Mouse Model. Arthritis & Rheumatism **60**, 813-823.

Kronenber, H. (2003). Developmental regulation of the growth plate. Nature 423, 332-336.

Le, A.X., Miclau, T., Hu, D., Helms, J.A. (2001). Molecular aspects of healing stabilized and non-stabilized fractures. J Orthop Res. 19(1):78-84.

Lehoczky, J.A., Robert, B., Tabin, C.J. (2011). Mouse digit tip regeneration is mediated by fate-restricted progenitor cells. Proc Natl Acad Sci U S A. 108(51):20609-14.

Merloz, P. (2011), Macroscopic and microscopic process of long bone fracture healing. Osteoporos Int. 22(6):1999-2001.

Minear, S., Leucht, P., Miller, S., Helms, J.A. (2010). rBMP represses Wnt signaling and influences skeletal progenitor cell fate specification during bone repair. J Bone Miner Res. 25(6):1196-207.

Mohammad, K. S., Day, F. A., Neufeld, D. A. (1999). Bone Growth is Induced by Nail Transplantation in Amputated Proximal Phalanges. Calcif Tissue Int 65, 408-410.

Mu, X., Bellayr, I., Pan, H., Choi, Y., Li, Y., (2013). Regeneration of soft tissues is promoted by MMP1 treatment after digit amputation in mice. PLoS One. 8(3):e59105.

Muller, T.L., Ngo-Muller, V., Reginelli, A., Taylor, G., Anderson, R., Muneoka, K. (1999). Regeneration in higher vertebrates: limb buds and digit tips. Semin Cell Dev Biol. 10(4):405-13.

Neufeld, D.A, Zhao W. (1993). Phalangeal regrowth in rodents: postamputational bone regrowth depends upon the level of amputation. Prog Clin Biol Res. 383A:243-52.

Reno, P.L., McBurney, D.L., Lovejoy, C.O., Horton, W.E. Jr. (2006). Ossification of the mouse metatarsal: differentiation and proliferation in the presence/absence of a defined growth plate. Anat Rec A Discov Mol Cell Evol Biol. 288(1):104-18.

Rinkevich, Y., Lindau, P., Ueno, H., Longaker, M.T., Weissman, I.L. (2011). Germ-layer and lineage-restricted stem/progenitors regenerate the mouse digit tip. Nature. 476(7361):409-13.

Rosen, V. (2009). BMP2 signaling in bone development and repair. Cytokine Growth factor Rev. 20(5-6):475-80.

Santos, E. M., Radin, S., Ducheyne, P. (1999). Sol-gel derived carrier for the controlled release of proteins. Biomaterials **20**, 1695-1700.

Sathyendra, V., Darowish, M. (2013). Basic science of bone healing. Hand Clin. (4):473-81.

Schindeler, A., McDonald, M.M., Bokko, P., Little, D. G. (2008). Bone remodeling during fracture repair: The cellular picture. Sem Cell Dev Biol 19, 459-466.

Shapiro, F. (2008). Bone Development and its Relation to Fracture Repair. The Role of Mesenchymal Osteoblasts and Surface Osteoblasts. European Cells and Materials 15, 53-76.

Taguchi, K., Ogawa, R., Migita, M., Hanawa, H., Ito, H., Orimo, H. (2005). The role of bone marrow-derived cells in bone fracture repaor in a green fluorescent protein chimeric mouse model. Biochem Biophys Res Commun. 331(1):31-6.

Thompson, Z., Miclau, T., Hu, D., Helms, J. A. (2001). A model for intramembranous ossification during fracture healing. J Orthop Res 20, 1091-1098.

Tsuji, K., Bandyopadhyay, A., Harfe, B. D., Cox, K., Kakar, S., Gerstenfeld, L., Einhorn, T., Tabin, C., Rosen, V. (2006). BMP2 activity, although dispensable for bone formation, is required for the initiation of fracture healing. Nature Genetics **38**, 1424-1429.

Turner, N.J., Johnson, S.A., Badylak, S.F. (2010). A histomorphologic study of the normal healing response following digit amputation in C57bl/6 and MRL/MpJ mice. Arch Histol Cytol. 73(2):103-11.

Urist, M.R. (1965). Bone: formation by autoinduction. Science. 150(3698):893-9.

Vortkamp, A., Pathi, S., Peretti, G. M., Caruso, E. M., Zaleski, D. J., Tabin, C. J. (1998). Recapitulation of signals regulating embryonic bone formation during postnatal growth and in fracture repair. Mech. Dev. 71, 65-76.

Wang, Q., Huang, C., Xue, M., Zhang, X. (2011). Expression of endogenous BMP-2 in periosteal progenitor cells is essential for bone healing. Bone. 48(3):524-32.

Welch, R.D., Jones, A.L., Bucholz, R.W., Reinert, C.M., Tjia, J.S.,Pierce, W.A., Wozney, J.M., Li, X.J. (1998). Effect of recombinant human bone morphogenetic protein-2 on fracture healing in a goat tibial fracture model. J Bone Miner Res. 13(9)1483-90.

Yu, L., Han, M., Yan, M., Lee, E., Lee, J., Muneoka, K. (2010). BMP signaling induces digit regeneration in neonatal mice. Development 137, 551-559.

Yu (a), Y.Y., Lieu, S., Lu, C., Colnot, C. (2010). Bone morphogenetic protein 2 stimulates endochondral ossification by regulating periosteal cell fate during bone repair. Bone 47, 65-73.

Yu (b), Y.Y., Lieu, S., Lu, C., Miclau, T., Marcucio, R.S., Colnot, C. (2010). Immunolocalization of BMPS, BMP antagonists, receptors, and effectors during fracture repair. 46(3):841-51.

Yu, L., Han, M., Yan, M., Lee, J., Muneoka, K. (2012). BMP2 indices segment-specific skeletal regeneration from digit and limb amputations by establishing a new endochondral ossification center. Dev Biol. 372(2):263-73.

Zhao, W., Neufeld, D.A. (1995) Bone regrowth in young mice stimulated by nail organ. J Exp Zool. 271(2):155-9

Biography

Lindsay Ann Dawson was born in sunny Santa Rosa, CA in 1981 to wonderful parents Rhonda Dawson and Jeff Dawson Sr. She and her brother, Jeff Dawson Jr. played outside in the creek, the apple orchards, and enjoyed childhood. High school was a trying time for Lindsay; she graduated from a California Continuation High School, a school designed for students at-risk of not graduating. She later enrolled at the Santa Rosa Junior College, and found her love of science. She earned her Associates Degree in 2003, yet remained at the SRJC to complete pre-requisites for a Bachelors Degree. In 2005, she transferred to Sonoma State University, and earned her B.S. degree in Molecular and Cellular Biology in the winter of 2007.

Lindsay moved to New Orleans, LA in late summer, 2008, to begin her studies towards earning her Ph.D. in Cell and Molecular Biology at Tulane University. She joined Ken Muneoka's Digit Regeneration Lab in February, 2009. She initially focused her studies on the SDF-1/CXCR4 signaling pathway, and eventually found her niche in integrating fracture healing and P2/P3 amputation.